DISSERTATION

INNOVATIONS IN MICROCHIP CAPILLARY ELECTROPHORESIS FOR THE DIRECT DETECTION OF BIOLOGICALLY IMPORTANT MOLECULES

Submitted by

Jonathan A. Vickers

Department of Chemistry

In partial fulfillment of the requirements

For the degree of Doctor of Philosophy

Colorado State University

Fort Collins, Co

Fall 2007

COLORADO STATE UNIVERSITY

MARCH 15, 2007

WE HEREBY RECOMMEND THAT THE DISSERTATION PREPARED UNDER OUR SUPERVISION BY JONATHAN A. VICKERS ENTITLED "INNOVATIONS IN MICROCHIP CAPILLARY ELECTROPHORESIS FOR THE DIRECT DETECTION OF BIOLOGICALLY IMPORTANT MOLECULES" BE ACCEPTED AS FULFILLING IN PART REQUIREMENTS FOR THE DEGREE OF DOCTOR OF PHILOSOPHY.

Committee on Graduate Work

Advisor: Charles S. Henry

Co-Advisor:

Department Head: Anthony K. Rappe

ABSTRACT OF DISSERTATION

INNOVATIONS IN MICROCHIP CAPILLARY ELECTROPHORESIS FOR THE DIRECT DETECTION OF BIOLOGICALLY IMPORTANT MOLECULES

Microchip capillary electrophoresis (MCE) and related techniques have benefits over conventional separation instrumentation, including small size, high speed (seconds time scale), and low sample consumption (pL injection volumes). These features make MCE an attractive separation method, particularly for point-of-measurement applications. This thesis will demonstrate improvements made to MCE coupled to electrochemical detection (EC) in the forms of increased sensitivity through the use of microwire detection electrodes and microwire decoupling electrodes, increased selectivity from the use of multiple detection techniques such as pulsed amperometric detection as well as dual electrode detection and improvements in the materials chemistry through the use of alternate microchip materials.

CE and MCE are relatively new separation techniques. CE was first developed by Jorgenson[1] in 1981 and MCE was developed shortly after that in 1992 by Manz.[2] Detection with MCE is most commonly accomplished using laser induced fluorescence (LIF). While LIF detection has the benefit of high sensitivity and low limits of detection it has some drawbacks, including difficulties in miniaturization, portability and higher

costs than some detection instrumentation used with microchip CE. EC was later coupled to MCE devices.[3] In contrast to LIF, EC is easily miniaturized and existing instrumentation is already portable. EC, however, has a few inherent problems: high noise levels limit sensitivity and in its most common form, DC amperometry, it is limited to a small number of easily oxidizable or reducible analytes. In my work I systematically addressed these issues by improving the design and construction of EC detection electrodes. I will show that increased sensitivity and decreased detection limits are possible through the incorporation of microwire working electrodes and a microwire decoupler. The incorporation of a palladium decoupler for the isolation of separation current from the detection current allows for decreased background, and in turn, lower detection limits. I will also address the low number of detectable analytes and the lack in selectivity of DC amperometry through the use of pulsed amperometric detection (PAD) and dual electrode detection, respectively. PAD will increase the number of detectable analytes allowing for the direct detection of carbohydrates, amines and thiols. Dual electrode detection will increase selectivity by allowing multiple potentials to be utilized for the selective detection of compound with reversible redox reactions as well as analytes with specific oxidation potentials in complex mixtures. As a final example of the applicability of the chemistry I have developed the direct detection of proteins using hemoglobin, myoglobin, albumin and concanavalin A as models.

Materials chemistry is also beginning to play a more important role in MCE because of the use of polymers as substrates. Poly(dimethylsiloxane) (PDMS) has become one of the most widely used materials for microchip capillary electrophoresis and microfluidics. The popularity of this material is the result of its low cost, simple

fabrication, and rugged elastomeric properties. The hydrophobic nature and lack of surface stability of PDMS limit its applicability for MCE. The surface of PDMS can be made hydrophilic using a simple air plasma treatment; however, this property is quickly lost through hydrophobic recovery caused by diffusion of unreacted oligomers to the surface. This hydrophobic recovery causes the MCE devices to have poor separation efficiencies and large peak tailing (peak skew). In my work I will address these issues through a simple extraction and oxidation of PDMS as well as exploring alternative microchip materials. PDMS can be extracted in a series of solvents designed to remove unreacted oligomers from the bulk phase. Then the oligomer-free PDMS is oxidized in a simple air plasma, generating a stable layer of hydrophilic SiO_2. The extracted oxidized PDMS (EO-PDMS) shows a dramatic increase in separation efficiencies and a decrease in peak skew from 3.2 on native PDMS to 1.2 on EO-PDMS. The introduction of thermoset polyester (TPE) as an alternative microchip material will also be presented. TPE shows promise as a merger between the ease of fabrication and cost effectiveness of PDMS and the higher separation efficiencies and increased surface stability of other polymers such as Poly(methylmethacrylate) (PMMA) and Poly(carbonate) (PC). These benefits will be shown in the form of increased separation efficiencies and decreased peak skews.

Jonathan A. Vickers

Chemistry Department

Colorado State University

Fort Collins, CO 80523

Fall 2007

(1) Jorgenson, J. W.; Lukacs, K. D. *Anal Chem* **1981**, *53*, 1298-1302.
(2) Manz, A.; Harrison, D. J.; Verpoorte, E. M. J.; Fettinger, J. C.; Paulus, A.; Ludi, H.; Widmer, H. M. *J. Chrom.* **1992**, *593*, 253-258.
(3) Woolley, A. T.; Lao, K.; Glazer, A. N.; Mathies, R. A. *Anal Chem* **1998**, *70*, 684-688.

ACKNOWLEDGEMENTS

To God: You stand above everyone and help to guide my life. Thank you.

To my Mother and Father: Thank you for everything you do for me. You have always stood behind me and supported me. Thank you for all of the prayers and love, I could never had done it without you.

To the woman who gives me strength in everything I do: Jennifer I love you and can't imagine my life without you in it. You make me a better person.

To Geof and Amanda: Geof you are the best brother I could ever had wished for. You were a good person to vent to and always had an open ear for me to talk to. Thank you.

To Chris Spann: Thank you for giving me someone to talk to about something other than chemistry and keeping me sane. Next time come up during the summer and there won't be any snow.

To my lab mates: Thank you for keeping the lab a relaxed and comfortable work environment.

To my committee: Thank you for your attention, advice and support.

To my Advisor: Dr. Charles Henry. Thank you for being the best advisor I could ever have wanted. Thank you for teaching me how to be a scientist and allowing me the freedom to explore my research while keeping me on track.

DEDICATION

This work is dedicated to my Father, Dr. Leland P. Vickers.

Table of Contents

Abstract iii

Acknowledgements vii

Dedication ix

List of Figures xiv

List of Abbreviations xxi

Chapters

1. Introduction

1.1 Capillary Electrophoresis 2
1.1a Modes of CE 2
1.1b Electroosmotic Flow 3
1.2 Microchip Capillary Electrophoresis 5
1.3 MCE-EC 7
1.4 Current Decoupler 12
1.5 Materials for MCE 15
1.5a Glass Microchips 15
1.5b Polymer Microchips 15
1.6 Important Electrochemically Active Analytes 17
1.6a Catecholamines 17
1.6b Carbohydrates 18
1.6c Thiols 20
1.6d Proteins 22
1.6e Summary 23
1.7 Research Goals 23

2. Mold and Microchip Fabrication

2.1 Mold Fabrication 29
2.2 Microchip Fabrication 32

2.2a PDMS Molding....32
2.2b Microwire Alignment....32
2.2c Microchip Sealing....33
2.3 Microchip Injection....36
2.4 Data Analysis....36
2.5 Conclusions....39

3. Simple and Sensitive Electrode Design for Microchip Electrophoresis/Electrochemistry
3.1 Experimental....42
3.1a Chemicals and Materials....42
3.1b Microchip CE-EC....42
3.2 Results and Discussion....45
3.2a Microwire Working Electrodes....45
3.2b Limits of Detection....45
3.2c Separation Efficiency....50
3.3 Conclusions....50
3.4 Acknowledgements....53

4. Incorporation of a Microwire Current Decoupler for Use with Microchip CE-EC
4.1 Experimental....57
4.1a Chemicals and Materials....57
4.1b Microchip CE-EC....57
4.1c Detection....63
4.2 Results and Discussion....63
4.2a Chip Design....64
4.2b Microchip CE-EC....64
4.2c Limits of Detection....68
4.2d Microchip CE-PAD....70
4.3 Conclusions....74
4.4 Acknowledgements....74

5. Microchip CE with Dual Electrode Electrochemical Detection
5.1 Experimental....78
5.1a Chemicals and Materials....78

5.1b Dual Electrode Microchip CE.....78
5.1c Dual Electrode Detection.....80
5.2 Results and Discussion.....82
5.2a Oxidation/Reduction Detection.....82
5.2b Increasing Potential Detection.....85
5.3 Conclusions.....87

6. Surface Modified PDMS for Use with Microchip CE-EC
6.1 Experimental.....90
6.1a Chemicals and Materials.....91
6.1b Fabrication of PDMS Microchips.....91
6.1c PDMS Extraction.....92
6.1d Surface Composition.....92
6.1e Microchip CE.....93
6.1f Detection.....94
6.2 Results and Discussion.....95
6.2a Surface Chemistry.....95
6.2b Oxidation Optimization.....99
6.2c Separation Efficiency.....101
6.2d Electroosmotic Flow.....103
6.2e Limits of Detection.....105
6.2f Pulsed Amperometric Detection.....105
6.3 Conclusions.....107
6.4 Acknowledgements.....109

7. Thermoset Polyester, an Alternative Microchip Material
7.1 Experimental.....113
7.1a Chemicals and Materials.....113
7.1b Microchip Fabrication.....113
7.1c Electroosmotic Flow.....116
7.1d Coating Procedures.....117
7.1e Electrochemical Detection.....117
7.2 Results and Discussion.....118
7.2a Electroosmotic Flow Studies.....118
7.2b Polyelectrolyte Modification.....122
7.2c Microchip CE-Amperometry.....124
7.2d Microchip CE-PAD.....128
7.3 Conclusions.....129

7.4 Acknowledgements 129

8. Microchip CE-EC for the Detection of Heme and non-Heme Proteins

8.1 Experimental 134
8.1a Chemicals and Materials.....134
8.1b Microchip CE-EC.....134
8.1c Detection.....135
8.2 Results and Discussion 136
8.2a Microchip MEKC-EC.....136
8.2b Hydrodynamic Voltamograms.....138
8.2c Hemoglobin Oxidation State.....144
8.3 Conclusions 148

9. Summary and Future Work

9.1 Dissertation Summary 152
9.2 Future Work 154

Appendix A: Publications.....158

Appendix B: Research Proposal.....159

List of Figures

Figure **Page**

Figure 1.1: **4**
A) Capillary zone electrophoresis, negatively charge capillary walls attract positive ions from the BGE. When a potential is applied across the capillary an electroosmotic flow is created causing flow through the capillary. Separation of analytes is based on charge to hydrodynamic radius with small highly positive ions (dark green) coming off first followed by larger less positive charged species (light green). Small highly negative charges come off last (dark red). Neutral analytes (yellow) travel with the EOF and are not separated. B) Micellar electrokinetic chromatography. Separation based on partitioning of analyte into and out of micelles.

Figure 1.2: **6**
A) Pressure induced flow through a capillary. Friction at the walls causes a parabolic flow profile. B) Electrophoretic flow through a capillary. Flow induced at the walls of the capillary causing a plug like flow.

Figure 1.3: **9**
Electrochemical detection techniques A) Amperometric detection, a constant potential is applied to the work electrode to oxidize or reduce the analytes of interest. B) Pulsed amperometric detection (PAD), a potential waveform is applied to the working electrode. An oxidative cleaning potential (high positive) is followed by a reductive regeneration potential (negative) is applied to clean the working electrode before a detection potential is applied to oxidize or reduce the analyte of interest.

Figure 1.4: **11**
Electrode alignment techniques. A, B) End channel detection, the working electrode is aligned outside of the separation channel. Is done either on or off chip. C) In channel detection, the working electrode is aligned in the separation channel. D) Off channel detection, the working electrode is aligned in the separation channel but outside of the separation potential. This is usually done through the incorporation of a current decoupler.

Figure 1.5: **13**
Current decoupler is placed in the separation channel upstream from the working electrode allowing the separation current to be grounded and isolate from the detection potential. This allows for the benefits of both end and in channel detection to be exploited. Electroosmotic flow is seen upstream from the decoupler while hydrodynamic flow is seen downstream from the decoupler and around the working electrode.

Figure 1.6: 19
Important electrochemically active catecholamines. Catechol is the building block behind all catecholamines. Dopamine, epinephrine (adrenalin) and norepinephrine (noradrenaline) are important for their effects on the nerous system, cardiovascular system, metabolic rate and helping control body temperature.

Figure 1.7: 21
Biologically important thiols. Cysteine and glutathione are important because of their role in the regulation of oxidative damage within the body. Homocysteine has shown to be an important biomarker in the diagnosis of cardiovascular disease.

Figure 2.1: 31
Schematic representation of mold fabrication process.

Figure 2.2: 34
Schematic representation of microchip fabrication process.

Figure 2.3: 35
Schematic representation and photograph of a decoupled microchip.

Figure 2.4: 37
Pinched injection schematic.

Figure 3.1: 46
Top) Schematic of the microchip showing placement of the electrode alignment channel. Bottom) Photograph showing electrode alignment in a completed microchip

Figure 3.2: 47
Electropherograms of 100 μM catechol: A) 25 μm Cu electrode B) 25 μm Au electrode C) 25 μm Pt electrode D) 50 μm Pt electrode. Experimental conditions: Separation voltage: 1500 V; Pinched injection time: 45 s; Running buffer: 20 mM TES (pH 7)

Figure 3.3: 48
A) LOD of dopamine for 25 μm Au electrode (250 nM). B) LOD of dopamine for 50 μm Pt electrode (100 nM). Experimental conditions were the same as Figure 3.2.

Figure 3.4: 51
Schematic of flow around the microwire electrode in microchannel, drawn to scale. Location of the 25 μm electrode can vary vertically in the channel.

Figure 3.5: 52
Separations of 100 μM dopamine and catechol. A) 25 μm Au electrode B) 50 μm Pt electrode. Experimental conditions were the same as Figure 3.2.

Figure 4.1: 59
A. Schematic of the microchip (50μm deep, 50μm wide, 5.1cm long separation channel) showing placement of the electrode alignment channels. Working electrode channel (50μm deep x 50μm wide). Decoupler electrode channel (50μm deep x 25μm wide, 50 μm gap to separation channel). Double-T injector (50μm × 50μm × 100μm) has a volume of 250 pL. The lower right is a photograph showing electrode alignment in a completed microchip. Left electrode is Pd microwire while the right electrode is the Pt working electrode. **B.** Decoupled microchip. Fluorescent image of 1 mM FITC as it passes the decoupler. No sample leakage was observed around the Pd microwire. Dotted lines indicate the outline of the channels in the PDMS.

Figure 4.2: 60
Representation of fluid flow in the first decoupled microchips. The red dotted line represents the flow of fluid in the very first decoupled microchips. Flow from the separation channel traveled down the electrode alignment channel and never made it to the working electrode. The Blue dashed line represents the desired flow in the chip.

Figure 4.3: 62
The second decoupled microchip design. RTV silicon sealant was forced down the alignment channel until it was 50-100 μm from the separation channel. This prevented flow down the alignment channel but increased band broadening because portions of the alignment channel were still open to the separation channel.

Figure 4.4: 65
Optimization of distance between the working electrode and decoupling electrode. Left axis (black), shows the background noise as a function of distance. Right axis (red), shows the peak width as a function of distance.

Figure 4.5: 67
The effect of applied voltage on the background noise measured at the working electrode with and without use of the decoupler. Peak-to-peak noise was measured at random points along the baseline. Error bars are for n > 30. Experimental parameters: Working electrode: 25 μm Au microwire; Pinched injection time: 15 s; Running buffer: 20 mM TES (pH 7.0).

Figure 4.6: 69
Representative electropherograms obtained using a decoupled system. A) 50 μM Dopamine, 50 μM Catechol, and 50 μM Ascorbic Acid; B) 5 μM Dopamine, 5 μM Catechol, and 5 μM Ascorbic Acid; C) 50 nM Dopamine, 500 nM Catechol, and 500 nM Ascorbic Acid. **Insert:** Limits of detection were seen as 5nM for dopamine (S/N = 3.34), 50 nM for catechol (S/N = 4.21), and 50 nM for ascorbic acid (S/N = 2.85). Experimental conditions: 0.7 V detection potential; Field strength: 200 V/cm; Pinched injection time: 15 s; Running buffer: 20 mM TES (pH 7).

Figure 4.7: 71
Hydrodynamic voltammograms for 1mM Glucose (■) Decoupled, (□) Non-decoupled, and 1 mM Cysteine (●) Decoupled, (○) Non- decoupled. Experimental conditions: Buffer: 20 mM Boric acid, 0.8 mM SDS (pH 12.0 for carbohydrates, pH 9.4 for thiols); Field Strength: 220 V/cm; Pinched injection time: 15s.

Figure 4.8: 72
A. Example electropherogram using a decoupled system for the separation of 1mM glucose and 1mM glucose-6-phosphate. PAD waveform: cleaning (1.6 V for 0.05s), regeneration (-0.5 V for 0.025s), detection (0.6 V for 0.15 s). Experimental conditions: Field strength: 220 V/cm; Pinched injection time: 15 s; Running buffer: 20 mM boric acid, 0.8 mM SDS (pH 12.0). **B.** Example electropherogram using a decoupled system for the separation of 1μM cysteine and 1μM glutathione. PAD waveform: cleaning (1.6 V for 0.05s), regeneration (-0.5 V for 0.025s), detection (1.3 V for 0.15 s). Experimental conditions: Field strength: 220 V/cm; Pinched injection time: 15 s; Running buffer: 20 mM boric acid, 0.8 mM SDS (pH 9.4).

Figure 5.1: 79
Photograph of a fully assembled microchip used in dual electrode electrochemical detection.

Figure 5.2: 83
Electropherograms for the oxidation/reduction dual electrode detection of 10 μM dopamine and catechol. Experimental conditions: Background electrolyte: 20 mM TES, pH 7.0, 1100 V separation potential, 0.8 V detection potential at first working electrode (upstream, black), 0.2 V detection potential at second working electrode (downstream, red)

Figure 5.3: 84
Electropherograms for the oxidation/reduction dual electrode detection of 10 μM dopamine, catechol and ascorbic acid. Blue electropherogram shows an oxidation of the analytes at the first working electrode. Red electropherogram shows a reduction of the reversible species in the sample at the second working electrode. Experimental conditions: Same as figure 5.2

Figure 5.4: 86
Electropherograms for the increasing potential dual electrode detection of 10 μM L-arginine, tyrosine, dopamine, ascorbic acid and 20 μM catechol. Blue electropherogram shows the easily oxidized analytes in the sample mixture oxidizing at a low potential. The red electropherogram show a separation and detection of all of the compounds in the sample mixture when oxidized at a high detection potential. Experimental conditions: Background electrolyte: 20 mM boric acid, pH 9.4, 1100 V separation potential, 0.2 V detection potential at first working electrode (upstream, blue), 1.5 V detection potential at second working electrode (downstream, red)

Figure 6.1: **96**
Si 2p peak measured by XPS. The Si 2p peaks are fit with a SiO_2 peak (blue) and a siloxane peak (green). Samples were scanned at 30 min, 3 hours and 7days after they were prepared and stored in air. A) Native PDMS with no plasma treatment. B) A 48% increase in SiO_2 can be seen 30 min after a 2 min plasma treatment. C) Hydrophobic recovery after 3 hrs seen on native PDMS. D) Extracted PDMS with no plasma treatment. E) A 54% increase in SiO_2 can be seen 3 hrs after a 2 min plasma treatment. F) Only a 7% decrease in SiO_2 can be seen 7 days after oxidation. All samples were stored in air.

Figure 6.2: **98**
% SiO_2 on surface as a factor of time. ▨ Represents % SiO_2 on the day the PDMS was oxidized. ■ Represents the % SiO_2 on the 7^{th} day after oxidation. 2 min air plasma prior to sealing the chips was used for oxidation. Percentage determined by area under the SiO_2 peak divided by total area of the Si 2p peak.

Figure 6.3: **100**
Light microscopy of oxidized extracted PDMS for oxidation times of 0, 120, 600 and 1200 s. No cracking can be seen in the 0 and 120s times while an increased amount of surface cracking can be seen in the longer oxidation time.

Figure 6.4: **102**
Example electropherograms for the separation of 1 μM dopamine, catechol and ascorbic acid using A) Native; B) Extracted; C) Extracted-oxidized PDMS. Experimental conditions: Field strength: 170 V/cm; Pinched injection time: 10 s for native and extracted, 7 s for extracted-oxidized; BGE: 20 mM TES (pH 7.0)

Figure 6.5: **104**
Run to run reproducibility over a period of 4 hrs (40 runs). Migration time for catechol was measured over 40 runs without retreating the microchips with NaOH for native PDMS ■ and extracted-oxidized PDMS ●.

Figure 6.6: **106**
Electropherograms showing limits of detection for the three model analytes A) 25 nM ascorbic acid (S/N = 4.23); B) 2.5 nM catechol (S/N = 4.28); C) 600 pM dopamine (S/N = 3.67). Experimental conditions: same as figure 4.4

Figure 6.7: **108**
Example electropherogram for the separation of 1 mM doxorubicin and daunorubicin by microchip CE-PAD. PAD waveform: cleaning (1.6 V for 0.05 s), regeneration (-0.5 V for 0.025 s), detection (0.8 V for 0.15 s). Experimental conditions: Field strength: 200 V/cm; Pinched injection: 15 sec; BGE: 20 mM boric acid (pH 10.0)

Figure 7.1: **115**
Schematic of the TPE microchips (50 μm x 50 μm x 6 cm) showing the double-T injector (100 μm, 250 nL) and electrode alignment channels (decoupler 25 μm x 50 μm and working 50 μm x 50 μm). A 50 μm gap separates the decoupler channel from the

separation channel. To the right is a photograph showing the electrode alignment in a completed microchip.

Figure 7.2: **119**
Day-to-day EOF reproducibility of TPE microchips. EOF stability is shown for native TPE over an 18 day period (■) and for plasma treated TPE over an 11 day period (●). EOF was determined by the current monitoring method. Experimental conditions: Field strength: 200 V/cm; Background electrolytes: 20 mM phosphate (high ionic strength) and 18 mM phosphate (low ionic strength).

Figure 7.3: **121**
EOF measured for five microchips made at different times from different batches of TPE. Each chip was run multiple times are varying pHs (4, 7 and 10) to determine pH effects on reproducibility. Other experimental protocols as in Figure 7.2.

Figure 7.4: **123**
EOF values of native TPE (●) modified with a single layer of polybrene (anionic polyelectrolyte) (◄) and a double layer of dextran sulfate (cationic polyelectrolyte) (■) over a pH range from 3 to 10. Other experimental protocols as in Figure 7.2.

Figure 7.5: **125**
Example electropherograms for 1 μM dopamine, catechol and ascorbic acid on a TPE microchip (Top) and PDMS microchip (bottom). Experimental conditions: Field strengths: 300 V/cm and 200 V/cm for TPE and PDMS microchips respectively; pinched injection time: 15 s; Background Electrolyte: 20 mM TES (pH 7.0)

Figure 7.6: **126**
Separation efficiencies for 1 μM dopamine, catechol and ascorbic acid on identical TPE (left) and PDMS (right) microchips.

Figure 7.7: **127**
Separation of 1 μM dopamine, catechol and ascorbic acid on a TPE microchip as a function of separation potential. Optimized separation potential is determined to be 266 V/cm (1600V). Experimental conditions as in Figure 7.5.

Figure 7.8: **130**
Electropherogram for the separation of 100 μM homocysteine, glutathione and cysteine on a TPE microchip. Experimental conditions: Field strength: 233 V/cm; Pinched injection time: 15 s; Background electrolyte: 20 mM boric acid (pH 10.0)

Figure 8.1: **138**
Proteins hemoglobin, albumin and concanavalin A run using microchip MEKC-PAD. Experimental conditions: 20 mM boric acid, 0.4 mM DDM (pH 9.4), Detection potential +1.2 V.

Figure 8.2: **139**
A) Structure of sodium dodecyl sulfate (SDS) surfactant. B) Structure of N-Dodecyl-B-D-Maltoside (DDM) surfactant

Figure 8.3: **141**
A) HDV for 1 mg/ml hemoglobin. B) HDV for 1 mg/ml concanavalin A. C) HDV for 1 mg/ml myoglobin. D) HDV for 1 mg/ml human serum albumin. All proteins were prepared in run buffer (20 mM boric acid, 0.4 mM DDM (pH 9.4))

Figure 8.4: **142**
The total number of electrochemically active residues vs the electrochemical signal based on peak height. The left axis (red) and the red bar represent the electrochemical signal (peak height) for each of the proteins. The right axis (blue) and the blue bars show the number of specific electrochemically active amino acid residues in each protein. This was made to determine if there was any correlation between a specific type of amino acid and the electrochemical signal observed.

Figure 8.5: **144**
Percentage of amine, alcohol and thiol containing residues on hemoglobin, albumin, concanavalin A and myoglobin.

Figure 8.6: **145**
HDV for oxidized hemoglobin run through a Sephadex G-25 column. Optimal detection potentials around 0.1V and 1.4 V. Experimental conditions same as Figure 8.1.

Figure 8.7: **146**
HDV for reduced hemoglobin. Hemoglobin was reduced by running a Sephadex G-25 column with sodium hydrosulfite. Samples were then dialyzed to remove excess sodium hydrosulfite from solution. Experimental conditions were the same as Figure 8.1.

Table of Common Abbreviations

BGE:	Background electrolyte
CE:	Capillary electrophoresis
CE-EC:	Capillary electrophoresis with electrochemical detection
CE-PAD:	Capillary electrophoresis with pulsed amperometric detection
Con A:	Concanavalin A
CV:	Cyclic voltammetry
Daun:	Daunorubicin
DDM:	N-dodecyl-B-D-maltoside
Dox:	Doxorubicin
DS:	Dextran Sulfate
EC:	Electrochemical detection
EOF:	Electroosmotic flow
E-PDMS:	Extracted poly(dimethylsiloxane)
FITC:	Fluorescein-5-isothiocyanate
Hb:	Hemoglobin
HDV:	Hydrodynamic voltammogram
HSA:	Albumin

LIF:	Laser induced fluorescence
LOD:	Limit of detection
MCE:	Microchip capillary electrophoresis
MEKC:	Micellar electrokinetic chromatography
Mb:	Myoglobin
PAD:	Pulsed amperometric detection
PB:	Polybrene
PC:	Poly(carbonate)
PDMS:	Poly(dimethylsiloxane)
PEM:	Polyelectrolyte multilayer
PMMA:	Poly(methylmethacrylate)
RSD:	Relative standard deviation
SDS:	Sodium dodecyl sulfate
TPE:	Thermoset polyester
XPS:	X-ray photoelectron spectroscopy

Chapter 1

An Introduction to Microchip Capillary Electrophoresis Coupled to Electrochemical Detection

1.1 Capillary Electrophoresis

Capillary electrophoresis (CE) is a separation technique based on the electrophoretic mobility of an analyte in an open tubular capillary in the presence of an electric field. In the late 1970's / early 1980's Mikkers[1] and Jorgenson and Lukacs [2, 3] showed CE to be a viable analytical separation technique. CE demonstrated the ability to produce high resolution separations of both large and small molecules while using very small sample (nL injection volumes) and reagent volumes (μL).

1.1a Modes of CE

Today, CE encompasses a collection of separation techniques which involve the use of high voltages applied across buffer filled capillaries to achieve separation. The various modes of separation are as follows: Capillary zone electrophoresis (CZE) or free solution CE (separation based on the ratio of charge to hydrodynamic radius between analytes)[1-3] (Figure 1.1A), micellar electrokinetic chromatography or MEKC (separation of compounds based on partitioning into and out of surfactant based micelles)[4, 5] (Figure 1.1B), capillary gel electrophoresis or CGE (sieving of solutes through a gel matrix),[6, 7] capillary isoelectric focusing or CIEF (separation within a pH gradient based on pI),[8] and capillary electrochromatography or CEC (capillary packed with a chromatographic stationary phase where separation selectivity is a combination of both electrophoretic and chromatographic processes).[9] Most of these CE separation techniques rely on the presence of an electrically induced flow of solution (electroosmotic flow, EOF) within the capillary to drive solutes towards the detector. CZEs primary use is in the separation of small charged analytes, while MEKC has more benefits when looking at neutral

analytes or large compounds such as proteins. Schematic drawings showing representations of CZE and MEKC are provided in Figure 1.1 since these two methods were used in the following work.

1.1b Electroosmotic Flow

Electroosmotic flow is a bulk fluid flow process that greatly aids in CE separations. The walls of a capillary are ionized when brought into contact with a high pH electrolyte solution. This produces a negatively charged capillary wall. Cations from a background electrolyte are attracted to the negatively charged wall and form an electrical double layer.[10] A voltage is applied and the cations associated with the wall migrate towards the cathode pulling the associated background electrolyte (BGE) with them. This flow effectively pumps solute ions along the capillary toward the anode. If the surface charge of the capillary is reversed, anions associate with the channel wall and the resulting flow direction is reversed. The extent of the flow is related to the charge on the capillary, the buffer viscosity and dielectric constant of the buffer. The magnitude (μ_{eof}) of the EOF is given by equation 1.1 and the linear velocity (ν_{eof}) is described in equation 1.2.

$$\mu_{eof} = (\varepsilon \zeta / 4 \pi \eta r) \qquad \text{Eq 1.1}$$

Where: μ_{eof} = EOF mobility (rate of EOF), η = viscosity, ζ = zeta potential (charge on capillary surface), r = capillary radius

$$\nu_{eof} = \mu_{eof}(V/L) \qquad \text{Eq 1.2}$$

Where V is the applied voltage, and L is the capillary length.

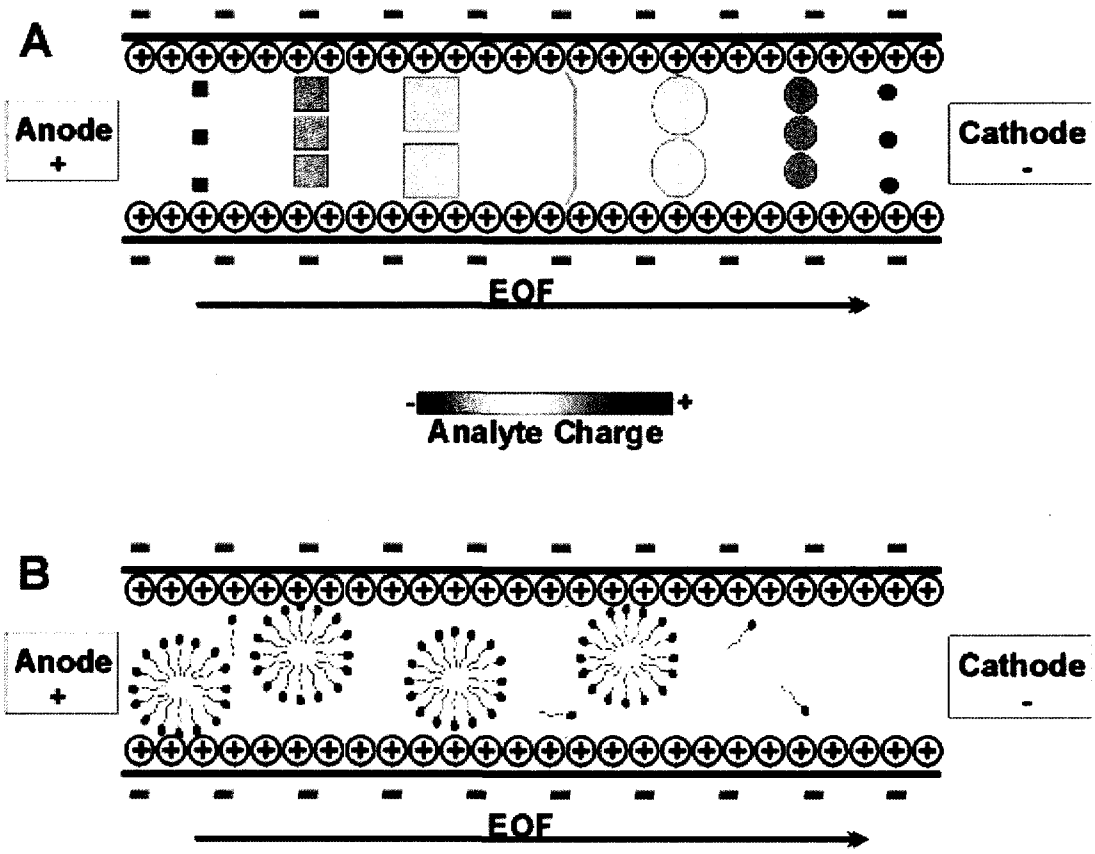

Figure 1.1: A) Capillary zone electrophoresis. Negatively charge capillary walls attract positive ions from the BGE. When a potential is applied across the capillary an electroosmotic flow is created causing flow through the capillary. Separation of analytes is based on charge to hydrodynamic radius with small highly positive ions (dark green) coming off first followed by larger less positive charged species (light green). Small highly negative charges come off last (dark red). Neutral analytes (yellow) travel with the EOF and are not separated. B) Micellar electrokinetic chromatography. Separation based on partitioning of analyte into and out of micelles.

The EOF is dependent upon BGE pH as the ζ is largely governed by the charge on the capillary wall. ζ is defined as the potential generated through electrostatics by the accumulation of ions at a surface arranged in an electrical double-layer.[2] Below pH 7, ζ is low and therefore EOF is small, while above pH 9, the capillary wall has a significant negative charge and the EOF is high. ζ is also affected as the ionic strength of the BGE changes. The EOF decreases as the BGE concentration increases because the zeta potential is reduced. The generation of flow at the capillary walls causes the flow profile of EOF to be plug-like, as shown in Figure 1.2, minimizing sample dispersion. [11] This plug-like flow is an advantage compared to the flow encountered in liquid chromatography (LC), which relies on high pressure pumps to induce flow and generates parabolic flow (Figure 1.2).

1.2 Microchip Capillary Electrophoresis

MCE has come about as an adaptation of conventional CE using microfabricated channels.[12] The driving forces behind this miniaturization include decreased sample volumes (from nL to pL), decreased analysis times (from min. to sec.) and the ability to incorporate multiple processes present in a conventional CE system onto a single device. Interest in these microanalytical devices has grown immensely recently and opened possibilities for the miniaturization of conventional chemical and biochemical analysis.[13-18] The ability to miniaturize analytical devices provides decreased analysis time (seconds scale), integration of sample processing, high portability, high throughput

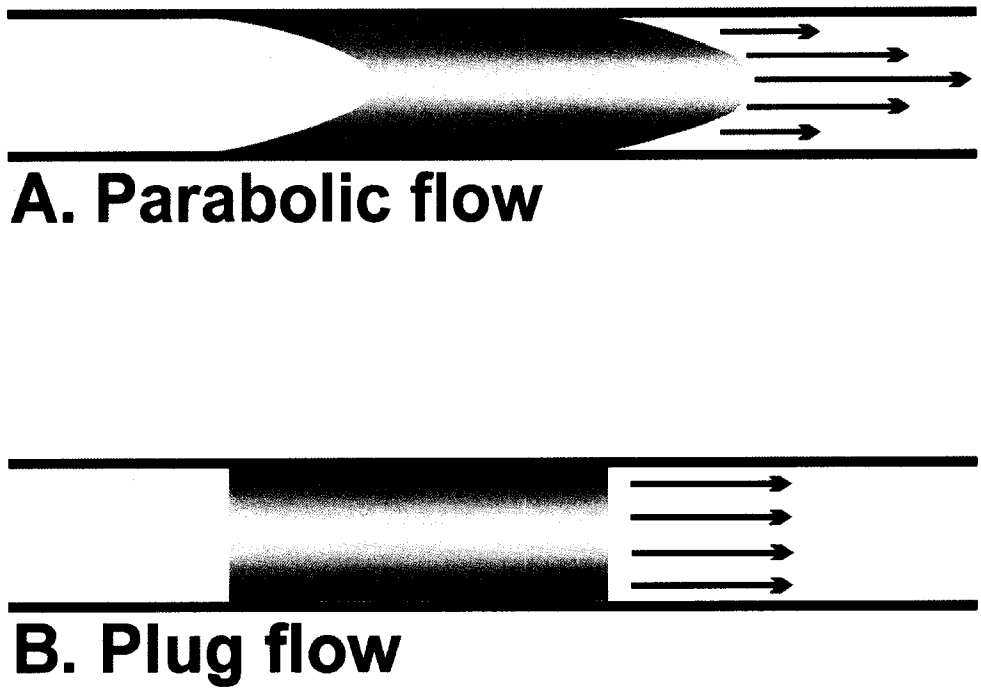

Figure 1.2: A) Pressure induced flow through a capillary. Friction at the walls causes a parabolic flow profile. B) Electrophoretic flow through a capillary. Flow induced at the walls of the capillary causing a plug like flow.

(hundreds of simultaneous runs), minimal reagent consumption (pL), and low cost (cents per chip).[19, 20] Two of the major limitations associated with MCE are the detection methods coupled to the microchip and the materials that the microchips are constructed from. This thesis focuses on the aspects needed to overcome these limitations.

1.3 MCE-EC

As the field of microfluidic devices continues to grow, there is an urgent need to develop suitable detection modes. Absorbance,[21, 22] mass spectrometry,[23, 24] laser-induced fluorescence (LIF),[25, 26] electrochemical techniques[27, 28] and other detection methods[29-32] have been coupled with MCE. Of these methods electrochemistry is arguably the most attractive for development of point of care devices.

Electrochemical detectors respond to substances that are either oxidizable or reducible and the electrical output results from an electron flow caused by the chemical reaction that takes place at the surface of the electrodes. The detector normally has three electrodes: the working electrode (where the oxidation or reduction takes place), the auxiliary electrode (supplies or accepts electrons to facilitate the oxidation or reduction) and the reference electrode (an electrode with a known half-cell potential that is not affected by the solution being studied, that the working electrode response is referenced to). Electrochemical detection (EC) instrumentation is attractive because it is less expensive and less complex than optical detection systems such as LIF [25, 26] and mass spectrometry [23, 33] while still offering comparable mass sensitivity levels. The most common EC detection technique is amperometry. In amperometry, a constant potential is applied to a working electrode and the analyte is oxidized or reduced and the current

measured (Figure 1.3A). Many compounds are electrochemically active,[19] but only a few of these analytes are easily detected with dc amperometry because of electrode fouling.[34, 35] Carbohydrates,[35] thiols, and phenols [34] are among the more common analytes that cause electrode fouling. To overcome this problem a potential waveform known as pulsed amperometric detection (PAD) can be applied[36-39] (Figure 1.3B). In PAD, a high positive potential is first applied to oxidize and clean the surface of a noble metal electrode (Pt or Au). Next, a negative potential step is applied to reduce and reactivate the electrode surface. A third potential is applied for detection. A typical PAD waveform is 250-300 ms and detection potential can be set to control selectivity. PAD has been shown to be useful for the detection of carbohydrates, amino acids, thiols, and alcohols when coupled to conventional CE and LC,[40-45] all of which are important in biological processes.[26, 46, 47]

The interest in MCE-EC has grown because the fabrication methods for both the microchips and the electrodes are similar. Although microfabricated electrodes have become widely used,[48-50] they have several disadvantages. First, the microfabrication process requires a clean-room facility, which increases the microchip cost. Second, the lifetime of a microfabricated electrode can be affected by the BGE and other experimental conditions.[51] Once the electrode fouls, a new chip must be made, which further increases the cost of the analysis. Microfabricated electrodes can also delaminate as a result of their use and/or cleaning. Finally, the alignment of the electrode is a significant concern when irreversible sealing is used for the assembly of the microchip.[52]

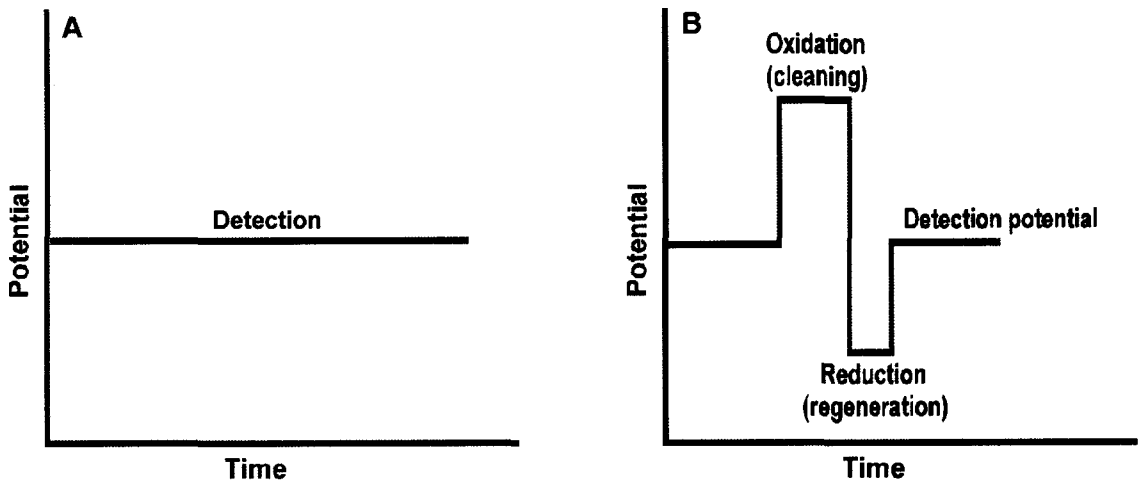

Figure 1.3: Electrochemical detection techniques: A) Amperometric detection, a constant potential is applied to the working electrode to oxidize or reduce the analytes of interest and B) Pulsed amperometric detection (PAD), a potential waveform is applied to the working electrode. An oxidative cleaning potential (high positive) is followed by a reductive regeneration potential (negative) to clean the working electrode before a detection potential is applied to oxidize or reduce the analyte of interest.

In an effort to develop a more versatile electrode system, end-channel working electrodes have been used. End-channel detection refers to the system where the detection electrode is placed just outside of the separation channel and is separate from the microchip.[53] Figure 1.4 shows a visual representation of multiple electrode alignment techniques. The systems are generally easier to construct than microfabricated systems. The coupling of end-channel electrodes with a MCE device, however, creates complications in obtaining precision spacing between the separation channel exit and the working electrode.[54] For instance, if the detection surface of the working electrode and the side of the microchip are not exactly parallel to one another, the working electrode collides with the edge of the microchip as it is moved toward the channel exit, preventing optimal alignment. If the gap between the separation channel exit and the working electrode is too large, the sample plug diffuses into the detection reservoir before the analyte can be detected. This diffusion results in a loss in peak efficiency and intensity. Finally, end-channel electrodes require an alignment device which reduces portability and increases the cost and complexity.

A new approach to the integration of electrodes in MCE-EC devices was presented by Martin et al.[55] Their system placed the working electrode directly in the separation channel. The results showed that aligning the electrode directly in the separation channel leads to a vast improvement in the performance of EC detection for MCE compared to the commonly used end-channel alignment even without use of

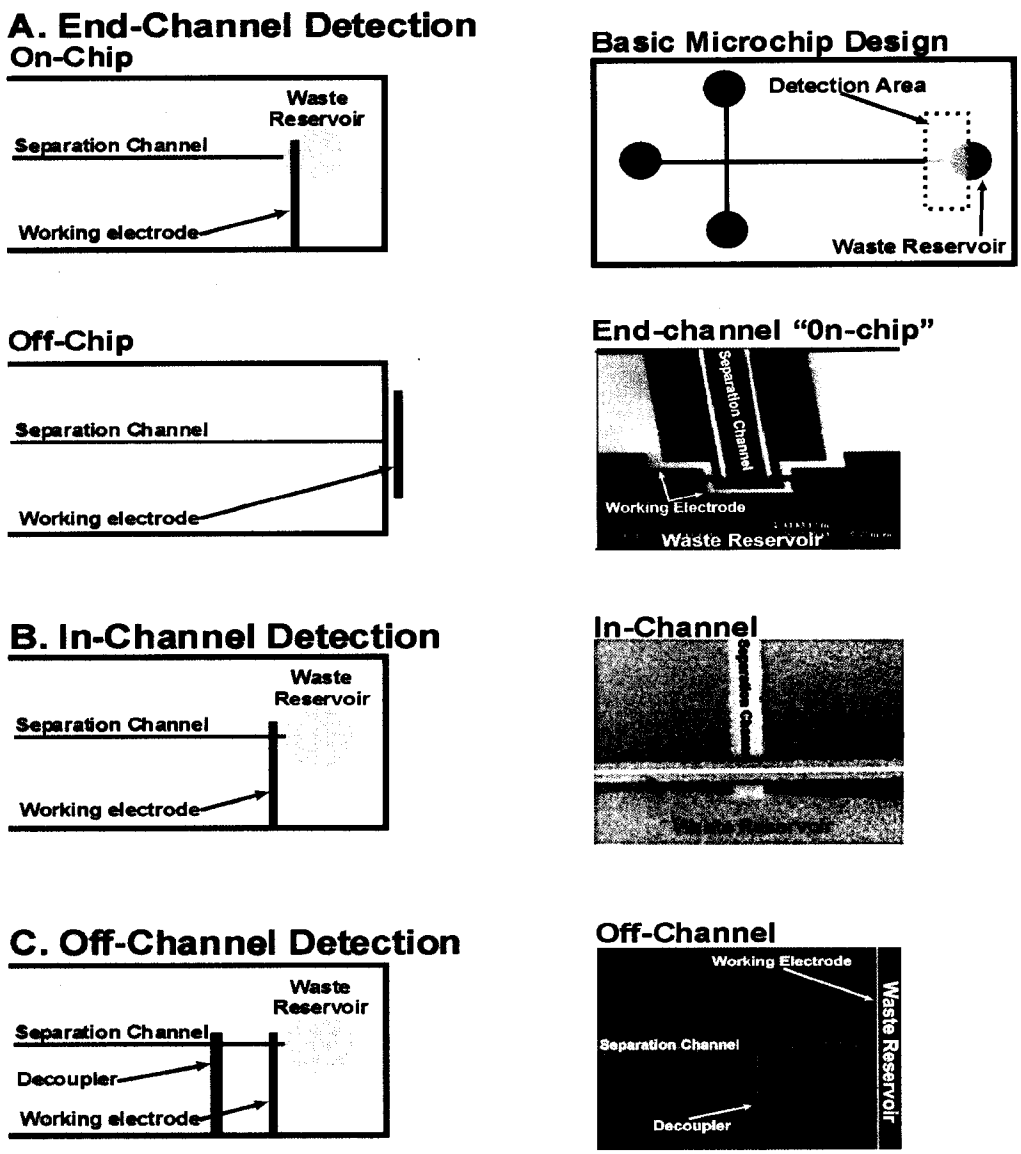

Figure 1.4: Electrode alignment techniques. A, B) End channel detection, the working electrode is aligned outside of the separation channel, either on or off chip. C) In channel detection, the working electrode is aligned in the separation channel. D) Off channel detection, the working electrode is aligned in the separation channel but outside of the separation potential. This is usually done through the incorporation of a current decoupler.

decoupler.[55] However, the system required an electrically isolated potentiostat making the instrumentation complex.[56]

A simple design using microwires as in-channel working electrodes for MCE-EC has been shown to alleviate many of the problems associated with more traditional thin film electrodes and is the focus of this thesis.[38, 57, 58] The microwire is aligned across the separation capillary using a channel patterned in the PDMS. The method provides excellent chip-to-chip reproducibility of the working electrode location. Furthermore, because the microwire has a larger surface area exposed to flow than conventional approaches, higher collection efficiencies can be achieved.

1.4 Current Decoupler

A current decoupler (decoupler) is used to isolate the separation potential/current from the detection current, eliminating noise in the system (Figure 1.5). The most commonly used material for this type of decoupler is palladium.[59, 60] Briefly, during electrophoretic separation, the high electric field seen in these microchips is sufficient for the electrolysis of water (see equation 1.3).

One of the most commonly used microchip decouplers is a thin film electrode that spans the separation channel upstream from the detection electrode.[59, 61, 62] The problem with thin film decouplers is the same as the thin film working electrodes discussed above. The fabrication of the electrode and alignment in the channel has been shown to be a tedious and irreproducible process.[26-29] Applications and rationale for the use of the Pd-metal decoupler have been shown by Kok and Sahin.[63]

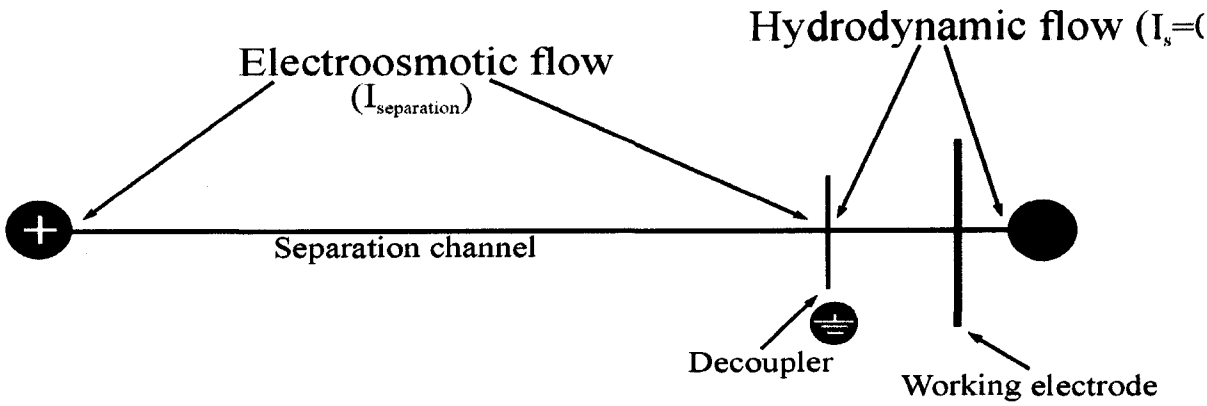

Figure 1.5: Current decoupler is placed in the separation channel upstream from the working electrode allowing the separation current to be grounded and isolated from the detection potential. This allows for the benefits of both end and in-channel detection to be exploited. Electroosmotic flow is seen upstream from the decoupler while hydrodynamic flow is seen downstream from the decoupler and around the working electrode.

$$\text{Anode(+)} \qquad 2H_2O \rightarrow O_2 + 4H^+ + 4e^- \qquad \text{Eq 1.3}$$

$$\text{Cathode(-)} \qquad 4H_2O + 4e^- \rightarrow 2H_2 + 4OH^-$$

This electrolysis causes H_2 gas evolution at the cathode which interferes with the separation as well as the electrochemical signal.[64] When H_2 bubbles fill the separation channel, EOF is lost due the removal of the electric field in the channel. Palladium decouplers absorb and pass hydrogen. This unique property is due to hydrogen gas being absorbed and quickly dissipated through the Pd and away from the BGE before bubbles can form.[63] The decoupler allows for a working electrode to be placed across the separation channel without the worry of hydrogen bubble formation. Without the decoupler in place, the working electrode acts as a pseudo ground for the separation potential and generate H_2 bubbles at the electrode. In an end channel configuration the working electrode is placed at the end of the separation channel directly in the waste reservoir. The placement of the working electrode here removes it from the separation field and in turn does not allow it to generate bubbles. With a decoupler, the alignment between the working electrode and the waste reservoir as seen in end-channel electrodes is no longer a major concern due to the elimination of the hydrogen bubbles at the working electrode by the decoupler. [59]

1.5 Materials for MCE

1.5a Glass Microchips

The first CE microchips were made from glass.[18] Glass provided an attractive initial material because the fabrication techniques were well established, the surface chemistry was similar to fused silica used with traditional CE, and the substrates had excellent optical clarity. Glass, however, is relatively difficult and expensive to micromachine, requiring expensive cleanroom time and corrosive etchants (hydrofluoric acid, HF). Thermal bonding, which is typically used in the fabrication of glass microchips, is also considered time consuming. The geometry (depth and width) of channels fabricated in glass is also limited by the etching technique used during fabrication. Finally, optical quality glass is expensive relative to many other materials that can be used for microfluidics and MCE.[65]

1.5b Polymer Microchips

As a result of the amount of time and high cost of fabricating glass chips there has been significant interest in the development and use of polymers as substrates for MCE.[66-68] Numerous polymers have been used as substrate materials, including poly(methylmethacrylate) (PMMA), [69-72] poly(carbonate) (PC),[73, 74] polyester,[75] thermoset polyester (TPE)[76, 77] and poly(dimethylsiloxane) (PDMS).[17, 78] A benefit of most polymeric devices is that they can be fabricated outside a cleanroom environment. A range of fabrication methods can be applied to polymers, including soft lithography,[79] casting,[17] laser ablation,[80] injection molding [81] and hot embossing.[69] Of the polymeric materials used, PDMS is the most popular because it is inexpensive, has good optical clarity and is elastomeric, giving it the ability to be used in active valving strategies.[82]

Polymers are not without disadvantages, particularly for separation-based applications. Polymer-based devices generally give lower separation efficiencies than glass, with PDMS being the most egregious offender.[83] The poor separation performance for PDMS is the result of the hydrophobicity of the bulk material and the ability of low molecular weight, non-cross-linked, oligomers to rapidly diffuse to the surface (< 30 min.), commonly termed hydrophobic recovery.[84-86] The result is an unstable hydrophobic material with a heterogeneous surface chemistry. Despite these limitations, PDMS remains an attractive material for MCE and microfluidics due to its ease of fabrication and low cost. A number of research groups have sought to overcome the problems of PDMS through careful control of the surface and/or bulk chemistry.[87-90] Whitesides' group was the first to address the problem in MCE by oxidizing the material in a simple oxygen plasma.[87] The treatment, however, was unstable due to hydrophobic recovery.[84-86] More sophisticated methods for surface modification of PDMS have followed with impressive results. Wirth's group used atom-transfer radical polymerization to coat the microchip surface with polyacrylamide.[90] The method generated high efficiency separations (> 33,000 N/m) for protein mixtures.[90] Allbritton's group demonstrated an alternative surface grafting approach.[91, 92] Surfaces were functionalized with acrylic acid, acrylamide, and poly(ethylene glycol) chemistries and showed a significant improvement in separation efficiency and contact angle relative to native PDMS. The Culbertson group recently published two methods for improving the separation efficiency of PDMS microchips.[89, 93] One method made use of a special micellar buffer that resulted in separations with theoretical plates over $1x10^6$ plates/m.[93] In this work, the surfactant (sodium dodecyl sulfate) played an important role in reducing absorption of hydrophobic

compounds while also increasing EOF. In a second approach, the same group reported the development of a novel sol-gel coating inside PDMS microchannels.[89, 93] The coatings improved separation efficiency while also providing the ability to control the surface chemistry by varying the sol composition. While all of these methods improve the performance of PDMS, none of them has been widely adopted because of either a limited set of surface chemistries or the apparent complexity of the treatment process. One aspect of this thesis focuses on modifying PDMS to address these limitations.

The introduction of thermoset polyester (TPE) as an alternative microchip material has shown promise as a merger between the ease of fabrication and cost effectiveness of PDMS with the higher separation efficiencies (~100,000 N/m for neutral compounds) and increased stability of PMMA and PC.[77] The process of fabricating TPE as a microfluidic device has been described previously by Fiorini et al.[76, 77] With fabrication techniques similar to PDMS, little to no modification to existing soft lithography techniques are needed.[38, 58]

1.6 Important Electrochemically Active Analytes

1.6a Catecholamines

Catecholamines are a group of compounds with active roles in the sympathetic and parasympathetic nervous systems.[94] Their chemical makeup is derived from tyrosine and secreted by the adrenal glands in the body. Catecholamines can act as hormones or neurotransmitters and are examples of phenethylamines. Important phenethylamines include epinephrine (adrenaline), norepinephrine and dopamine (Figure 1.6). Each

phenethylene consists of a benzene ring with two ortho hydroxyl groups and an ethylamine side chain. The production and regulation of these compounds has a profound effect on the nervous system, cardiovascular system, metabolic rate and body temperature. Dopamine and catechol also serve as standards for the development of new electrochemical detection methods when coupled with separation techniques. In this thesis dopamine and catechol will be used as model analytes in DC amperometry experiments.

1.6b Carbohydrates

Carbohydrates are the most abundant organic molecules in nature and are used in a wide variety of biological processes.[95] One function of carbohydrates in the body is to produce energy. As carbohydrates are introduced into metabolic pathways such as glycolysis they are broken down and in turn produce energy the body needs. A second function of carbohydrates is as a structural element of proteins. Glycoproteins and peptides are of great interest to many scientists for their roles in the body. Certain glycoproteins have been shown to be biomarkers for various diseases. For example glycated hemoglobin is a good indicator for how well a diabetic patient has controlled their glucose levels over a 3 month period. The ability to detect carbohydrates, whether they are small molecules or a component of large proteins, without a need for derivatization and at biological concentrations is a useful tool in monitoring a person's

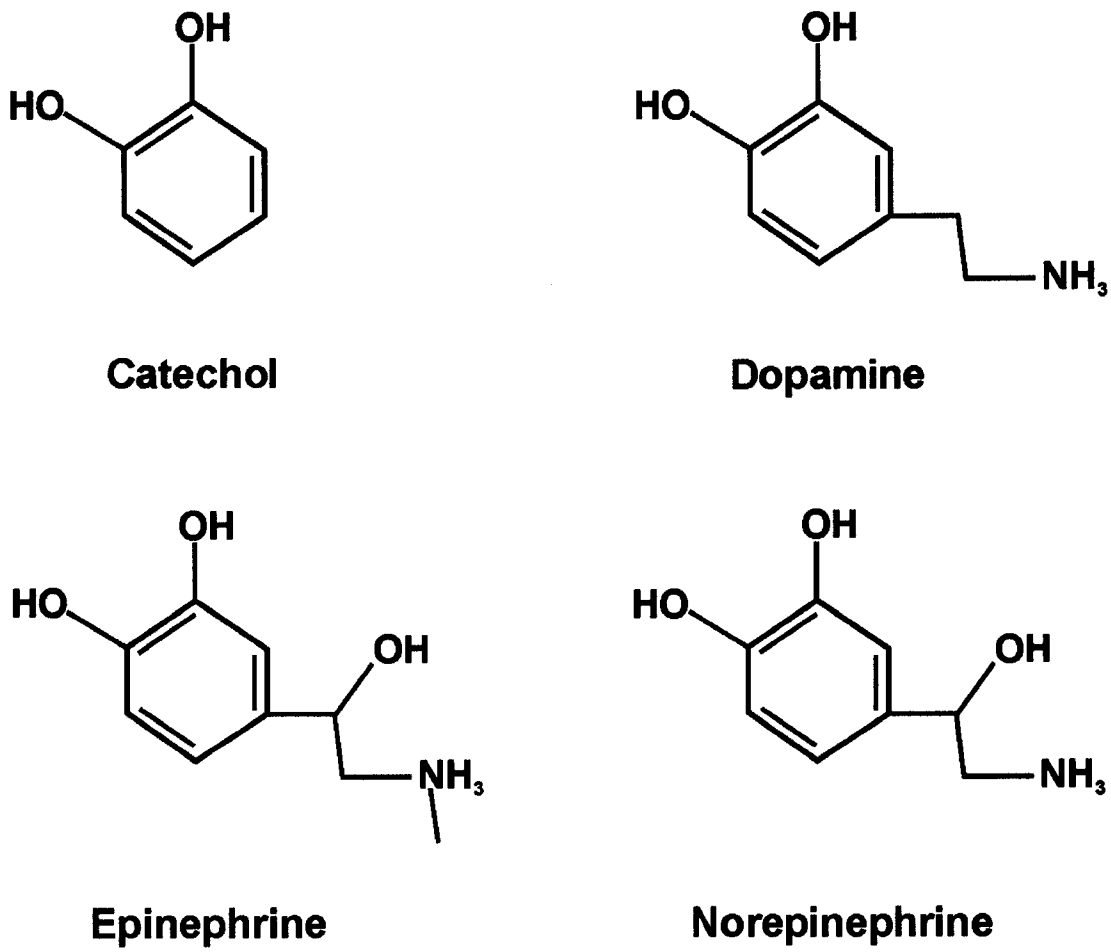

Figure 1.6: Important electrochemically active catecholamines. Catechol is the building block behind all catecholamines. Dopamine, epinephrine (adrenaline) and norepinephrine (noradrenaline) are important for their effects on the nervous system, cardiovascular system, metabolic rate and control of body temperature.

health. Simple carbohydrates such as glucose will be used in my research to demonstrate the functionality of PAD.

1.6c Thiols

Thiol containing compounds are known to play a multitude of roles within physiological systems. As we learn more about their significance, attention is drawn to a specific group of thiols, the sulfhydryl thiols (R-SH).[96, 97] Attention to sulfhydryls has come about because of the association of these compounds with oxidative damage and stress in the body. Information on specific sulfhydryls/thiols can provide scientists with a versatile diagnostic handle through which the pathology of a variety of conditions can be indirectly monitored. Among the major targets of interest are cysteine, glutathione and homocysteine (Figure 1.7). Cysteine and glutathione depletion in the body is believed by some to accompany many diseases such as leukemia, cervical cancer, diabetes as well as others.[98-100] An increase in these thiols has been found to be present in patients with Alzheimer's, Parkinson's and stroke victims.[101] Elevated levels of homocysteine have been proposed as a biomarker for cardiovascular disease.[102-104] Whether measuring elevated or depleted levels, these electrochemically active analytes will be important in the diagnosis of diseases. Here thiols will be used to demonstrate the use of PAD coupled to MCE.

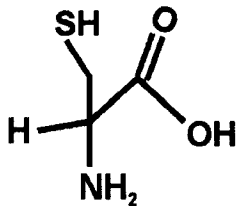

Cysteine

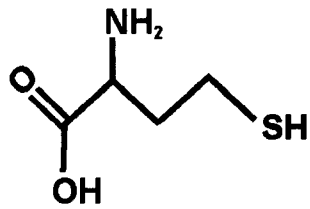

Homocysteine

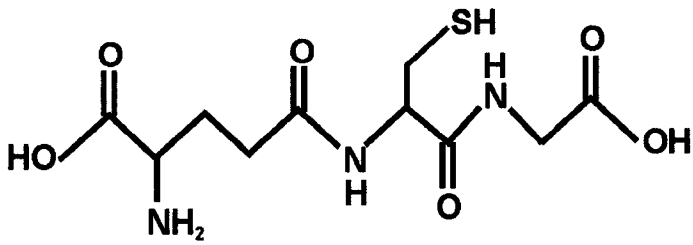

Glutathione

Figure 1.7: Biologically important thiols. Cysteine and the ratio of oxidized to reduced glutathione are important because of their role in the regulation of oxidative damage within the body. Homocysteine has shown to be an important biomarker in the diagnosis of cardiovascular disease.

1.6d Proteins

Proteins serve many biological functions. Some of these functions include transport, structural, storage and receptors. Enzymatic proteins are probably the most varied and most highly specialized proteins and virtually all the chemical reactions of organic biomolecules in cells are catalyzed by enzymes. Transport proteins act as carriers for other substances in the body. For example, hemoglobin, an iron-containing protein of blood, transports oxygen from the lungs to other parts of the body. Other proteins transport molecules across cell membranes. Structural proteins are very important for providing physical support. Collagen provides a fibrous framework in animal connective tissues, such as tendons and ligaments. Other proteins provide structure to things such as hair, horns and feathers. Storage proteins store chemicals such as amino acids and lipids. Ovalbumin is a protein found in egg whites and is used as an amino acid source for the developing embryo. Casein, the protein of milk, is a major source of amino acids for babies. Receptor proteins make up the major signaling molecules in biological membranes. In nerve cell membranes they are used to detect chemical signals released by other nerve cells. Proteins have many functions and the ability to measure proteins could lead to the ability to diagnoses or monitor diseases such as cardiovascular disease, diabetes or Alzheimer's. A detection of specific proteins will be shown in this thesis to demonstrate the ability of our MCE-PAD devices in the detection of proteins.

1.6e Summary

When looking at some of the important electrochemically active analytes and their functions within the body, it is evident that new chemistry is needed for rapid,

sensitive and selective detection of analytes and its correlation to a disease of interest. In this thesis I demonstrate a method for the rapid separation (second scale) and sensitive/selective detection of many of these electrochemically active compounds using MCE.

1.7 Research Goals

The overall goal of this research has been the development of MCE-EC devices for the rapid separation and sensitive detection of specific compounds from biological samples. The first milestone toward reaching the overall goal of this project was to improve the sensitivity and selectivity of these microchips. The development of MCE with a microwire electrochemical working electrode design will be discussed as a solution to this problem. The use of various electrode materials, types, sizes and the incorporation of multiple electrochemical detection techniques provides an improvement in the ability to use MCE-EC. The second millstone was to improve separation efficiencies of PDMS microchips in order to better separate complex samples. Vast improvements in separation efficiencies and peak skew were achieved through the use of alternative materials used for the construction of our microchips. The third and final millstone of this project was to incorporate the improvements in detection from millstone one and improvements in separation from millstone two for the analysis of proteins in a biological sample. This is accomplished through the detection of hemoglobin from human red blood cell lysate.

(1) Mikkers, F. E. P.; Everaerts, F. M.; Verheggen, T. P. E. M. *J Chrom* **1979**, *169*, 11-20.
(2) Jorgenson, J. W.; Lukacs, K. D. *Clin Chem* **1981**, *27*, 1551-1553.
(3) Jorgenson, J. W.; Lukacs, K. D. *Anal Chem* **1981**, *53*, 1298-1302.
(4) Terabe, S.; Otsuka, K.; Ando, T. *Anal Chem* **1985**, *57*, 834-841.
(5) Terabe, S.; Otsuka, K.; Ichikawa, K.; Tsuchiya, A.; Ando, T. *Anal Chem* **1984**, *56*, 111-113.
(6) Cohen, A. S.; Najarian, D. R.; Karger, B. L. *J Chrom* **1990**, *516*, 49-60.
(7) Garcia-Canas, V.; Gonzalez, R.; Cifuentes, A. *J Sep Sci* **2002**, *25*, 577-583.
(8) Hjerten, S.; Zhu, M. D. *J Chrom* **1985**, *346*, 265-270.
(9) Chee, G. L.; Wan, T. S. M. *J Chrom-Biomed App* **1993**, *612*, 172-177.
(10) Jorgenson, J. W.; Lukacs, K. D. *Science* **1983**, *222*, 266-272.
(11) Hayes, M. A.; Kheterpal, I.; Ewing, A. G. *Anal Chem* **1993**, *65*, 27-31.
(12) Harrison, D. J.; Manz, A.; Fan, Z.; Luedi, H.; Widmer, H. M. *Anal Chem* **1992**, *64*, 1926-1932.
(13) Beard, N. P.; Zhang, C. X.; DeMello, A. J. *Electrophoresis* **2003**, *24*, 732-739.
(14) Breadmore, M. C.; Wolfe, K. A.; Arcibal, I. G.; Leung, W. K.; Dickson, D.; Giordano, B. C.; Power, M. E.; Ferrance, J. P.; Feldman, S. H.; Norris, P. M.; Landers, J. P. *Anal Chem* **2003**, *75*, 1880-1886.
(15) Ceriotti, L.; Shibata, T.; Folmer, B.; Weiller, B. H.; Roberts, M. A.; de Rooij, N. F.; Verpoorte, E. *Electrophoresis* **2002**, *23*, 3615-3622.
(16) Chen, Y. H.; Wang, W. C.; Young, K. C.; Chang, T. T.; Chen, S. H. *Clin Chem* **1999**, *45*, 1938-1943.
(17) Effenhauser, C. S.; Bruin, G. J. M.; Paulus, A.; Ehrat, M. *Anal Chem* **1997**, *69*, 3451-3457.
(18) Manz, A.; Harrison, D. J.; Verpoorte, E. M. J.; Fettinger, J. C.; Paulus, A.; Luedi, H.; Widmer, H. M. *J Chrom* **1992**, *593*, 253-258.
(19) Vandaveer, W. R. I. V.; Pasas, S. A.; Martin, R. S.; Lunte, S. M. *Electrophoresis* **2002**, *23*, 3667-3677.
(20) Vilkner, T.; Janasek, D.; Manz, A. *Anal Chem* **2004**, *76*, 3373-3385.
(21) Liang, Z.; Chiem, N.; Ocvirk, G.; Tang, T.; Fluri, K.; Harrison, D. J. *Anal Chem* **1996**, *68*, 1040-1046.
(22) Salimi-Moosavi, H.; Jiang, Y.; Lester, L.; McKinnon, G.; Harrison, D. J. *Electrophoresis* **2000**, *21*, 1291-1299.
(23) Xue, Q.; Foret, F.; Dunayevskiy, Y. M.; Zavracky, P. M.; McGruer, N. E.; Karger, B. L. *Anal Chem* **1997**, *69*, 426-430.
(24) Ramsey, R. S.; Ramsey, J. M. *Anal Chem* **1997**, *69*, 2617.
(25) Jacobson, S. C.; Ramsey, J. M. *Electrophoresis* **1995**, *16*, 481-486.
(26) Jakeway, S. C.; de Mello, A. J.; Russell, E. L. *Fresenius' J Anal Chem* **2000**, *366*, 525-539.
(27) Mayrhofer, K.; Zemann, A. J.; Schnell, E.; Bonn, G. K. *Anal Chem* **1999**, *71*, 3828-3833.
(28) Wang, J.; Polsky, R.; Tian, B.; Chatrathi, M. P. *Anal Chem* **2000**, *72*, 5285-5289.
(29) Ocvirk, G.; Tang, T.; Jed Harrison, D. *Analyst* **1998**, *123*, 1429-1434.

(30) Burggraf, N.; Krattiger, B.; de Rooij, N. F.; Manz, A.; de Mello, A. J. *Analyst* **1998**, *123*, 1443-1447.
(31) Walker, P. A., 3rd; Morris, M. D.; Burns, M. A.; Johnson, B. N. *Anal Chem* **1998**, *70*, 3766-3769.
(32) Hashimoto, M.; Tsukagoshi, K.; Nakajima, R.; Kondo, K.; Arai, A. *J Chrom A* **2000**, *867*, 271-279.
(33) Ramsey, R. S.; McLuckey, S. A. *J Microc Sep* **1997**, *9*, 523-528.
(34) Garcia, C. D. O., P.I. *Electroanalysis* **2000**, *12*, 1074-1076.
(35) Hughes, S., Johnson, D.C. *Anal. Chim. Acta* **1981**, *132*, 11-22.
(36) Owens, G. S.; LaCourse, W. R. *J Chrom, B: Biomed Sci App* **1997**, *695*, 15-25.
(37) Hompesch, R. W.; Garcia, C. D.; Weiss, D. J.; Vivanco, J. M.; Henry, C. S. *Analyst* **2005**, *130*, 694-700.
(38) Garcia, C. D.; Henry, C. S. *Anal Chem* **2003**, *75*, 4778-4783.
(39) Garcia, C. D.; Henry, C. S. *Anal Chim Acta* **2004**, *508*, 1-9.
(40) Zhong, M.; Lunte, S. M. *Anal Chem* **1996**, *68*, 2488-2493.
(41) Weber, P. L.; Lunte, S. M. *Electrophoresis* **1996**, *17*, 302-309.
(42) Oshea, T. J.; Lunte, S. M.; Lacourse, W. R. *Anal Chem* **1993**, *65*, 948-951.
(43) Lacourse, W. R.; Johnson, D. C. *Anal Chem* **1993**, *65*, 50-55.
(44) LaCourse, W. R.; Johnson, D. C. *Carbohydrate Research* **1991**, *215*, 159-178.
(45) LaCourse, W. R.; Mead, D. A., Jr.; Johnson, D. C. *Anal Chem* **1990**, *62*, 220-224.
(46) Thormann, W.; Wey, A. B.; Lurie, I. S.; Gerber, H.; Byland, C.; Malik, N.; Hochmeister, M.; Gehrig, C. *Electrophoresis* **1999**, *20*, 3203-3236.
(47) Hutterer, K.; Dolnik, V. *Electrophoresis* **2003**, *24*, 3998-4012.
(48) Wang, J.; Pumera, M.; Chatrathi, M. P.; Rodriguez, A.; Spillman, S.; Martin, R. S.; Lunte, S. M. *Electroanalysis* **2002**, *14*, 1251-1255.
(49) Woolley, A. T.; Lao, K.; Glazer, A. N.; Mathies, R. A. *Anal Chem* **1998**, *70*, 684-688.
(50) Martin, R. S.; Gawron, A. J.; Lunte, S. M.; Henry, C. S. *Anal Chem* **2000**, *72*, 3196-3202.
(51) Lunte, S. M.; Martin, R. S.; Lunte, C. E. *Electroanal Methods Biol Mat* **2002**, 461-490.
(52) Holland, L. A.; Lunte, S. M. *Anal Comm* **1998**, *35*, 1H-4H.
(53) Lacher, N. A.; Garrison, K. E.; Martin, R. S.; Lunte, S. M. *Electrophoresis* **2001**, *22*, 2526-2536.
(54) Fanguy, J. C.; Henry, C. S. *Electrophoresis* **2002**, *23*, 767-773.
(55) Martin, R. S.; Ratzlaff, K. L.; Huynh, B. H.; Lunte, S. M. *Anal Chem* **2002**, *74*, 1136-1143.
(56) Vandaveer, W. R. I. V.; Pasas-Farmer, S. A.; Fischer, D. J.; Frankenfeld, C. N.; Lunte, S. M. *Electrophoresis* **2004**, *25*, 3528-3549.
(57) Liu, Y.; Vickers, J. A.; Henry, C. S. *Anal Chem* **2004**, *76*, 1513-1517.
(58) Vickers, J. A.; Henry, C. S. *Electrophoresis* **2005**, *26*, 4641-4647.
(59) Chen, D. C.; Hsu, F. L.; Zhan, D. Z.; Chen, C. H. *Anal Chem* **2001**, *73*, 758-762.
(60) Wu, C. C.; Wu, R. G.; Huang, J. G.; Lin, Y. C.; Hsien-Chang, C. *Anal Chem* **2003**, *75*, 947-952.
(61) Osbourn, D. M.; Lunte, C. E. *Anal Chem* **2001**, *73*, 5961-5964.
(62) Osbourn, D. M.; Lunte, C. E. *Anal Chem* **2003**, *75*, 2710-2714.

(63) Kok, W. T., Sahin, Yuksel *Anal Chem* **1993**, *65*, 2497.
(64) Slater, J. M.; Watt, E. J. *Analyst* **1994**, *119*, 2303-2307.
(65) Vickers, J. A.; Caulum, M. M.; Henry, C. S. *Anal Chem* **2006**, *78*, 7446-7452.
(66) Belder, D.; Ludwig, M. *Electrophoresis* **2003**, *24*, 3595-3606.
(67) Dolnik, V. *Electrophoresis* **2004**, *25*, 3589-3601.
(68) Soper, S. A.; Ford, S. M.; Qi, S.; McCarley, R. L.; Kelly, K.; Murphy, M. C. *Anal Chem* **2000**, *72*, 545A.
(69) Martynova, L.; Locascio, L. E.; Gaitan, M.; Kramer, G. W.; Christensen, R. G.; MacCrehan, W. A. *Anal Chem* **1997**, *69*, 4783-4789.
(70) Soper, S. A.; Ford, S. M.; Xu, Y.; Qi, S.; McWhorter, S.; Lassiter, S.; Patterson, D.; Bruch, R. C. *J Chrom A* **1999**, *853*, 107-120.
(71) Kelly, R. T.; Woolley, A. T. *Anal Chem* **2003**, *75*, 1941-1945.
(72) Jikun Liu, T. P.; Woolley, A. T.; Lee, M. L. *Anal Chem* **2004**, *76*, 6948-6955.
(73) Liu, Y.; Ganser, D.; Schneider, A.; Liu, R.; Grodzinski, P.; Kroutchinina, N. *Anal Chem* **2001**, *73*, 4196-4201.
(74) Wen, J.; Lin, Y.; Xiang, F.; Matson, D. W.; Udseth, H. R.; Smith, R. D. *Electrophoresis* **2000**, *21*, 191-197.
(75) Uchiyama, K.; Xu, W.; Qiu, J.; Hobo, T. *Fresenius J Anal Chem* **2001**, *371*, 209-211.
(76) Fiorini, G. S.; Jeffries, G. D. M.; Lim, D. S. W.; Kuyper, C. L.; Chiu, D. T. *Lab Chip* **2003**, *3*, 158-163.
(77) Fiorini, G. S.; Lorenz, R. M.; Kuo, J. S.; Chiu, D. T. *Anal Chem* **2004**, *76*, 4697-4704.
(78) Fogarty, B. A.; Heppert, K. E.; Cory, T. J.; Hulbutta, K. R.; Martin, R. S.; Lunte, S. M. *Analyst* **2005**, *130*, 924-930.
(79) McDonald, J. C.; Duffy, D. C.; Anderson, J. R.; Chiu, D. T.; Wu, H.; Schueller, O. J.; Whitesides, G. M. *Electrophoresis* **2000**, *21*, 27-40.
(80) Roberts, M. A. *Anal Chem* **1997**, *69*, 2035-2042.
(81) McCormick, R. M., Nelson, R.J., Alonso-Amigo, M.G., Benvegnu, J., Hoopwer, H.H. *Anal Chem* **1997**, *69*, 2626-2630.
(82) McDonald, J. C.; Whitesides, G. M. *Acc Chem Res* **2002**, *35*, 491-499.
(83) Lacher, N. A.; de Rooij, N. F.; Verpoorte, E.; Lunte, S. M. *J Chrom A* **2003**, *1004*, 225-235.
(84) Fritz, J. L.; Owen, M. J. *J Adhesion* **1995**, *54*, 33-45.
(85) Kim, J.; Chaudhury, M. K.; Owen, M. J. *J Colloid Interface Sci* **2000**, *226*, 231-236.
(86) Kim, J.; Chaudhury, M. K.; Owen, M. J.; Orbeck, T. *J Colloid Interface Sci* **2001**, *244*, 200-207.
(87) Duffy, D. C.; McDonald, J. C.; Schueller, O. J. A.; Whitesides, G. M. *Anal Chem* **1998**, *70*, 4974-4984.
(88) Hu, S. *Electrophoresis* **2003**, *24*, 3679-3688.
(89) Roman, G. T.; Hlaus, T.; Bass, K. J.; Seelhammer, T. G.; Culbertson, C. T. *Anal Chem* **2005**, *77*, 1414-1422.
(90) Xiao, D.; Le, T. V.; Wirth, M. J. *Anal Chem* **2004**, *76*, 2055-2061.
(91) Hu, S. W.; Ren, X. Q.; Bachman, M.; Sims, C. E.; Li, G. P.; Allbritton, N. L. *Anal Chem* **2004**, *76*, 1865-1870.

(92) Hu, S. W.; Ren, X. Q.; Bachman, M.; Sims, C. E.; Li, G. P.; Allbritton, N. L. *Langmuir* **2004**, *20*, 5569-5574.
(93) Roman, G. T.; Culbertson, C. T. *Langmuir* **2006**, *22*, 4445-4451.
(94) Atuk, N. O.; Hanks, J. B.; Weltman, J.; Bogdonoff, D. L.; Boyd, D. G.; Vance, M. L. *J Clin Endocrin Metabo* **1994**, *79*, 1609-1614.
(95) Ymateos, A. G. D.; Culebras, J. M. *Nutrition* **1991**, *7*, 163-167.
(96) Lawrence, N. S.; Davis, J.; Compton, R. G. *Talanta* **2001**, *53*, 1089-1094.
(97) White, P. C.; Lawrence, N. S.; Davis, J.; Compton, R. G. *Electroanalysis* **2001**, *14*, 89.
(98) Evans, S. M.; Lew, R.; Kochman, M. L.; Wileyto, E. P.; Baum, E.; Safford, K. M.; Koch, C. J. *Dig Dis Sci* **2002**, *47*, 2743-2750.
(99) Goncalves, T. L.; Erthal, F.; Corte, C. L. D.; Muller, L. G.; Piovezan, C. M.; Nogueira, C. W.; Rocha, J. B. T. *Clin Biochem* **2005**, *38*, 1071-1075.
(100) Malinow, M. R. *J Internal Med* **1994**, *236*, 603-617.
(101) Kleinman, W. A.; Richie, J. P. *Biochem Pharmacology* **2000**, *60*, 19-29.
(102) Barter, P. J.; Rye, K. A. *Circulation Res* **2006**, *99*, 565-566.
(103) Refsum, H.; Ueland, P. M.; Nygard, O.; Vollset, S. E. *Ann Rev Med* **1998**, *49*, 31-62.
(104) Liao, D.; Tan, H. M.; Hui, R. T.; Li, Z. H.; Jiang, X. H.; Gaubatz, J.; Yang, F.; Durante, W.; Chan, L.; Schafer, A. I.; Pownall, H. J.; Yang, X. F.; Wang, H. *Circula Res* **2006**, *99*, 598-606.

Chapter 2

Microchip Fabrication, Use and Data Analysis

This chapter describes the major methods used for microchip fabrication, use and data analysis from dissertation. While the overall concepts and methods in this chapter were not developed in the Henry lab, all of the microchip designs and injection specifications were developed in our laboratory.

2.1 MOLD FABRICATION

Mold and PDMS microchip fabrication techniques have been published previously by a variety of groups.[1-6] The procedure that follows is included in this thesis to demonstrate the fabrication processes used in making our Poly(dimethylsiloxane) (PDMS) MCE devices. Slight variations in this procedure are noted in the following chapters if needed. 100 mm Si wafers were obtained from Silicon Inc. (Boise, ID) The wafers were cleaned and oxidized with HF (1:10 48%HF:H_2O) solution for 5 min followed by Piranha (2:1 18M H_2SO_4: 30% H_2O_2) solution for 10 min (*Caution! Piranha solution is a powerful oxidizing agent that reacts violently with organic compounds and should be handled with extreme care*). Once the wafer was removed from the Piranha solution, it was rinsed with deionized water and allowed to dry in a 65° C oven for 30 min. The wafer was then coated with SU-8 2035 negative photoresist (1mL photoresist for every 2.5 cm of wafer) using a spin coater (Laurell WS-400A-6NPP/LITE) (Figure 2.1A). The spin coater was programmed to spin the wafer at 500 rpm for 30 sec and then ramp to 2100 rpm for 45 seconds. This spin rate generates a photoresist thickness of 50 ± 3 μm (measured by profilometry). A soft bake is then performed by placing the coated wafer on a digital hotplate (Fisher) at 65°C for 3 min and then moving it to a 95°C

hotplate for 6 min. A digitally produced vector image (Corel Draw or Adobe Illustrator) printed in high resolution (2400-3600 dpi, CSU) on a transparent background was placed on the photoresist coated wafer (Figure 2.1B). The mask was held in place with a 2 mm thick glass slide and spring loaded clips to ensure the mask was flat against the photoresist and to prevent the it from moving during exposure. The mask and wafer were then exposed to near UV light (Intella-ray 400, 100 W) at 100% power for 7 sec at a distance of 8" (Figure 2.1C). After exposure a post baking step was used to fully adhere the photoresist to the silicon wafer. The post bake is performed by placing the exposed wafer on a 65° C hotplate for 1 min and then transferring it to a 95° C hotplate for 6 min (digital hotplate from Fisher Scientific). After the post bake, the wafer was rinsed and allowed to sit in a developing agent (propylene glycol-methyl ether acetate) for at least 10 min. The developer removed any unexposed photoresist leaving a positive relief of the channels on the silicon wafer (Figure 2.1D). The mold was then put back in the oven and allowed to fully dry for 30 min. After exposure and developing, patterned silicon masters are treated with hexamethyldisilazane (HMDS) by vapor deposition to aid in the removal of the both thermoset polyester (TPE) and PDMS. Vapor deposition was performed by placing the wafer and a small vial containing 500 μL of HMDS in a crystallization dish. The dish was then covered with foil and placed in a 65° C oven for 4-6 hrs.

2.2 MICROCHIP FABRICATION

2.2a PDMS Molding

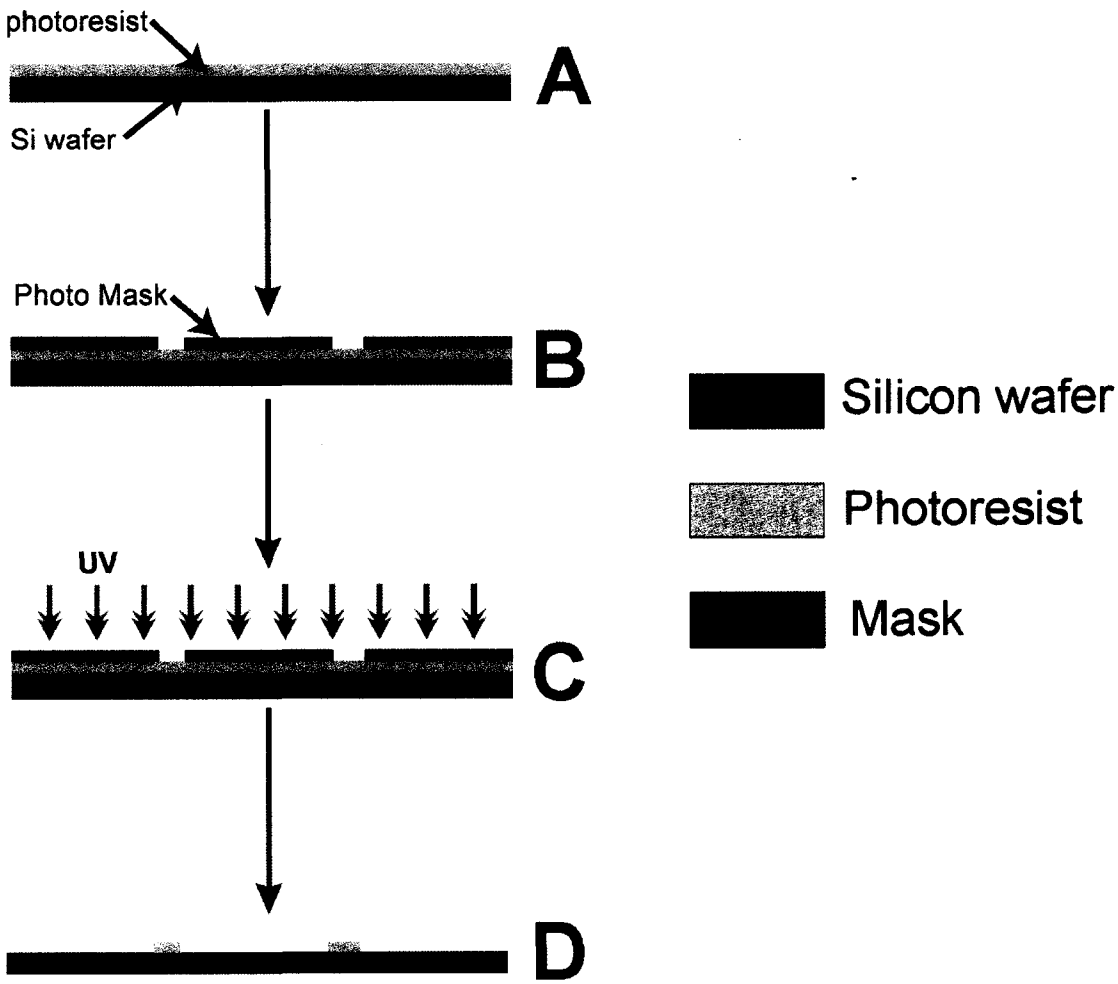

Figure 2.1: Schematic representation of mold fabrication process.

Once the master was completed (Figure 2.2A), replica molding was used to create PDMS microchips. Dimethylsiloxane monomer and Sygard 184 elastomer curing agent were mixed thoroughly in a 10:1 ratio and degassed in a vacuum desiccator. The mixture was then carefully poured onto the silicon master so as not to reintroduce any air bubbles (Figure 2.2B). The mold was then placed in an oven and allowed to cure at 65°C for at least 2 hours to cure the PDMS. The fully cured PDMS was cut to shape with a razor blade and peeled off the silicon wafer, leaving a negative relief of the channels and reservoirs. A blank piece of PDMS (formed on a blank Si wafer) (no channels) was also made to act as the 4^{th} wall of the capillary upon completion of the microchip. A 6mm punch (6mm biopsy punch, Robbins instruments) was used to open the reservoirs on the molded PDMS and the PDMS was trimmed to size with a razor blade.[7]

2.2b Microwire Alignment

The microwire electrodes were aligned in pre-designated electrode channels fabricated on the mold with the separation channel.[7] The electrode channels were molded into the PDMS for reproducible alignment of the microwire decoupler and working electrodes during the initial fabrication. 25-50 μm wide channels were molded into the PDMS near the waste reservoir, perpendicular to the separation channel. 25-50 μm microwire electrodes, ~ 4 cm in length, were placed on the chip and held down with scotch tape. The wires were manipulated into their designated channels with a fine tip needle. Caution was taken when moving the electrodes with the needle to not kink, bend or break them.

2.2c Microchip Sealing

Irreversible PDMS sealing was used for the assembly of the microchips according to published procedures.[3, 5, 8] The molded PDMS replica with the microwire electrodes and a blank piece of PDMS were placed in an air plasma cleaner (Harrick plasma cleaner/sterilizer PDG-32G) and oxidized for 45 s on the high setting (18 W) (Figure 2.2C). Upon removal from the plasma, the two pieces were brought into conformal contact and pressed firmly together (Figure 2.2D). The plasma forms radicals on the surface of the PDMS that when brought into contact with another plasma treated PDMS pieces forms a bond.[9] Caution needs to be taken when applying pressure around the microwires not to bend or break them. The sealed microchips were then placed in the oven for an additional 10-30 min to allow complete sealing of the chip. After removal from the oven, a 0.80 mm copper wire was attached to the exposed microwire end with conductive silver paint and held in place with glue to facilitate electrical contact. A schematic and photograph of a decoupled microchip are shown in Figure 2.3

2.3 MICROCHIP INJECTION AND SEPARATION

In this thesis all experiments were done with a pinched injection. Pinched injection is described in detail in a paper published by Garcia and Henry.[10] Briefly, during injection a high electric field (~285 V/cm) was applied between the sample (+410 V) and sample waste (-160 V) reservoirs on the microchip while the separation field was lowered from ~250 V/cm to 60 V/cm (1500V to 410V, buffer reservoir). This drives

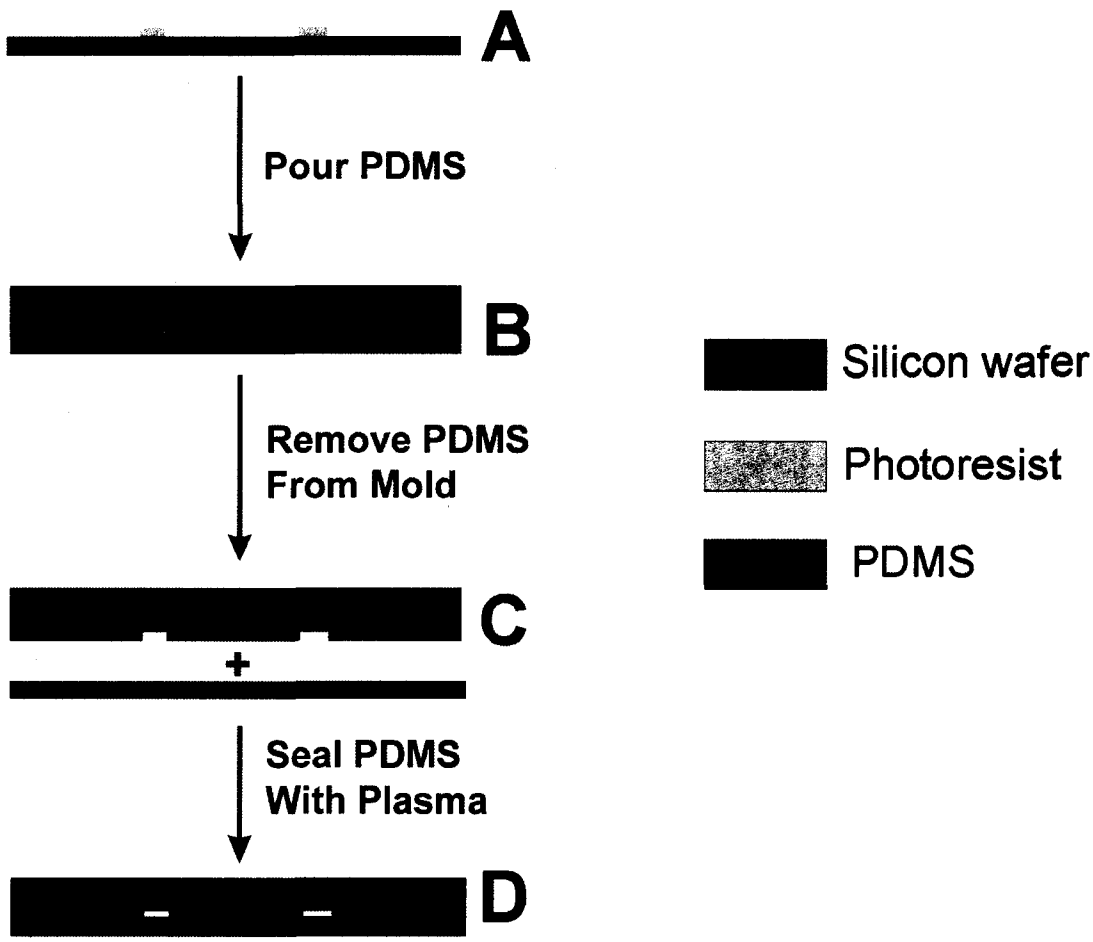

Figure 2.2: Schematic representation of microchip fabrication process.

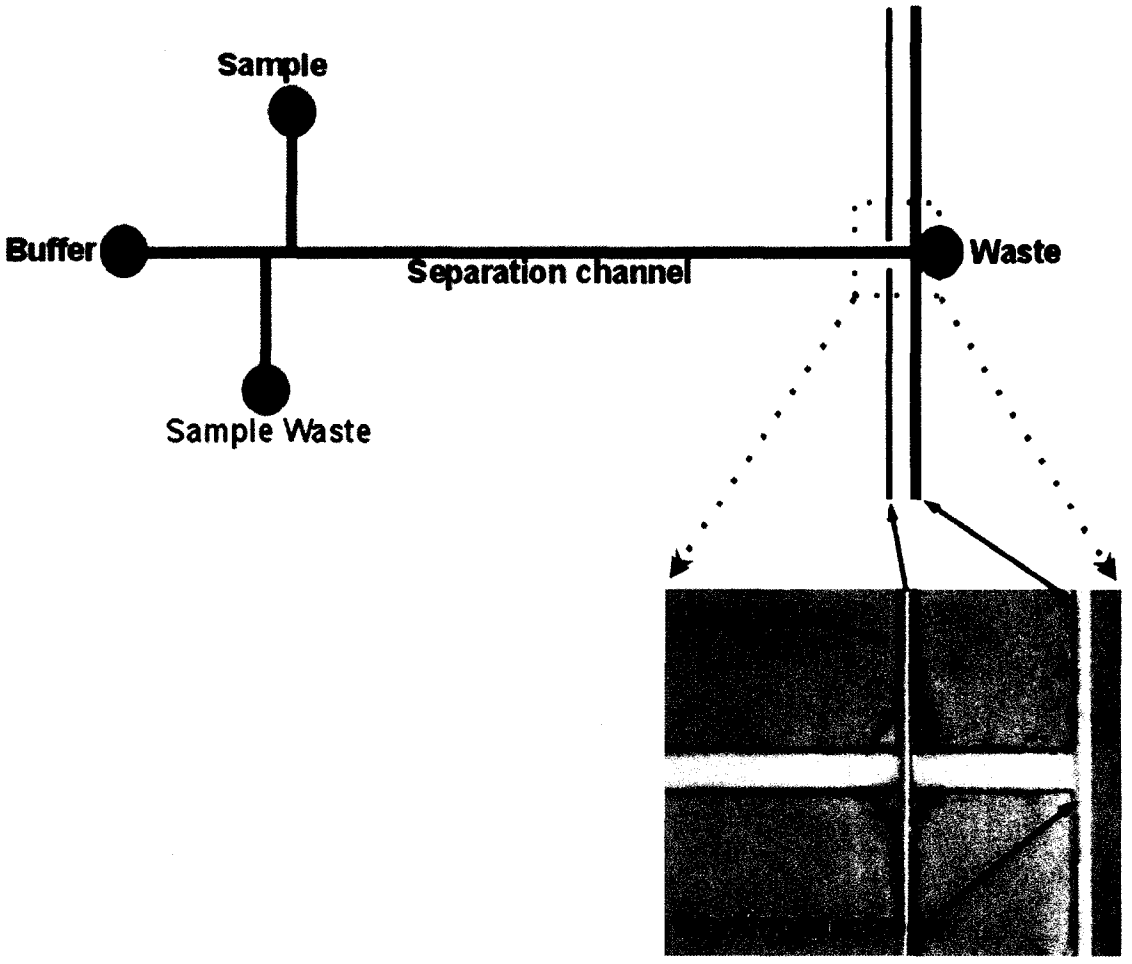

Figure 2.3: Schematic representation and photograph of a decoupled microchip.

solution from the sample reservoir through the double T and toward the sample waste reservoir (Figure 2.4B). Once the double T was filled with sample, voltages were switched to perform separation. The separation field was increased by applying 1500 V between the buffer reservoir and the waste reservoir (250 V/cm) while the injection field was removed. During separation both of the sample and sample waste reservoirs were placed at a lower positive potential (+410 V) for push back (Figure 2.4C). Push back voltage is a small amount of flow from the buffer reservoir to the sample and sample waste to keep any unwanted leaking to a minimum during separation. This process can be repeated to perform subsequent injections.

2.4 DATA ANALYSIS

Hydrodynamic voltamograms (HDV) were used to determine optimal detection potentials for analytes. To obtain HDVs peak height was measured as a function of detection potential. Optimal detection potentials for single analytes were determined to be the detection potential which produced the highest electrochemical signal (peak height). Optimal detection potentials for groups of analytes were determined from the HDV of the individual analytes. A detection potential was chosen that did not favor a specific analyte rather the potential which showed the highest signal in all of the individual HDVs.

Statistical calculations were also performed as data analysis methods of MCE-EC experiments. Limits of detection (LOD) were calculated as a function of peak height relative to the peak to peak baseline noise. Baseline noise was measured at an n = 30

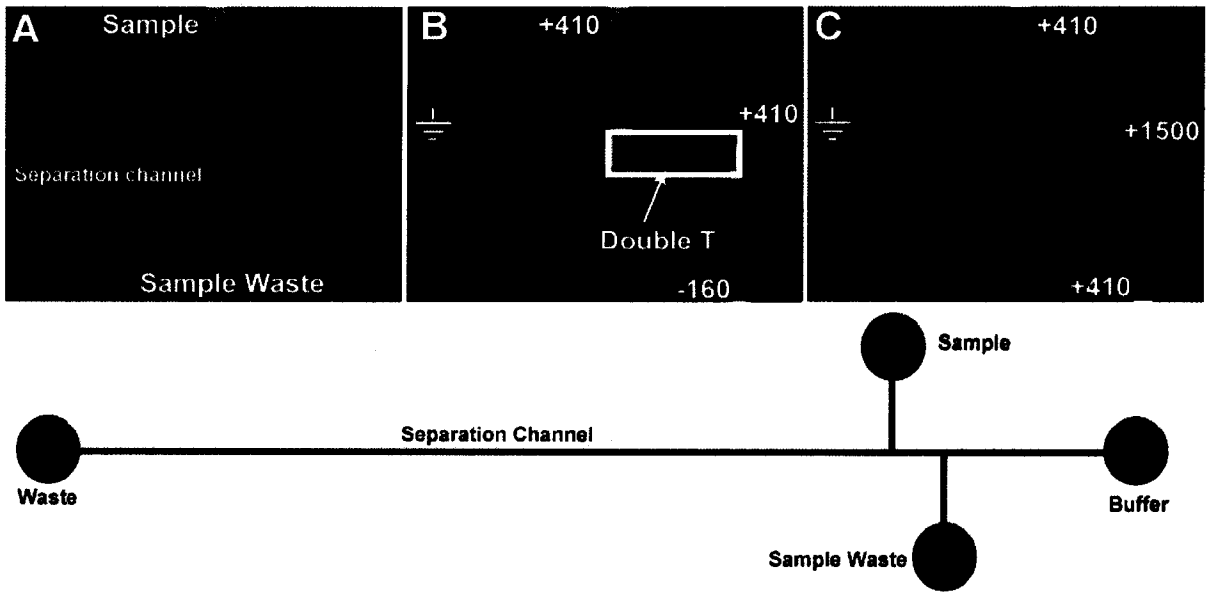

Figure 2.4: Pinched injection schematic.

with 15 point coming from the baseline prior to the peak and 15 point from the baseline after the peak being analyzed. All LOD measurements were done experimentally at a signal to noise ratio of 3. Separation efficiencies were calculated using equation 2.1.

$$N = 5.54 (t_m/w_{1/2})^2 \qquad \text{Eq 2.1}$$

Where: N = number of theoretical plates, t_m = migration time of the analyte and $w_{1/2}$ = is the peak width at half the maximum height.

N was then divided by the length of the separation channel from the injection to the detection electrode to get N/m. Peak skew was the determination of peak symmetry. Peak skew was calculated at 10% of the height of the peak using equation 2.2.

$$S = b/a \qquad \text{Eq 2.2}$$

Where: b = the distance from peak center to the back edge of the peak at 10% height and a = the distance from peak center to the front edge of the peak at 10% height. a and b were determined using data processing software (Origin Pro 7.0).

2.5 CONCLUSIONS

Fabrication of these devices is simple and relatively fast. The entire mold fabrication process, depending upon the HMDS vapor deposition, takes 1-7 hours while the PDMS molding process takes a little over 2 hours. All in all, it is possible to go from blank silicon wafer to a functioning microchip in as little as 3 hours. The processes for

making the mold, microchips, and data analysis were constant throughout my research unless otherwise noted. Any changes to these procedures will be discussed in the appropriate chapters.

(1) Effenhauser, C. S.; Bruin, G. J. M.; Paulus, A.; Ehrat, M. *Anal Chem* **1997**, *69*, 3451-3457.
(2) Martin, R. S.; Gawron, A. J.; Lunte, S. M.; Henry, C. S. *Anal Chem* **2000**, *72*, 3196-3202.
(3) McDonald, J. C.; Duffy, D. C.; Anderson, J. R.; Chiu, D. T.; Wu, H.; Schueller, O. J.; Whitesides, G. M. *Electrophoresis* **2000**, *21*, 27-40.
(4) Hong, J. W.; Hosokawa, K.; Fujii, T.; Seki, M.; Endo, I. *Biotechnol Prog* **2001**, *17*, 958-962.
(5) McDonald, J. C.; Metallo, S. J.; Whitesides, G. M. *Anal Chem* **2001**, *73*, 5645-5650.
(6) Yan, J.; Du, Y.; Liu, J.; Cao, W.; Sun, X.; Zhou, W.; Yang, X.; Wang, E. *Anal Chem* **2003**, *75*, 5406-5412.
(7) Liu, Y.; Vickers, J. A.; Henry, C. S. *Anal Chem* **2004**, *76*, 1513-1517.
(8) Liu, Y.; Fanguy, J. C.; Bledsoe, J. M.; Henry, C. S. *Anal Chem* **2000**, *72*, 5939-5944.
(9) Duffy, D. C.; McDonald, J. C.; Schueller, O. J. A.; Whitesides, G. M. *Anal Chem* **1998**, *70*, 4974-4984.
(10) Garcia, C. D.; Liu, Y.; Anderson, P.; Henry, C. S. *Lab Chip* **2004**, *3*, 324-328.

Chapter 3

Simple and Sensitive Electrode Design for Microchip Electrophoresis/Electrochemistry

Two general approaches for integration of electrodes in MCE-EC are commonly used; end-channel and microfabrication.[1] The end-channel approach allows for electrode cleaning and the use of chemically modified electrodes. However, the designs generally lack portability and the ability to incorporate multiple electrodes. Microfabrication allows the incorporation of multiple electrodes and is easily made portable; however it requires the use of expensive metallization, cleanroom facilities and the challenge of integrating more than one electrode material. The first step in my graduate work was to help develop a new detection electrode configuration that combined the advantages of both approaches. A novel, simple and sensitive design using a microwire as the in-channel working electrode for MCE-EC was developed. The microwire is aligned across the separation capillary using a channel patterned in the PDMS. The approach aligns a solid metal microwire through the separation channel allowing integration of multiple electrodes and the use of different electrode materials without sacrificing portability. Furthermore, because a larger area of the wire is exposed to flow than with previous approaches, higher collection efficiencies are achieved. This work was performed with another graduate student, Yan Liu, and was published in *Analytical Chemistry*.[2] In this chapter all of the data collected with a 50 μm electrode was generated by me while the data taken with 25 μm working electrodes was generated by Yan.

The work in this chapter for the development of microwire working electrodes was done to improve the sensitivity of our MCE-EC devices over more traditional methods such as thin film electrodes. The improvements demonstrated here lead to a large linear range and decreased limits of detection when compared to similar

microchips with thin film electrodes and set the stage for additional developments in the remaining chapters.

3.1 EXPERIMENTAL

3.1a Chemicals and Materials.

The following chemicals and materials were used as received: SU-8 2035 photoresist (Micro Chem. Corp., Newton, MA), propylene glycol methyl ether acetate (Aldrich), 3" silicon wafers (Silicon Inc., Boise, ID), poly(dimethylsiloxane) (PDMS) (Dow Corning), Sygard 184 elastomer curing agent (Dow Corning), sodium hydroxide (Fisher), N-tris[Hydroxymethyl]methyl-2-aminoethanesulfonic acid (TES, >99% pure) (Sigma), methanol (Fisher, ACS grade), 2-propanol (Fisher, ACS grade), catechol (Sigma, 99%), and 3,4-dihydroxyphenethylamine dopamine (Sigma, 99%). Microwires made of 99.9 % platinum (diameter 0.025 and 0.050 mm), 99.99 % gold wire (diameter 0.025 mm) and 99.99 % copper wire (diameter 0.025mm) were obtained from Goodfellow (Huntingdon, England).

3.1b MCE-EC.

A double-T injector along with pinched injection[3-6] was employed for these experiments as discussed in chapter 2. Channels were first treated with 0.1 M NaOH for 30 min in order to give the surface of the channel a negative charge through the deprotonation of silanol groups. The channels and reservoirs were then filled with the buffer solution by applying pressure to a reservoir containing buffer while the other reservoirs were empty. Buffer located in the sample reservoir was replaced with sample

solution prior to experiments. For separations, a high positive potential (1200-1500 V) was applied to the buffer reservoir while the buffer waste was kept at ground and the sample and sample waste reservoirs were held at a constant lower positive potential, termed the pull back voltage. Injections were performed by applying the lower positive potential (410 V) to the sample reservoir and a negative potential (-160 V) to the sample waste reservoir while, simultaneously, decreasing the high positive separation potential of the buffer and keeping the waste reservoir at electrical ground. In all situations, Pt wires (1 mm diameter) were used as electrodes in the reservoirs for electrophoresis.

The amperometric mode of electrochemical detection was employed (CHI812, CH Instruments) in a two-electrode configuration. A platinum wire (1 mm diameter) was employed as a counter electrode while the working electrode materials and sizes varied between experiments. The electrode materials studied were platinum, gold, and copper, with diameters of 25 and 50 μm. The microwire electrodes were placed in an electrode channel fabricated in the microchip at the end of the separation channel and the beginning of the waste reservoir as shown in Figure 3.1. Cleaning of the working electrode was performed every 20 runs via cyclic voltammetry with 20 sweep segments from 0 V to 1.2V at the rate of 0.1 V/s while the separation potential was being applied to the electrode. This cleans the electrode by forming a metal oxide layer on the electrode surface in order to remove adsorbed species and then reducing the oxide layer back to the native form of the electrode.

3.2 RESULTS AND DISCUSSION

3.2a Microwire Working Electrode

One advantage of the microwire electrode design is the wide variety of the electrode materials that can be incorporated.[7] The influence of different electrode materials was investigated. Cu, Au, and Pt microwires were each used as working electrodes. Electropherograms of catechol at each electrode material is shown in Figure 3.2. Catechol was choosen because at pH 7.0 it is neutral and will travel with the EOF. For the Cu electrode, the baseline current decreased with time. This can be attributed to the oxidation of the Cu electrode caused because our detection potential (0.8 V) is higher than copper oxidation potential (0.35 V). Cu electrodes are not commonly used for direct amperometric detection, but were used in this case is a simple demonstration of the concept and for comparison to other electrode materials. Migration times for catechol vary in each electropherogram, this is attributed to inconsistent EOF (Chip to chip), common in irreversibly sealed PDMS microchips.[8] Surface modification can minimize this problem.[9, 10] Results from the Au and Pt electrodes are consistent with other reports for similar systems with the same electrode materials.[11]

3.2b Limits of Detection

Limits of detection (LOD) for dopamine were determined as a function of electrode size. Electropherograms for 100 nM (62 femtomoles) dopamine detected at a 50 μm electrode and 250 nM (156 fmoles) dopamine measured at a 25 μm electrode are

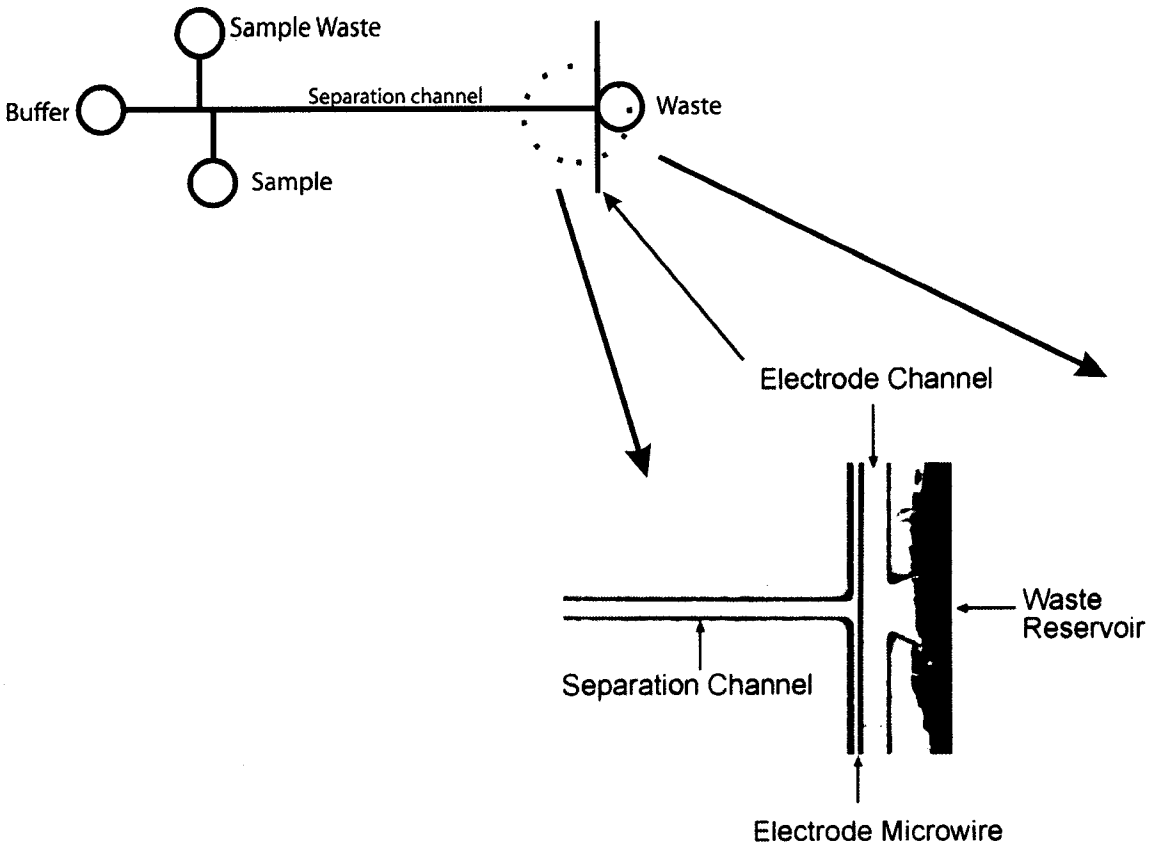

Figure 3.1: Top) Schematic of the microchip showing placement of the electrode alignment channel. Bottom) Photograph showing electrode alignment in a completed microchip

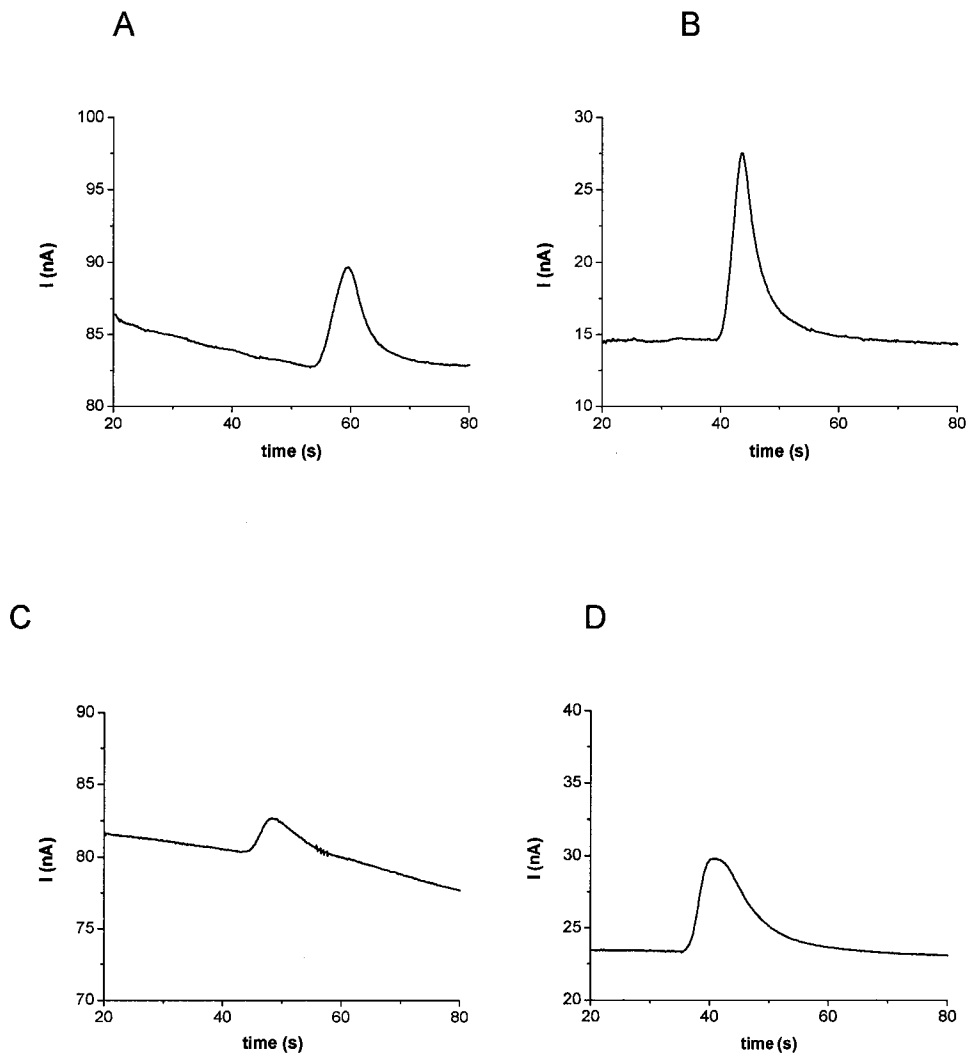

Figure 3.2: Electropherograms of 100 μM catechol: A) 25 μm Au electrode B) 50 μm Pt electrode C) 25 μm Cu electrode D) 25 μm Pt electrode. Experimental conditions: Separation voltage: 1500 V; Pinched injection time: 45 s; Running buffer: 20 mM TES (pH 7). Copper and Gold electrode were run by Yan Liu.

A

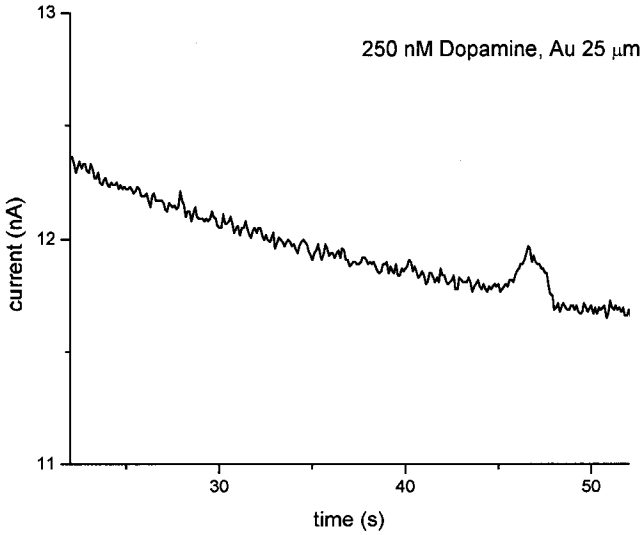

B

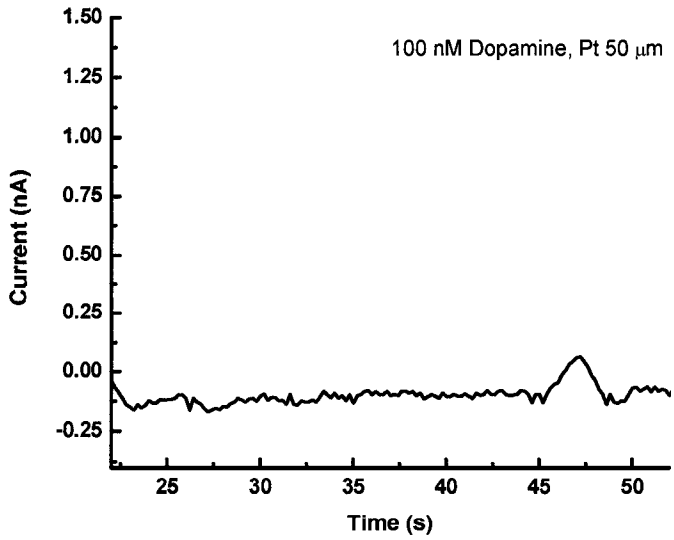

Figure 3.3: A) LOD of dopamine for 25 μm Au electrode (250 nM). B) LOD of dopamine for 50 μm Pt electrode (100 nM). Experimental conditions were the same as Figure 3.2.

shown in Figure 3.3. Peak heights at the LODs were 0.22 ± 0.053 nA and 0.189 ± 0.49 nA for the 25 μm Au and 50 μm Pt electrodes, respectively. Standard deviations were calculated using n = 3. Detection limits are the lowest reported without the use of a decoupler.[12] The dynamic range of dopamine detection for 25 μm Pt electrode microchip was also investigated. The linear range for dopamine was found to be from 0.1 to 100 μM with an R^2 value of 0.993 and a sensitivity of 12.445 nA/μM.

The low detection limit achieved with the 50 μm wire cannot only be attributed to the difference in the electrode surface area. Another consideration is the diffusion of analytes to the electrode surface. Figure 3.4 shows a schematic of the flow around the electrode in the separation channel. For the 25 μm electrode, there is a greater distance for diffusion between analytes in solution and the electrode when compared to the 50 μm electrode. Comparing the velocity of the analyte (1 mm/s) to the rate of diffusion of a small molecule in the BGE (1 x 10^{-6} cm^2/s) allowed us to determine the distance a molecule could diffuse in the amount of time the sample would spend in contact with the working electrode. Using $v = \sqrt{Dt}$ the distance the analyte can diffuse while the sample plug is in contact with working electrode was calculated to be 2.24 μm for the 50 μm electrode and 1.58 μm for the 25 μm electrode. This resulted in higher collection efficiency at 50 μm electrode when compared to the 25 μm electrode. Collection efficiency were calculated for both electrode sizes using Faraday's equation (Q = nFC). Where n= number of electrons, F= faradays constant and C is the concentration. Theoretically, 1.2 nL of dopamine (100 μM) injected into the separation channel should have a peak area of 11.58 nC. The total charge passed as measured by the peak area was 4.21 nC and 10.49 nC for 25 μm and 50 μm electrodes, respectively. Therefore, the

collection efficiency given by the ratio of measured value to theoretical value for 25 μm and 50 μm electrode is 36% and 90% respectively. The results demonstrate that the 50 μm electrode dramatically improves the collection efficiency as a result of electrode alignment in the channel. This improvement in the collection efficiency results from a combination of shorter diffusional pathlengths for the analytes to the electrode surface and larger surface area of the 50 μm electrode. Dr. Yan Liu was responsible for LOD experiments with the 25 μm working electrodes and calculation of collection efficiencies.

3.2c Separation Efficiency.

The electrode size plays a role in the separation efficiency. The separation efficiencies for dopamine and catechol were measured for 25 and 50 μm electrodes (Figure 3.5). For the 25 μm electrode, the two peaks from the oxidation of dopamine and catechol were well resolved (R = 1.54), while for 50 μm electrode, the resolution was 0.85. Resolution is calculated by $R= \Delta t_m/w_{avg}$. Where Δt_m is the difference in migration times and w_{avg} is the average width of the peaks. The difference in the resolution could be attributed to restriction of flow with the 50 μm electrode. The separation efficiencies for the dopamine peak were 3623 plates/m for the 25 μm electrode and 3838 plates/m for the 50 μm electrode, respectively. The corresponding plate heights (H) are 0.52 mm and 0.75 mm for the 25 μm and 50 μm electrodes respectively, mirroring the increase in electrode area. Although the separation efficiencies are low, they can be improved for both electrodes by reducing the injection volume and modifying the surface of the PDMS. The trends in the separation efficiency and resolution are still valid regardless of the injection volume.

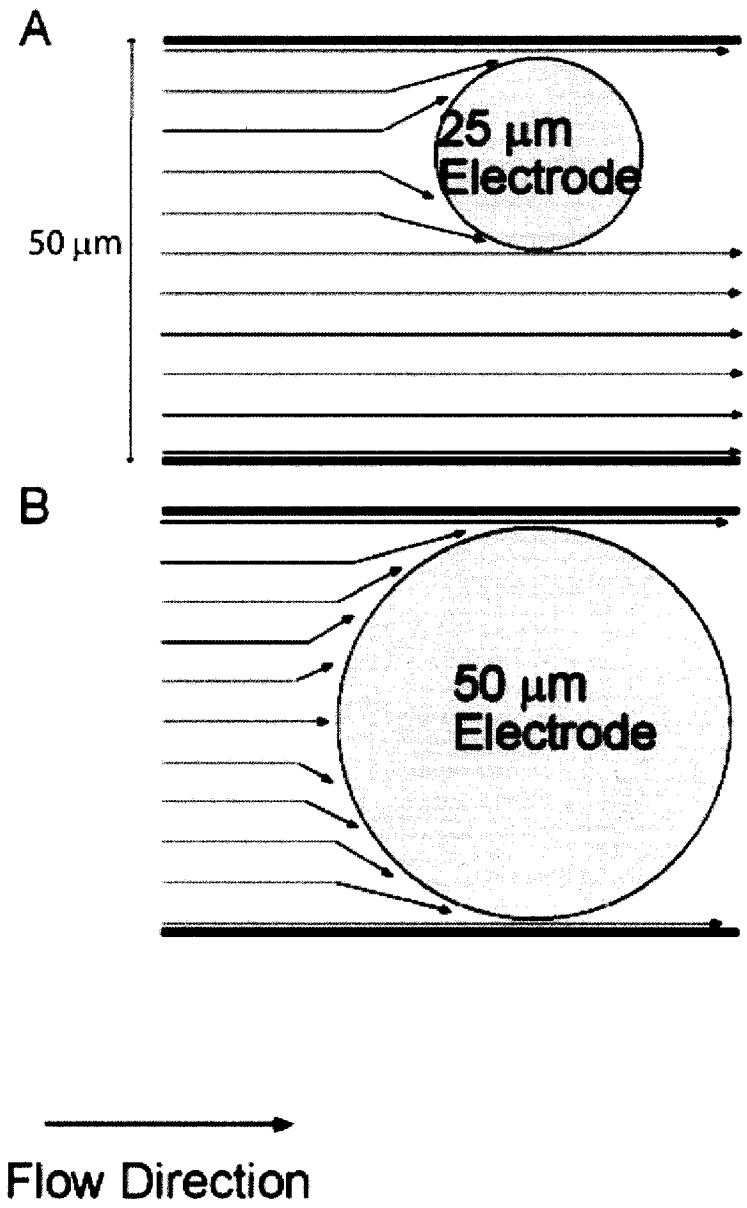

Figure 3.4: Schematic of flow around the microwire electrode in microchannel, drawn to scale. Location of the 25 μm electrode can vary vertically in the channel.

A

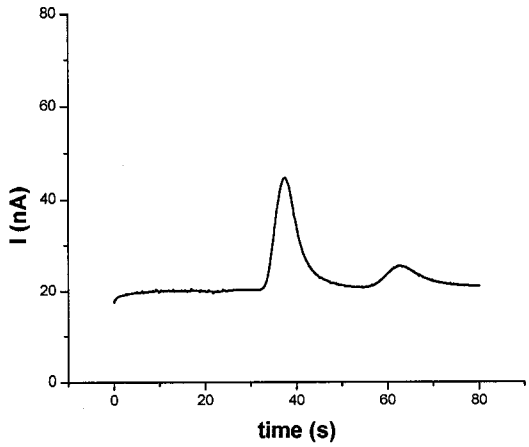

B

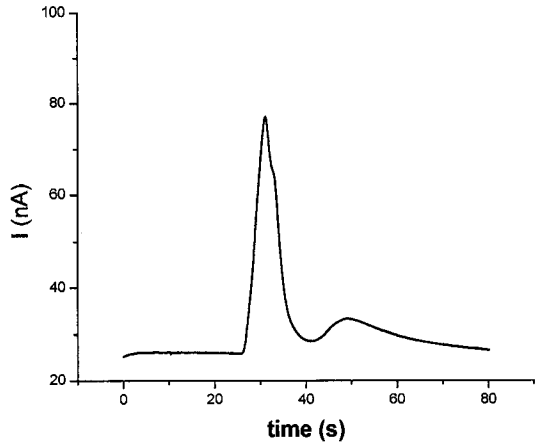

Figure 3.5: Separations of 100 μM dopamine and catechol. A) 25 μm Au electrode B) 50 μm Pt electrode. Experimental conditions: Separation voltage: 1500 V; Pinched injection time: 45 s; Running buffer: 20 mM TES (pH 7).

3.3 Conclusions

Microwire working electrodes have been shown to be easily incorporated in PDMS microchips, with the aid of electrode channels fabricated on chip, as a working electrode for electrochemical detection. Microwire electrodes have shown to be a viable alternative to thin film electrodes for use with MCE-EC. Microwire electrodes yield high collection efficiencies, large linear ranges and limits of detection as low as 100 nM (62 fmoles). The use of microwire electrodes also allows for the use of various electrode materials which will be beneficial when trying to incorporates multiple electrode materials onto a single microchip. Issues that still need to be addressed with these microchips are high background noise, low separation efficiencies and large peak skews. These problems will be discussed in more detail in the following chapters.

3.4 Acknowledgment

This work was done in coordination with Dr. Yan Liu for the research and data analysis of the MCE devices with 25 μm working electrodes and collection efficiency calculations. I would like to thank Dr. Kevin Lear for access to microfabrication equipment in the department of Electrical Engineering at Colorado State University.

(1) Vandaveer, W. R. I. V.; Pasas-Farmer, S. A.; Fischer, D. J.; Frankenfeld, C. N.; Lunte, S. M. *Electrophoresis* **2004**, *25*, 3528-3549.
(2) Liu, Y.; Vickers, J. A.; Henry, C. S. *Anal Chem* **2004**, *76*, 1513-1517.
(3) Shultz-Lockyear, L. L.; Colyer, C. L.; Fan, Z. H.; Roy, K. I.; Harrison, D. J. *Electrophoresis* **1999**, *20*, 529-538.
(4) Jacobson, S. C.; Hergenroder, R.; Koutny, L. B.; Warmack, R. J.; Ramsey, J. M. *Anal Chem* **1994**, *66*, 1107-1113.
(5) Garcia, C. D.; Henry, C. S. *Anal Chem* **2003**, *75*, 4778-4783.
(6) Garcia, C. D.; Liu, Y.; Anderson, P.; Henry, C. S. *Lab Chip* **2004**, *3*, 324-328.
(7) Lacher, N. A.; Garrison, K. E.; Martin, R. S.; Lunte, S. M. *Electrophoresis* **2001**, *22*, 2526-2536.
(8) Ocvirk, G.; Munroe, M.; Tang, T.; Oleschuk, R.; Westra, K.; Harrison, D. J. *Electrophoresis* **2000**, *21*, 107-115.
(9) Liu, Y.; Fanguy, J. C.; Bledsoe, J. M.; Henry, C. S. *Anal Chem* **2000**, *72*, 5939-5944.
(10) Liu, Y.; Wipf, D. O.; Henry, C. S. *Analyst* **2001**, *126*, 1248-1251.
(11) Martin, R. S.; Gawron, A. J.; Lunte, S. M.; Henry, C. S. *Anal Chem* **2000**, *72*, 3196-3202.
(12) Osbourn, D. M.; Lunte, C. E. *Anal Chem* **2003**, *75*, 2710-2714.

Chapter 4

Incorporation of a Microwire Current Decoupler for Use with Microchip CE-EC

Increasing sensitivity for DC amperometry and PAD requires the isolation of detection current (nA) from the separation current (μA) in a process generally referred to as current decoupling as discussed in more detail in Chapter 1. Current decouplers have been shown to improve the sensitivity of conventional as well as MCE-EC through a significant reduction of noise.[1-6] Microchip decouplers have taken on two forms; laser etched and Pt or Pd cathodes. Pd[1, 5] and, to lesser extent, Pt[6] are used in decouplers because they absorb H_2 gas that is formed at the cathode with good efficiency and thus prevent it from interfering with the electrophoretic separation.[7] In this thesis I present the development of a simple integrated decoupler to improve sensitivity and its coupling with PAD and DC amperometry in MCE devices. A Pd microwire is used as the cathode for decoupling and a second Au or Pt wire is used as the working electrode for either DC amperometry or PAD. The electrode system is easy to make, requiring no cleanroom facilities or specialized metallization systems. Sensitive detection of a wide range of analytes is shown to be possible using this system. This was published in *Electrophoresis*.[8]

The work presented in this chapter was done to further increases the sensitivity of our MCE-EC devices and to demonstrate the ability to incorporate multiple electrochemical detection techniques. The incorporation of the current decoupler demonstrated here decreases the background noise in the system and allows for lower LODs to be achieved. Amperometry provides a simple but sensitive detection technique, but it's ability to detect electrode fouling analytes limits it usefulness with biological samples. Pulsed amperometric detection will be used to demonstrate the ability to use a different detection techniques as well as to increase the number of detectable analytes.

4.1 Experimental

4.1a Chemicals and Materials.

The following chemicals and materials were used as received: SU-8 2035 photoresist (Micro Chem. Corp., Newton, MA), propylene glycol methyl ether acetate (Aldrich, 98%), 4" silicon wafers (Silicon Inc., Boise, ID), poly(dimethylsiloxane) (PDMS) (Dow Corning), Sygard 184 elastomer curing agent (Dow Corning), sodium hydroxide (Fisher, 99%), N-tris[Hydroxymethyl]methyl-2-aminoethanesulfonic acid (TES) (Sigma, 99%), boric acid (Fisher, 99%), sodium dodecyl sulfate (SDS) (Fisher, 97%), methanol (Fisher, ACS), 2-propanol (Fisher, ACS), catechol (Sigma, 99%), 3,4-dihydroxyphenethylamine; (dopamine) (Sigma, 99%), ascorbic acid (Sigma, 99%)), β-D-glucose-6-phosphate (Aldrich, >99%), dextrose (Fisher, >99%), cysteine (Sigma), glutathione (Sigma) and fluorescein-5-isothiocyanate (FITC, >95%) (Invitrogen). Microwires made of 99.9 % Pt (diameter 0.050 mm), 99.99 % Pd (diameter 0.025 mm) and 99.99 % Au (diameter 0.025 mm) were obtained from Goodfellow (Huntingdon, England).

4.1b Microchip CE-EC.

Pinched injection through a double-T injector was employed for these experiments as described in chapter 2.[9-11] The double-T gave an injection volume of 250 pL based on the channel dimensions. The channels were first treated with 0.1M NaOH for at least 30 min to give the channel walls a negative charge. Reservoirs were filled with background electrolyte (BGE) and pressure was applied to one of the reservoir to

displace e the NaOH in the channels with BGE. Before analysis, buffer in the sample and sample waste reservoirs was replaced with sample solution. The microchip was designed with two electrode channels spanning the separation channel in order to incorporate the decoupler and working electrodes shown in Figure 4.[12] A Pd microwire (25 μm) was placed in the first electrode channel (25 μm wide) for use as the cathode (Figure 4.1). The working electrode was placed downstream in the second electrode channel (Figure 4.1). The distance between the two electrodes was fixed at 250 μm based on previous work by Lacher *et al.* [1] and experiments in our laboratory. Noise and peak width (base) were measured at various distances between the working electrode and decoupler to evaluate this effect. The fully assembled microchips were allowed to sit for 24 hours before use in experiments to allow the EOF of plasma sealed chips to decrease to a stable level through hydrophobic recovery. The typical lifetime of these devices was one to two weeks although a new microchip was used everyday for these experiments to show chip to chip reproducibility. For separations, 800-1500 V was applied to the buffer reservoir while the Pd microwire decoupler was kept at ground. The sample and sample waste reservoirs were held at 450 V for push back. The first microchip design had electrode alignment channels that were 50 μm wide and intersected the separation channel fully. While not problematic for the working electrode, complications were seen when dealing with the decoupler. BGE as well as sample were seen flowing through the separation channel and down the decoupler electrode channel rather than passing by the decoupler toward the working electrode as shown schematically in Figure 4.2. To alleviate this problem, RTV

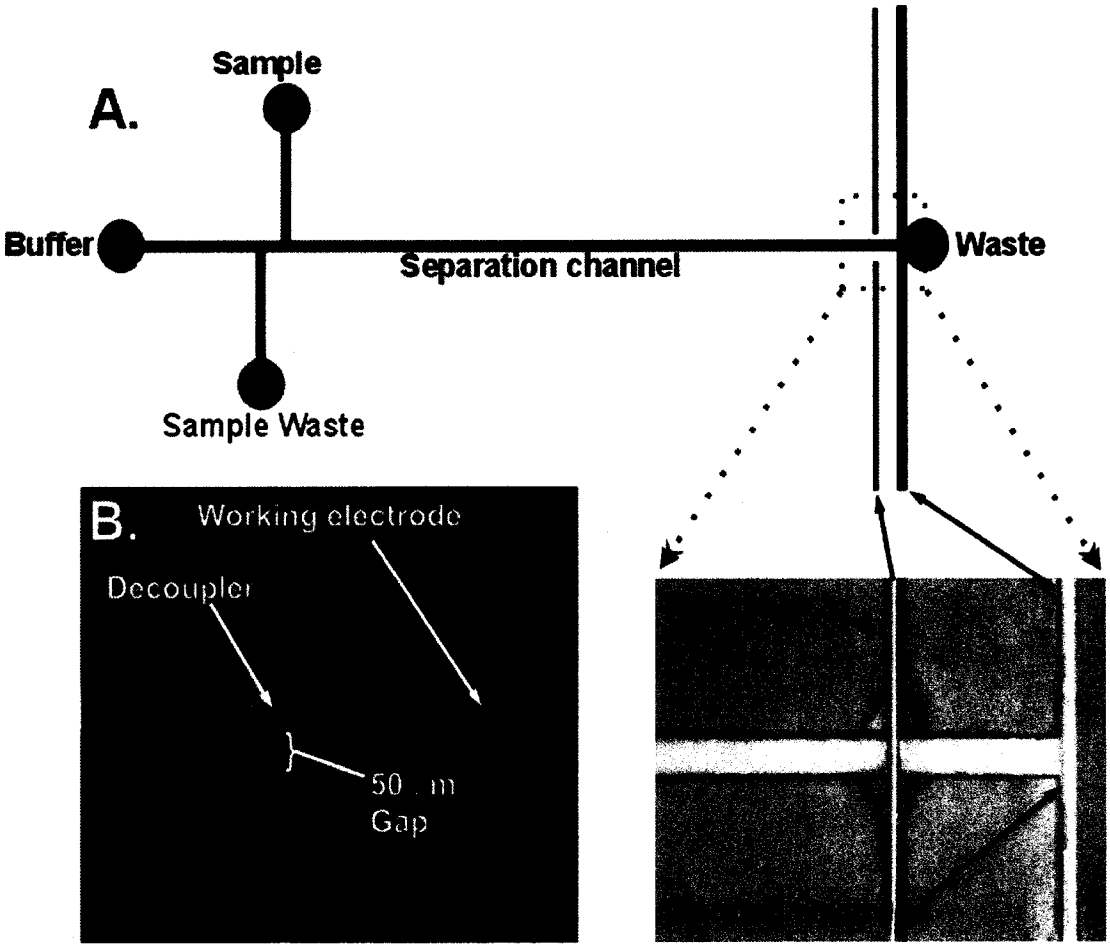

Figure 4.1: **A.** Schematic of the microchip (50μm deep, 50μm wide, 5.1cm long separation channel) showing placement of the electrode alignment channels. Working electrode channel (50μm deep x 50μm wide). Decoupler electrode channel (50μm deep x 25μm wide, 50 μm gap to separation channel). Double-T injector (50μm × 50μm × 100μm) has a volume of 250 pL. The lower right is a photograph showing electrode alignment in a completed microchip. Left electrode is Pd microwire while the right electrode is the Pt working electrode. **B.** Decoupled microchip. Fluorescent image of 1mM FITC as it passes the decoupler. No sample leakage was observed around the Pd microwire. Dotted lines indicate the outline of the channels in the PDMS.

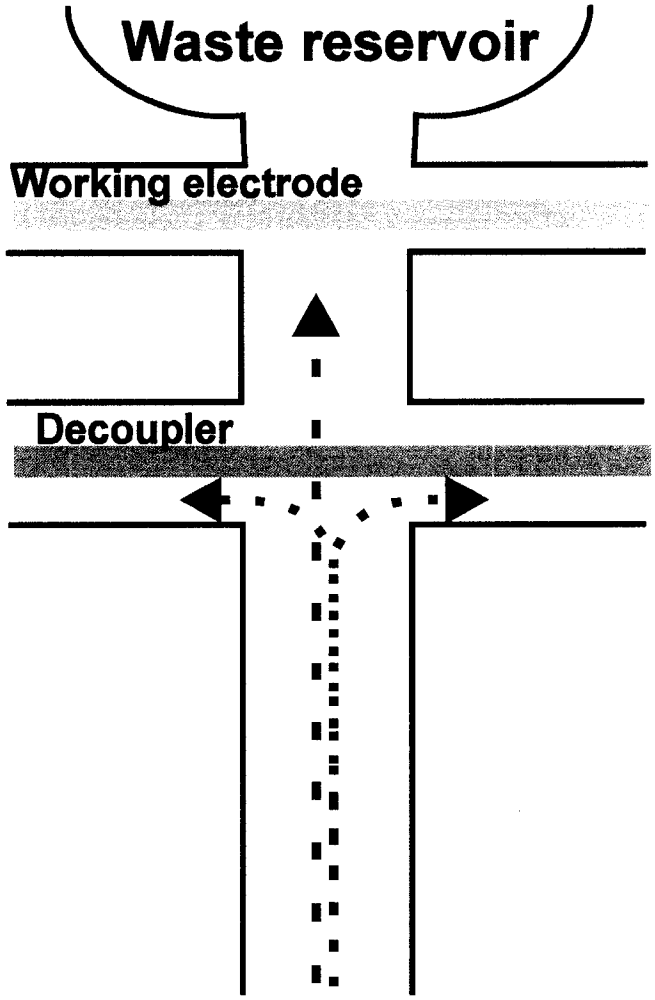

Figure 4.2: Representation of fluid flow in the first decoupled microchips. The red dotted line represents the flow of fluid in the very first decoupled microchips. Flow from the separation channel traveled down the electrode alignment channel and never made it to the working electrode. The blue dashed line represents the desired flow in the chip.

silicon sealant was forced down the decoupler alignment channel with pressure after the microwires were in place and the chip was fully assembled (Figure 4.3). This allowed the BGE and injected sample to flow past the decoupler toward the working electrode. The RTV could not be forced all the way to the separation channel because it would coat the area of the decoupler in the separation channel and would leak into and plug the separation channel once it cured. 3 out of 5 microchips were unusable because of the human error associated with forcing the RTV down the electrode channel. The inabilities to force RTV to the point were it directly contacted the separation channel also introduced dead volume in the microchip around the decoupler (Figure 4.3). To overcome this problem, a decrease in size of the alignment channel from 50 to 25 μm wide and the incorporation of a small (50μm) gap between the decoupler alignment channel and the separation channel was used (Figure 4.1). When sealed together, the PDMS forms around the microwire holding it in place. This design does not allow solution to flow down the decoupler alignment channel, eliminating the human error associated with forcing the RTV sealant into the channels. After each electrode was aligned and sealed in place, a 0.80 mm copper wire was attached to the exposed microwire end with conductive silver paint and held in place with glue. In situ cleaning of the working electrode was done while using direct amperometric detection every 15 runs via cyclic voltammetry (CV) with 20 sweep segments from -1.0V to 1.0V at the rate of 0.1 V/s while buffer was electrokinetically pumped over the electrode to ensure a clean and uniform electrode surface.[12] The Pd decoupler was cleaned and conditioned initially by running a CV from -1.0V to 1.0V at 0.1 V/s for 50 cycles.

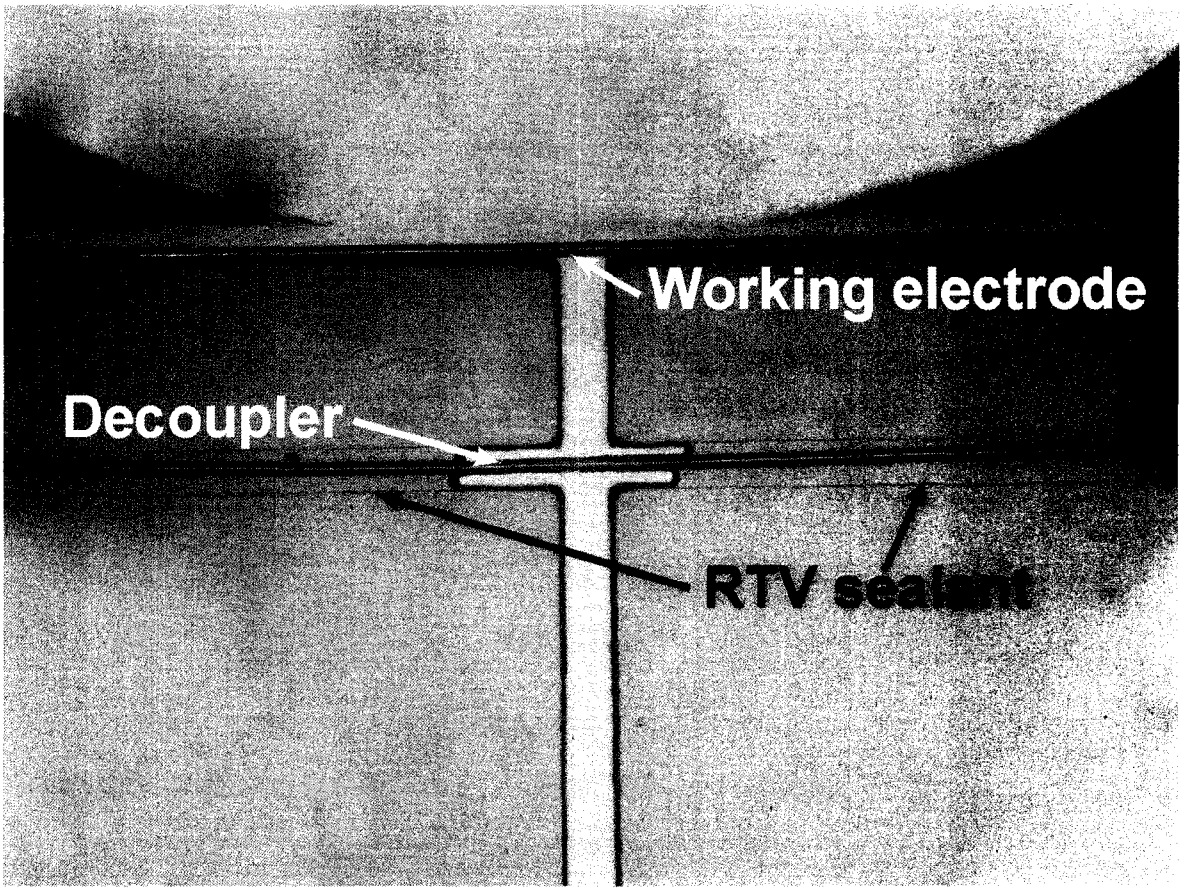

Figure 4.3: The second decoupled microchip design. RTV silicon sealant was forced down the alignment channel until it was 50-100 μm from the separation channel. This prevented flow down the alignment channel but increased band broadening because portions of the alignment channel were still open to the separation channel.

4.1c Detection.

Amperometry was used for the detection of catecholamines and PAD was used for carbohydrates and thiols using a commercially available potentiostat (CHI812, CH Instruments). For PAD, the cleaning/oxidation potential was held at 1.6 V for 0.05 s, the reduction/regeneration potential was -0.5 V for 0.025 s and the detection potential was varied between 0.6 V and 1.4 V versus a Pt counter electrode for 0.15 s depending on the analyte of interest. All experiments were run in a two-electrode configuration with a Pt wire (1 mm diameter) in the waste reservoir used as the counter electrode. A Pt working electrode (50μm diameter wire) was used for DC amperometry, while a Au working electrode (25 μm) was used for PAD. Noise was determined by measuring peak-to-peak current at random points along the baseline.

Fluorescent images were acquired using a Nikon Eclipse TE2000-U microscope equipped with a CCD camera (Photometrics Cool Snap cf) and MetaMorph software. In order to determine if solution was leaking down the electrode channels, 1mM FITC was injected into the separation channel and imaged as it passed the electrodes.

4.2 Results and Discussion

4.2a Chip Design.

In initial iterations of the microwire design the electrode channel was sealed with RTV silicone to prevent leakage into the side channels. In the development of the decoupler here, a small (50 μm) gap was used to block flow down the electrode channels. The PDMS forms around the wire, preventing flow down the electrode channel. It is

obvious from the microscope image that a gap exists between the wire and the PDMS (Figure 4.1). In order to evaluate the amount of leakage through the electrode channel, we injected a fluorescent dye (FTIC) into the channel and imaged the electrode intersection (Figure 4.1B). As is seen in these images no dye enters the electrode channel despite the presence of small gaps between the electrode and the PDMS. A more sensitive fluorescent detection system may have the ability to visualize a leakage; however, at the limits we were able to detect we saw no leakage. The mechanism preventing flow down these channels is under investigation. It should be noted, however, that these results are consistent with the work of Kovarik *et al.*[13] when they sealed PDMS over a raised carbon electrode and saw no leaking of solution around the electrode.

4.2b MCE-EC.

The optimization of the distance between the working electrode and decoupling electrode is shown in Figure 4.4. A decreasing trend in background noise was seen when separating the decoupler and working electrode by 50 – 250 μm. At distances above 250 μm the background noise leveled off and no statistical improvement was seen. Figure 4.2 also shows an increase in peak width based on the distance between the decoupler and working electrode due to the change from plug flow (before the decoupler) to hydrodynamic flow (after the decoupler). Due to the parabolic shape of hydrodynamic flow the longer the distance the analyte has to travel before reaching the working electrode the wider the peaks become. 250 μm was chosen as the optimal distance for both low noise levels and smaller peak widths. The effect of applied separation

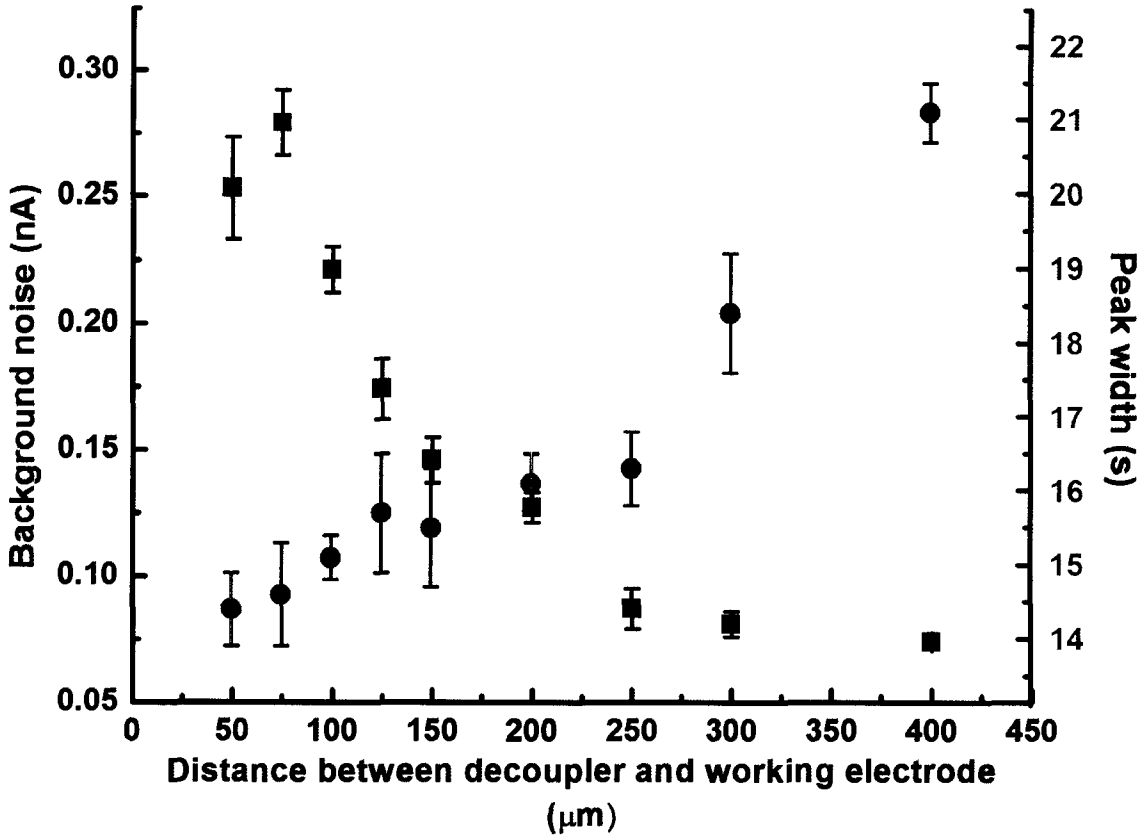

Figure 4.4: Optimization of distance between the working electrode and decoupling electrode. Left axis (black), shows the background noise as a function of distance. Right axis (red), shows the peak width as a function of distance.

voltage on baseline noise for EC was also evaluated at a 250 μm separation between the electrodes (Figure 4.5). The applied separation voltage was varied from 800 to 1500V (131 V/cm – 245 V/cm) while the baseline noise was measured at a 25 μm Au working electrode using either the decoupler or a Pt wire in the waste reservoir as the cathode. Due to channel dimensions the PDMS channels have been seen to fail at separation voltages above 1500-1600 V. A significant decrease in noise was noted when using the Pd microwire as the cathode, especially at higher separation potentials. An increase in noise was observed with the increase in separation potential for the decoupled system, indicating that the EC was still being partially influenced by the separation current. The addition of a second decoupler wire in the decoupler channel was explored to see if a further reduction in noise was possible with an increased electrode area/volume. No significant improvement over the use of only a single decoupling wire was seen, indicating that the decoupling was not influenced by the microwire volume or surface area in the present design.

Dopamine, catechol, and ascorbic acid were chosen as model analytes to characterize the decoupled CE-EC microchips with amperometric detection to provide a comparison to previous work in the field.[1, 5, 6, 12, 14] Representative electropherograms for the separation of dopamine, catechol and ascorbic acid at different concentrations are shown in Figure 4.6. All separations were performed using 20mM TES buffer (pH 7.0) at an electric field of 200 V/cm and a 15 s injection time. All three electropherograms in

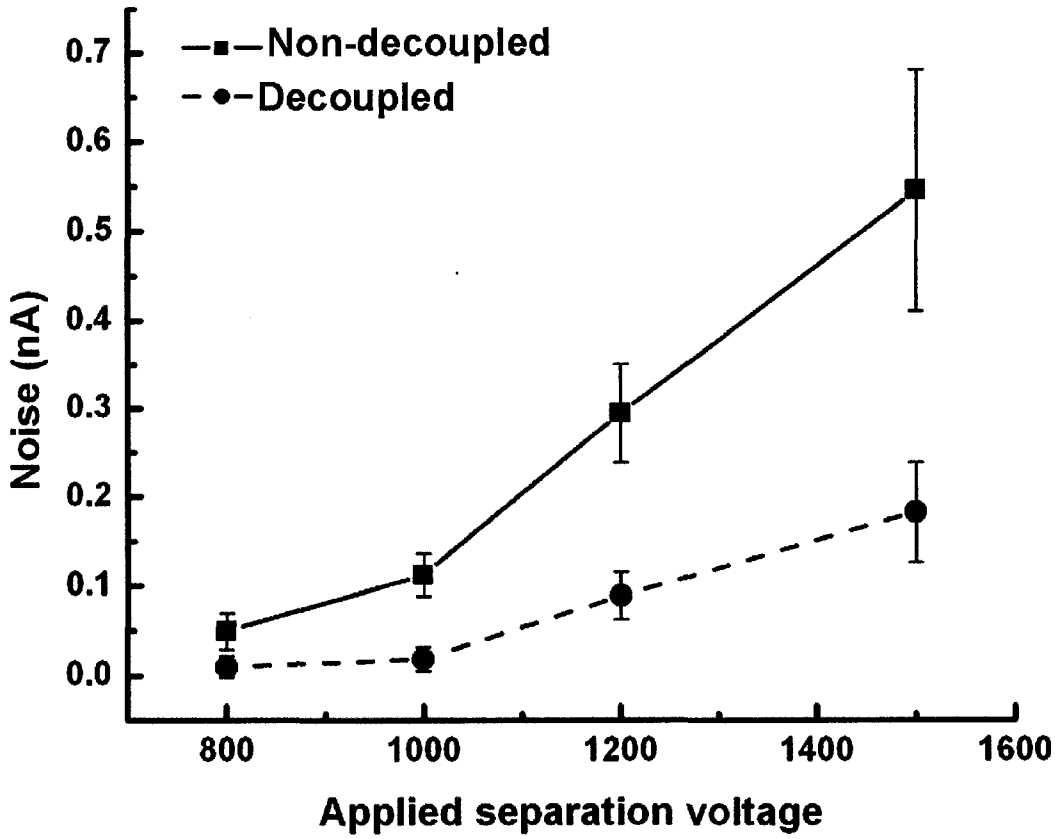

Figure 4.5: The effect of applied voltage on the background noise measured at the working electrode with and without use of the decoupler. Peak-to-peak noise was measured at random points along the baseline. Standard deviations were calculated at $n \geq 30$. Experimental parameters: Working electrode: 25 μm Au microwire; Pinched injection time: 15 s; Running buffer: 20 mM TES (pH 7.0).

Figure 4.6 were achieved using optimized conditions and showed baseline resolution for the separation of dopamine, catechol and ascorbic acid. As expected, a linear decrease in signal was observed with decreasing analyte concentration. The linear ranges for catechol and ascorbic acid were established over a range from 50 nM-100 μM using 6 points. The linear range for dopamine was determined by 7 concentration measurements over a range from 5 nM-100 μM. Separation efficiencies measured from the 100 μM separation were 15207.7, 32628.5 and 25261.6 N/m for dopamine, catechol and ascorbic acid, respectively.[8]

4.2c Limits of Detection.

An electropherogram of the measured limit of detection is shown in the insert of Figure 4.6. The measured detection limits were 5 nM dopamine (S/N = 3.34), 50 nM catechol (S/N = 3.21) and 50 nM ascorbic acid (S/N = 2.85). Based on 5nM detection for dopamine with a 250 pL injection volume, a detection limit of 1.25 zeptomoles (10^{-18}) was achieved for dopamine. The detection limit of 5 nM for dopamine is the lowest to date for microchip CE-EC to the best of our knowledge. The relative standard deviation of the peak height from electropherograms of dopamine, catechol and ascorbic acid at their LODs were 8.1%, 10.1%, and 10.0% respectively (n=6).

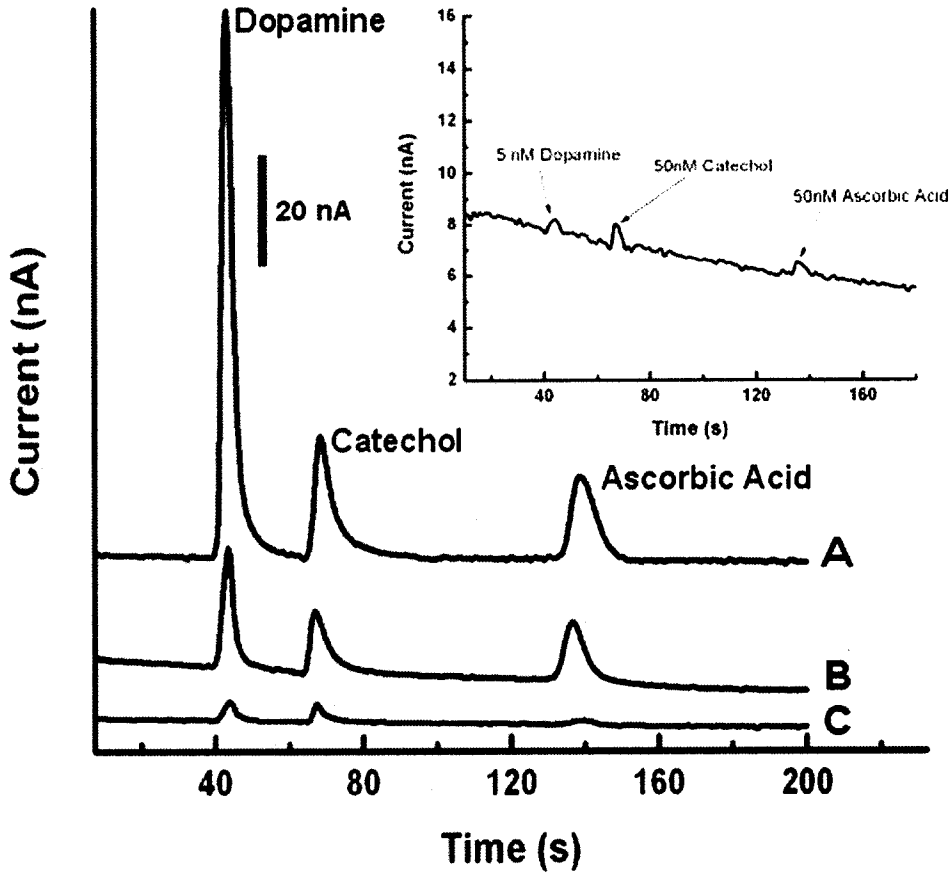

Figure 4.6: Representative electropherograms obtained using a decoupled system. A) 50 μM dopamine, 50 μM catechol, and 50 μM ascorbic acid; B) 5 μM dopamine, 5 μM catechol, and 5 μM ascorbic acid; C) 50 nM dopamine, 500 nM catechol, and 500 nM ascorbic acid. **Insert:** Limits of detection were seen as 5nM for dopamine (S/N = 3.34), 50 nM for catechol (S/N = 4.21), and 50 nM for ascorbic acid (S/N = 2.85). Experimental conditions: 0.7 V detection potential; Field strength: 200 V/cm; Pinched injection time: 15 s; Running buffer: 20 mM TES (pH 7).

4.2d Microchip CE-PAD.

Glucose, glucose-6-phosphate, cysteine and glutathione were chosen as model carbohydrate and thiol analytes to characterize decoupled MCE-PAD because of their tendencies to foul Au electrodes. The effect of detection potential on the signal was analyzed between 0.1 and 1.6 V for all four analytes on both non-decoupled and decoupled microchips. Figure 4.7 shows the resulting hydrodynamic voltamograms (HDV) for glucose and cysteine as representatives of each analyte class. The peak current increases as the potential increases until current maxima are obtained. When the detection potential is increased further the peak current decreases. This decrease can be attributed to the formation of an insulating Au oxide layer on the working electrode.[15] HDVs for 1mM samples on a decoupled microchip show an increase in signal as well as a shift in the optimal detection potential over non-decoupled microchips (Figure 4.7). The increased signal as well as the shift in optimal detection potential in the decoupled chips can be attributed to a reduction in the separation field felt by the working electrode and is consistent with previous work.[16] Optimal detection potentials for the carbohydrates and thiols were determined to be 0.6 V and 1.4V, respectively, using the decoupler.

Carbohydrates, glucose and glucose-6-phosphate play an important role in biological systems and were chosen for these experiments because of their tendencies to foul Au electrodes. An electropherogram for the separation of these carbohydrates is shown in Figure 4.8A. The separation was performed using 20mM boric acid, 0.8mM SDS (pH 12.00) BGE at a field strength of 200 V/cm with a 15 sec. injection time. Migration times of 47 ± 1.2 s (n=5) for

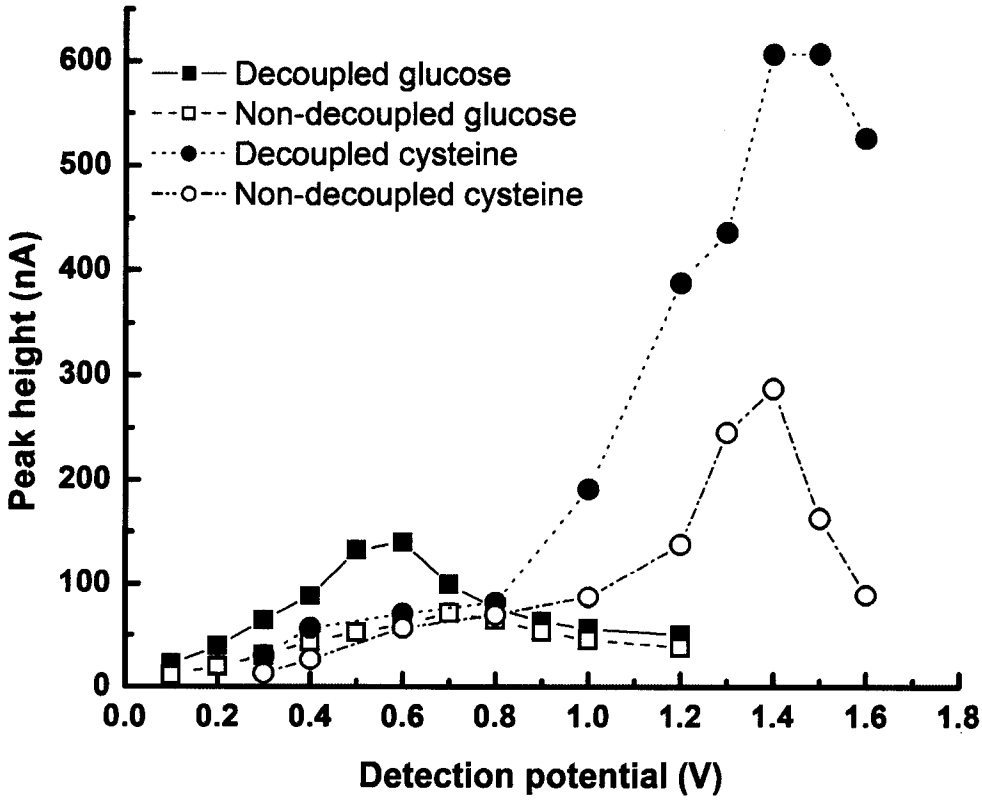

Figure 4.7: Hydrodynamic voltammograms for 1mM glucose (■) decoupled, (□) non-decoupled, and 1 mM cysteine (●) decoupled, (○) non-decoupled. Experimental conditions: Buffer: 20 mM boric acid, 0.8 mM SDS (pH 12.0 for carbohydrates, pH 9.4 for thiols); Field Strength: 220 V/cm; Pinched injection time: 15s.

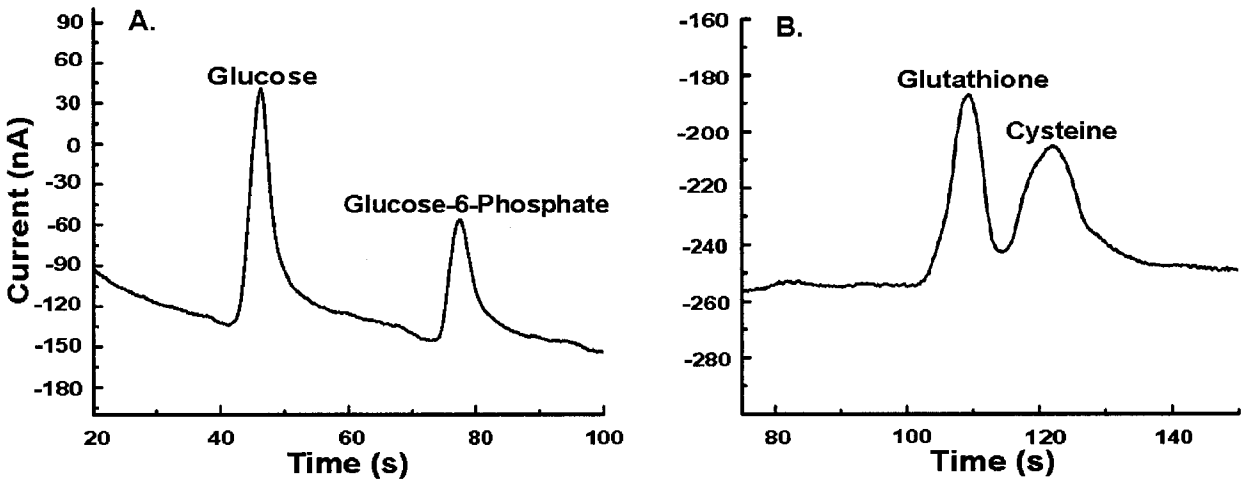

Figure 4.8: **A.** Example electropherogram using a decoupled system for the separation of 1mM glucose and 1mM glucose-6-phosphate. PAD waveform: cleaning (1.6 V for 0.05s), regeneration (-0.5 V for 0.025s), detection (0.6 V for 0.15 s). Experimental conditions: Field strength: 220 V/cm; Pinched injection time: 15 s; Running buffer: 20 mM boric acid, 0.8 mM SDS (pH 12.0). **B.** Example electropherogram using a decoupled system for the separation of 1μM cysteine and 1μM glutathione. PAD waveform: cleaning (1.6 V for 0.05s), regeneration (-0.5 V for 0.025s), detection (1.3 V for 0.15 s). Experimental conditions: Field strength: 220 V/cm; Pinched injection time: 15 s; Running buffer: 20 mM boric acid, 0.8 mM SDS (pH 9.4).

glucose and 79 ± 1.6 s (n=5) for glucose-6-phosphate were observed. The electropherogram in Figure 4.8A was obtained using optimal conditions for carbohydrates and showed baseline resolution with separation efficiencies of 10300 N/m for glucose and 42520 N/m for glucose-6-phosphate. The linear range based on peak height for both glucose and glucose-6-phosphate had R^2 values of >0.992 (101nM - 1mM and 590nM -1mM respectively). The chip-to-chip reproducibility, expressed as a RSD of peak height was found to be 9.1% for three runs on each of three different chips for 1 mM glucose.

The direct detection of thiols has the potential to simplify the quantification of these important biological compounds. Glutathione and cysteine are present in high concentrations (μM) in various body fluids and tissues and were chosen as model analytes for this work.[17] An electropherogram for the separation of cysteine and glutathione is shown in Figure 4.8B. The separation was performed using 20mM boric acid, 0.8mM SDS (pH 9.4) buffer solution at an electric field of 200 V/cm with a 15 s injection time. Migration times of 109 ± 3.6 s (n=5) for glutathione and 123 ± 2.3 s (n=5) for cysteine were observed. The electropherogram in Figure 4.8B was achieved using 1.3 V as the detection potential. The linear range based on peak height for both cysteine (614nM - 1mM) and glutathione (74nM - 1mM) had R^2 values of 0.992 and 0.988 respectively. Separation efficiencies of 22828.5 and 35979.4 N/m were seen for cysteine and glutathione respectively. Although not completely baseline resolved, a distinct separation between the two thiols can be seen (R_s=0.949). The peak broadness and the inability to resolve them can be attributed to both poor separation efficiency of all

electrophoretic separations performed on PDMS[18] as well as the formation of parabolic flow after the decoupler .

4.3 Conclusions

We have presented a simple and successful incorporation of microwires as working electrodes and decouplers in PDMS microchips for CE-EC and CE-PAD. We have demonstrated the ability to incorporate multiple electrodes with differing electrode materials in the same microchip. This ability allows the use of Au and Pt as the working electrodes and Pd as a decoupling electrode. The circuitry of EC detection is decoupled from that of CE separation, dramatically decreasing the noise from 0.3 to 0.05 nA when comparing non-decoupled to a decoupled microchip at 1200 V separation potential. This decrease in noise allows us to achieve low detection limits (5 nM) and extend the application of microchip CE-EC and CE-PAD to many more analyte classes than previously possible.

4.4 Acknowledgements

I would like to thank Dr. Carlos Garcia and Dr. Yan Liu for useful discussions regarding microchip design and fabrication.

(1) Lacher, N. A.; Lunte, S. M.; Martin, R. S. *Anal Chem* **2004**, *76*, 2482-2491.
(2) Rossier, J. S.; Ferrigno, R.; Girault, H. H. *J Electroanall Chem* **2000**, *492*, 15-22.
(3) Osbourn, D. M.; Lunte, C. E. *Anal Chem* **2001**, *73*, 5961-5964.
(4) Osbourn, D. M.; Lunte, C. E. *Anal Chem* **2003**, *75*, 2710-2714.
(5) Chen, D. C.; Hsu, F. L.; Zhan, D. Z.; Chen, C. H. *Anal Chem* **2001**, *73*, 758-762.
(6) Wu, C. C.; Wu, R. G.; Huang, J. G.; Lin, Y. C.; Hsien-Chang, C. *Anal Chem* **2003**, *75*, 947-952.
(7) Kok, W. T., Sahin, Yuksel *Anal Chem* **1993**, *65*, 2497.
(8) Vickers, J. A.; Henry, C. S. *Electrophoresis* **2005**, *26*, 4641-4647.
(9) Shultz-Lockyear, L. L.; Colyer, C. L.; Fan, Z. H.; Roy, K. I.; Harrison, D. J. *Electrophoresis* **1999**, *20*, 529-538.
(10) Jacobson, S. C.; Hergenroeder, R.; Koutny, L. B.; Ramsey, J. M. *Anal Chem* **1994**, *66*, 2369-2373.
(11) Garcia, C. D.; Henry, C. S. *Anal Chem* **2003**, *75*, 4778-4783.
(12) Liu, Y.; Vickers, J. A.; Henry, C. S. *Anal Chem* **2004**, *76*, 1513-1517.
(13) Kovarik, M. L.; Li, M. W.; Martin, R. S. *Electrophoresis* **2005**, *26*, 202-210.
(14) Lai, C. C.; Chen, C. H.; Ko, F. H. *J Chrom A* **2004**, *1023*, 143-150.
(15) Garcia, C. D.; Henry, C. S. *Electroanalysis* **2005**, *17*, 1125-1131.
(16) Martin, R. S.; Ratzlaff, K. L.; Huynh, B. H.; Lunte, S. M. *Anal Chem* **2002**, *74*, 1136-1143.
(17) Sato, K.; Yamanaka, M.; Takahashi, H.; Tokeshi, M.; Kimura, H.; Kitamori, T. *Electrophoresis* **2002**, *23*, 734-739.
(18) Hu, S. W.; Ren, X. Q.; Bachman, M.; Sims, C. E.; Li, G. P.; Allbritton, N. L. *Langmuir* **2004**, *20*, 5569-5574.

Chapter 5

Microchip CE with Dual Electrode Electrochemical Detection

Electrochemical detection is considered a selective detection technique.[1, 2] Selectivity for carbohydrates, amines, alcohols or thiols is achieved by varying the potential of the working electrode. However, there are often situations where even greater selectivity is desired. An example of one of these situations is in the analysis of complex biological samples such as blood, serum or urine. Increased selectivity can be achieved with electrochemical detection by using chemically modified electrodes or multiple-electrode systems. Chemically modified electrodes, while useful to increase selectivity, are more difficult to incorporate into a microchip than standard gold electrodes. The development of a PDMS MCE-EC system employing dual electrode detection is described. The device consists of PDMS fabricated MCE devices with incorporated Pd and Au microwires used as the decoupler and working electrodes, respectively. Dual-electrode detection in a series configuration is shown to be useful for the selective analysis of analytes that undergo chemically reversible redox reactions and for the selective detection of easily oxidizable analytes in a more complex mixture. The use of dual electrode detection presented in this chapter was performed to further demonstrate the ability to incorporate multiple detection techniques and to improve the selectivity of our microwire devices. Two different modes of dual electrode detection were used to show selectivity for analytes with reversible redox reactions and easily oxidizable analytes.

5.1 EXPERIMENTAL

5.1a Chemicals and Materials.

The following chemicals and materials were used as they were received: SU-8 2035 photoresist (Micro Chem. Corp., Newton, MA), propylene glycol methyl ether acetate (Aldrich), 4" silicon wafers (Silicon Inc., Boise, ID), poly(dimethylsiloxane) (PDMS) (Dow Corning), Sylgard 184 elastomer curing agent (Dow Corning), sodium hydroxide (Fisher, ACS), boric Acid (Fisher, 99%), sodium dodecyl sulfate (SDS) (Fisher, 97%), methanol (Fisher, ACS), 2-propanol (Fisher, ACS). Electrochemically active analytes used were catechol (Sigma), 3,4-dihydroxyphenethylamine (dopamine) (Sigma, 99%), ascorbic acid (Sigma, 99%), tyrosine (Sigma, 99%) and l-arginine (Sigma, 99%). Microwires made of 99.99 % Pd (diameter 0.025 mm) and 99.99 % Au (diameter 0.025 mm) were obtained from Goodfellow (Huntingdon, England).

5.1b Dual Electrode Microchip CE.

The dual electrode microchips were designed with three electrode channels spanning the separation channel in order to incorporate the decoupler and two working electrodes.[3] A Pd microwire was placed in the most upstream electrode channel (25 μm wide) for use as the cathode as discussed in chapter 4. The working electrodes were placed downstream in the two other electrode channels. The distance between the decoupler electrode and the closest working electrode was fixed at 250 μm based on results presented in chapter 4. The second working electrode was placed 70 μm downstream from the first working electrode and 320 μm from the decoupler (Figure 5.1). The fully assembled microchips were allowed to sit for 24 hours

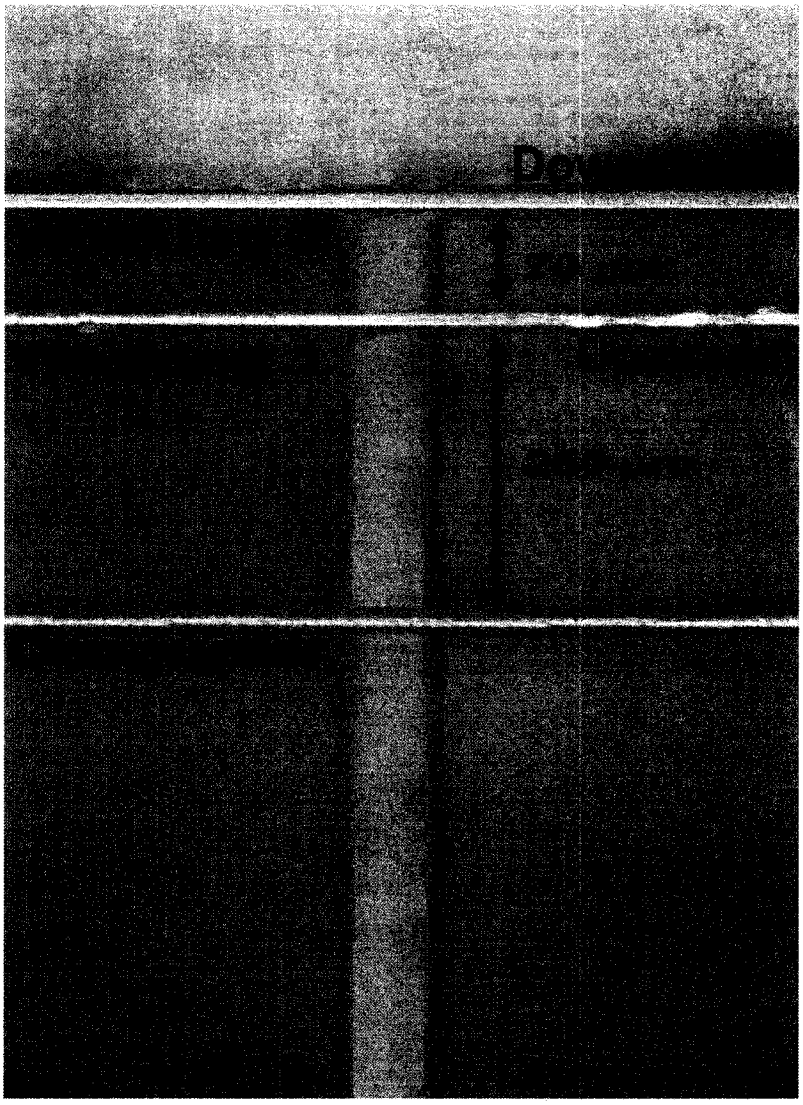

Figure 5.1: Photograph of a fully assembled microchip used in dual electrode electrochemical detection.

before use in experiments. This was done to allow the EOF of plasma sealed chips to decrease to a stable level. For separations, 800-1500 V was applied to the buffer reservoir while the Pd decoupler was kept at ground. The sample and sample waste reservoirs were held at 450 V for push back. Pinched injection through a 250 pL double-T injector was employed for all experiments.[4-6]

The microchip was designed to prevent solution from flowing down the decoupler electrode channel. The decoupler and working electrode channels were fabricated with a 50 μm gap between the separation and electrode channels as seen in chapter 4, Figure 4.1. The gap allows the PDMS to form a seal around the microwire, isolating the electrode channel from the separation channel. After all three electrodes were aligned and sealed in place, a 0.80 mm copper wire was attached to the exposed microwires with conductive silver paint and held in place with glue. In situ cleaning of both working electrodes was done every 15 - 20 runs via cyclic voltammetry (CV) with 20 sweep segments from -1.0V to 1.0V at the rate of 0.1 V/s while buffer was electrokinetically pumped over the electrode. [3] The Pd decoupler was cleaned initially by running a CV from -1.0V to 1.0V at 0.1 V/s for 50 cycles.

5.1c Dual Electrode Detection.

Amperometry was used at both working electrodes for the detection of all analytes (CHI812, CH Instruments). All experiments were run in a two-electrode configuration with a Pt wire (1 mm diameter) in the waste reservoir used as the counter electrode. Au working electrodes (25 μm diameter wire) were used for dual electrode amperometry. Noise was determined by measuring peak-to-peak current at random

points along the baseline. Two different modes of dual electrode detection were used. The first is an oxidation/reduction mode, in which a high oxidizing potential is applied to the first working electrode (upstream) while a low reducing potential is applied to the second working electrode (downstream) (Figure 5.1). This mode allows for the selective detection of redox reversible analytes. Dopamine, catechol and ascorbic acid were chosen as model analytes for this mode of detection. Dopamine and catechol have a reversible electrochemistry while ascorbic acid doesn't show a reduction once it has been oxidized.[7] The lack of a reduction peak for ascorbic acid is due to the instability of dehydroascorbic acid and/or the slow kinetics of the reverse reaction.

The second mode involves an increasing detection potential from the first to the second working electrode. This allows for selective detection of analytes with low detection potentials. Dopamine, catechol, ascorbic acid, tyrosine and L-arginine were chosen as model analytes to show the abilities of this detection mode. Detection potentials were determined experimentally versus a Pt counter electrode (Table 5.1). Dopamine and catechol are oxidizable at lower detection potentials while ascorbic acid, tyrosine and L-arginine require higher potentials for oxidation.

Table 5.1: Detection Potentials for Analytes used in Dual Electrode Detection

Analyte	Minimum Detection Potential (V)	Maximum Signal (V)
Dopamine	0.1	0.8
Catechol	0.1	0.8
Ascorbic Acid	0.5	1.1
Arginine	0.8	1.5
Tyrosine	0.7	1.2

Minimum detection potential is the lowest potential at which an electrochemical signal is seen in an HDV
Maximum Signal is the detection potential at which the maximum peak height is achieved
All potentials are measured versus a platinum counter electrode

5.2 RESULTS AND DISCUSSION

5.2a Oxidation/Reduction Detection

Oxidation/reduction dual electrode detection was done using 10 μM dopamine, catechol and ascorbic acid with a 20 mM TES BGE at pH 7.0. The first working electrode was set at a detection potential of 0.8 V and the second working electrode was set at a detection potential of 0.2 V based on the experimentally determined E_{oxd} for the analytes in question. Figure 5.2 shows representative electropherograms of dopamine and catechol as they are detected using dual electrode detection in the oxidation/reduction mode. The black electropherogram represents an oxidation of the analytes as they pass the first working electrode while the red electropherogram is the reduction of the oxidized compounds as they pass the second working electrode. An irreversible analyte (ascorbic acid) was added to the dopamine and catechol to show the selectivity of this mode of dual electrode detection (Figure 5.3). The blue electropherogram comes from the first working electrode (upstream electrode) where the analytes are oxidized as they pass over the electrode with the high detection potential. This oxidation is represented by positive peaks. The red electropherogram represents the signal seen for the second working electrode (downstream electrode) as the already oxidized analytes are reduced at the lower potential applied to the second electrode. Three positive peaks can be seen for the oxidation of all three analytes at the first working electrode but reduction peaks can only be seen for dopamine and catechol at the second working electrode. The ability to look selectively at reversible versus irreversible analytes has many benefits, especially when analyzing complex samples such as blood or urine. The decrease in peak

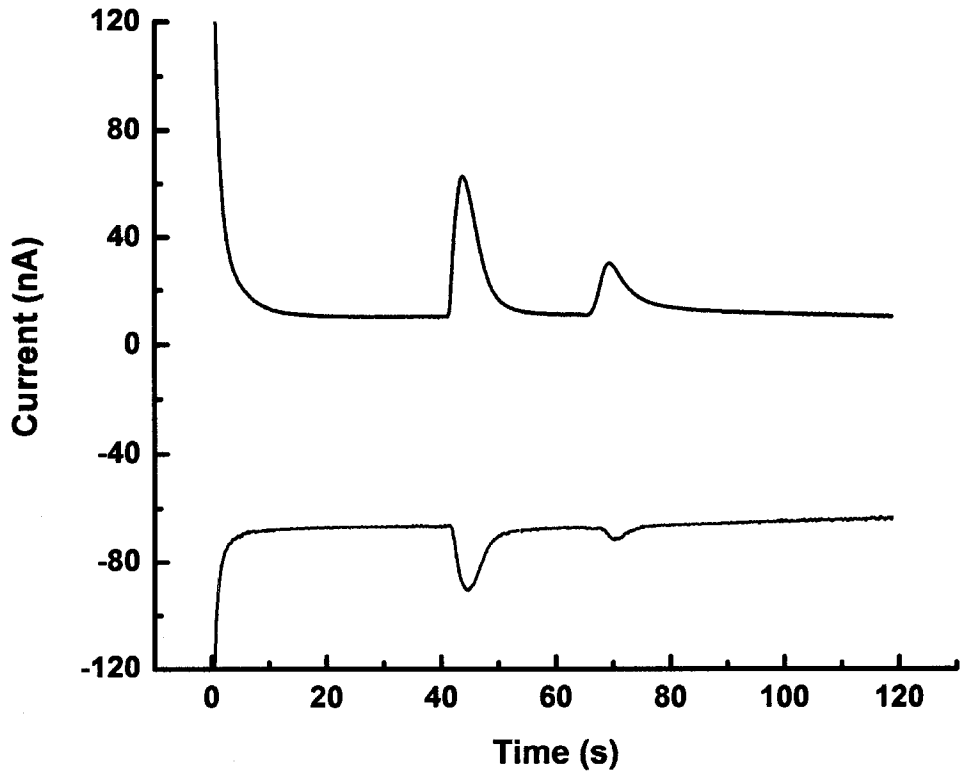

Figure 5.2: Electropherograms for the oxidation/reduction dual electrode detection of 10 μM dopamine and catechol. Experimental conditions: Background electrolyte: 20 mM TES, pH 7.0, 1100 V separation potential, 0.8 V detection potential at first working electrode (upstream, black), 0.2 V detection potential at second working electrode (downstream, red)

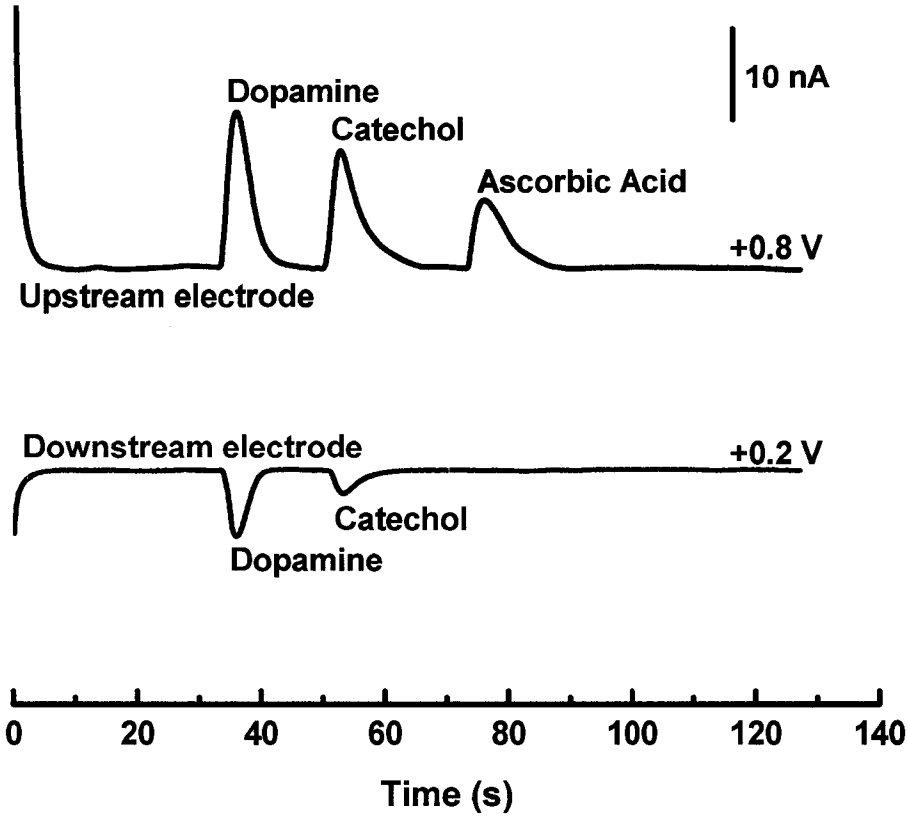

Figure 5.3: Electropherograms for the oxidation/reduction dual electrode detection of 10 μM dopamine, catechol and ascorbic acid. Blue electropherogram shows an oxidation of the analytes at the first working electrode. Red electropherogram shows a reduction of the reversible species in the sample at the second working electrode. Experimental conditions: Same as Figure 5.2

magnitude from the first working electrode to the second working for dopamine and catechol can be explained by the collection efficiencies of the electrodes (chapter 3). A collection efficiency of 36% is seen at both working electrodes. The concentration of analyte before oxidation at the first working electrode is much higher than the concentration of analyte in the oxidized form, that will be reduced at the second working electrode.

5.2b Increasing Potential Detection

Increasing potential dual electrode detection was done using 10 μM dopamine, ascorbic acid, tyrosine, L-arginine and 20 μM catechol with a 20 mM boric acid BGE at pH 9.4. The first working electrode was set at a detection potential of 0.2 V and the second working electrode was set at a detection potential of 1.5 V based on the E_{oxd} of the analytes of interest (Table 5.1). Figure 5.4 shows electropherograms for the dual electrode detection of L-arginine, tyrosine, dopamine, catechol and ascorbic acid. The blue electropherogram is from the first working electrode (upstream electrode) and show the easily oxidizable analytes, dopamine and catechol. The red electropherogram is at a high detection potential (1.5 V) and allows all of the analytes in the sample to be oxidized. The increasing potential method allowed for the detection of specific analytes with low detection potentials to be selectively chosen from a more complex group of electrochemically active analytes. This method can be beneficial when deciphering complex mixtures in which important compounds with low oxidation potentials can co-migrate or overlap with compounds that have higher oxidation potentials. In this detection mode dopamine and catechol were oxidized and showed positive peaks at a

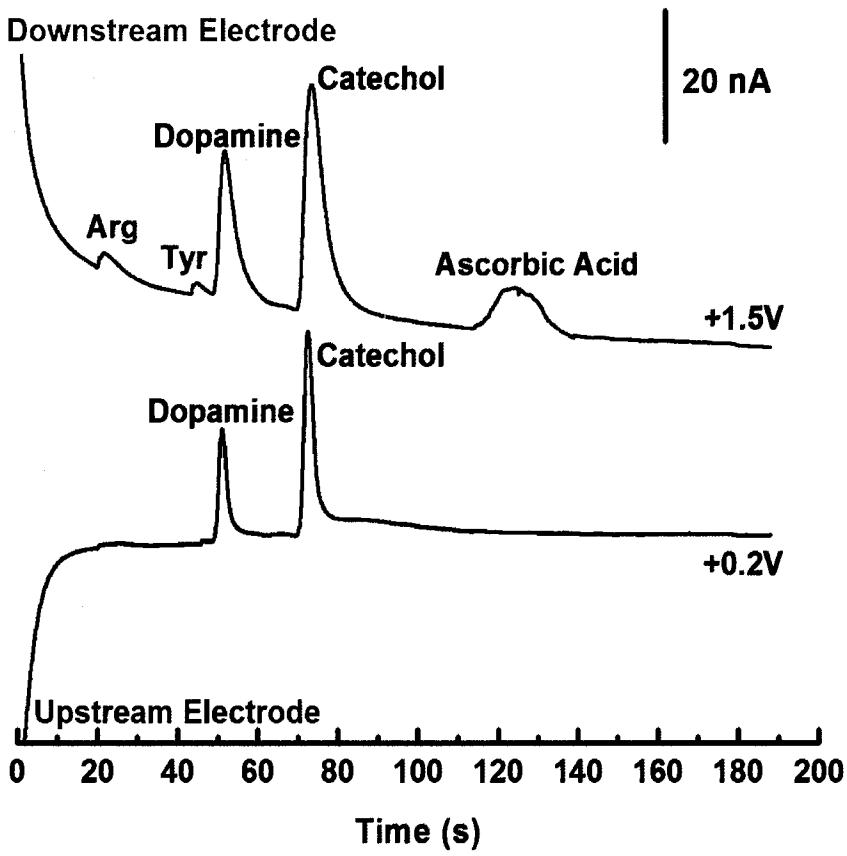

Figure 5.4: Electropherograms for the increasing potential dual electrode detection of 10 μM L-arginine, tyrosine, dopamine, ascorbic acid and 20 μM catechol. Blue electropherogram shows the easily oxidized analytes in the sample mixture oxidizing at a low potential. The red electropherogram show a separation and detection of all of the compounds in the sample mixture when oxidized at a high detection potential. Experimental conditions: Background electrolyte: 20 mM boric acid, pH 9.4, 1100 V separation potential, 0.2 V detection potential at first working electrode (upstream, blue), 1.5 V detection potential at second working electrode (downstream, red)

detection potential of 0.2 V (Figure 5.4) while in the oxidation/reduction mode dopamine and catechol are reduced and show negative peaks in the electropherogram at the same detection potential (+0.2 V, Figure 5.3). This is due to the oxidation state at which the analytes are in when they come into contact with the working electrode. In the oxidation/reduction mode, both compounds were in an oxidized state after they came into contact with the first working electrode. In the increasing potential mode the compounds not previously oxidized by the upstream electrode can become oxidized when they come in contact with the downstream electrode.

5.3 CONCLUSIONS

Dual electrode detection shows an improved selectivity for specific analytes over standard amperometry because it allows for the manipulation of multiple detection potentials to see specific compounds selectively. Here I have shown the feasibility of this method of electrochemical detection. An increased selectivity was seen when looking for analytes with reversible redox reactions and easily oxidized analytes in a five component mixture. A multitude of analytes could be looked at selectively by this method depending on the detection potentials chosen for each electrode. Future experiments with this method of electrochemical detection will revolve around the incorporation of PAD. DC amperometry at the up stream electrode followed by PAD at the downstream electrode will allow for the simultaneous detection of both DC amperometry active and PAD active analytes in a single sample.

(1) Voegel, P. D.; Baldwin, R. P. *Electrophoresis* **1997**, *18*, 2267-2278.
(2) Lawrence, N. S.; Davis, J.; Compton, R. G. *Talanta* **2001**, *53*, 1089-1094.
(3) Liu, Y.; Vickers, J. A.; Henry, C. S. *Anal Chem* **2004**, *76*, 1513-1517.
(4) Shultz-Lockyear, L. L.; Colyer, C. L.; Fan, Z. H.; Roy, K. I.; Harrison, D. J. *Electrophoresis* **1999**, *20*, 529-538.
(5) Jacobson, S. C.; Hergenroeder, R.; Koutny, L. B.; Ramsey, J. M. *Anal Chem* **1994**, *66*, 2369-2373.
(6) Garcia, C. D.; Henry, C. S. *Anal Chem* **2003**, *75*, 4778-4783.
(7) Ruiz, J. J.; Rodriguezmellado, J. M.; Dominguez, M.; Aldaz, A. *J Chem Soc-Faraday Trans I* **1989**, *85*, 1567-1574.

Chapter 6

Surface Modified PDMS for Use with Microchip CE-EC

The hydrophobic nature of PDMS contributes in the limitations of its applicability for MCE, microfluidic patterning and other non-electrophoresis applications. The surface of PDMS can be made hydrophilic using a simple air plasma treatment;[1] however, this property is quickly lost through hydrophobic recovery caused by diffusion of unreacted oligomer to the surface as discussed in chapter 1.[2, 3] Here, a simple approach for the generation of hydrophilic PDMS with long term stability (days) in air is presented. PDMS was rendered hydrophilic as determined by contact angle measurements through a simple two-step extraction/oxidation process. First, PDMS was extracted in a series of solvents designed to remove unreacted oligomers from the bulk phase. Second, the oligomer-free PDMS was oxidized in a simple air plasma, generating a stable layer of hydrophilic SiO_2 as determined by XPS. The result of this modification was a significant improvement in the performance of PDMS for microchip electrophoresis and microfluidic applications. This work has been previously published in *Analytical Chemistry*.[4] While this paper had a co-author, Meghan Caulum, all of the presented work was done by the author.

The research presented in this chapter was done in order to improve separation properties of our microfluidic devices. Improvements in separation efficiencies and peak skews are needed in order to separate complex biological samples. In this work I show a dramatic increase in separation efficiencies and a decrease in peak skew through a simple extraction and oxidation procedure.

6.1 EXPERIMENTAL

6.1a Chemicals and Materials.

The following chemicals and materials were used as received: SU-8 2035 photoresist (MicroChem. Corp., Newton, MA), propylene glycol methyl ether acetate (Aldrich, St. Louis, MO), 4" silicon wafers (Silicon Inc., Boise, ID), poly(dimethylsiloxane) (PDMS) (Dow Corning, San Diego, CA), Sygard 184 elastomer curing agent (Dow Corning), sodium hydroxide (Fisher, ACS, Pittsburgh, PA), N-tris[Hydroxymethyl]methyl-2-aminoethanesulfonic acid (TES) (Sigma, 99%), boric acid (Fisher, 99%), methanol (Fisher, ACS), 2-propanol (Fisher, ACS), catechol (Sigma, ACS), 3,4-dihydroxyphenethylamine (dopamine, 99%, Sigma), ascorbic acid (Sigma, 99%), doxorubicin (Fluka, 99%), daunorubicin (Fluka, 99%), triethylamine (Sigma, ACS), ethyl acetate (Sigma,ACS), 1,4-diaminobutane (Sigma, 99%), and fluorescein isothiocyanate (FITC) (Molecular Probes, 95%). Microwires made of 99.99 % Pd (diameter 0.025 mm) and 99.99 % Au (diameter 0.025 mm) were obtained from Goodfellow (Huntingdon, England).

6.1b Fabrication of PDMS Microchips.

The fabrication of poly(dimethylsiloxane) (PDMS) microchips using SU-8 molding has been described in detail previously in chapter 2.[5-9] For extraction of unreacted oligomers, the imprinted PDMS and an unpatterned PDMS piece were placed in a series of three organic solvents for extraction. These solvents were selected based on work published by Lee *et al.*[1] After extraction, electrodes were aligned in pre-designated electrode channels for chips used with electrochemical detection.[6, 10] The extracted PDMS replica and a blank piece of extracted PDMS were placed in an air plasma cleaner (Harrick plasma cleaner/sterilizer PDG-32G) and oxidized for 30 sec at 18 W unless

otherwise noted. The two pieces were brought into conformal contact directly after removal from the plasma to form an irreversible seal.[5, 8, 11]

6.1c PDMS Extraction

For PDMS extraction, a molded PDMS piece and a blank PDMS piece were immersed in 200 mL of a triethylamine solution at 25° C for 2 hrs. The triethylamine was refreashed after 1 hr. The PDMS was removed from the triethylamine and placed in 200 mL of an ethyl acetate at 25° C for 2 hrs, replacing with fresh solvent after 1 hr. The PDMS pieces were then placed in 200 mL of acetone for 2 hrs. The solvents were stirred during the PDMS extraction steps. Finally the pieces were allowed to dry completely in a 65° C oven for 2 – 6 hrs. The percent extracted PDMS (w/w) was calculated by determining the difference in the mass between the native and extracted PDMS and dividing by the mass of the native PDMS.

6.1d Surface Composition

Determination of PDMS surface chemistry was performed by X-ray Photoelectron Spectroscopy (XPS) and contact angle measurements. XPS (PHI 5800 ESCA System) was used with an Al monochromatic X-ray source at a 45° incidence angle with a pass energy of 23.5 eV. XPS of native and extracted PDMS was performed for non-oxidized and oxidized pieces. Measurements of the same PDMS piece were done at 30 min, 3 hrs and 7 days after oxidation with samples stored in air in a pétri dish between runs. Oxidized and non-oxidized samples of both native and extracted PDMS were cut to 1 cm x 1 cm x 1 mm with a razor blade for contact angle measurements.

Measurements were taken on day one and day seven at 25° C using a Kruss drop shape analysis system DSA 10.

6.1e MCE

A 250 μm double-T injector was employed for all experiments.[12-14] An injection volume of 1.1 nL was obtained for the microchips used with electrochemical detection The large injection volume on the chips is the result of the need to apply a constant ground potential in the waste reservoir to prevent overloading of the detection circuitry. The constant ground potential applied to the waste reservoir causes some sample to flow down the separation channel during the injection and thus increasing the sample plug size. The application of the electrical ground is necessary with EC detection to prevent exposing the detector electronics to high voltage. A reservoir was filled with 1.0 M NaOH; capillary action caused the solution to flow through the microchannels freely and was used to pretreat the channels at the beginning of each day for 30 min. The channels were then filled with background electrolyte (BGE) by applying a vacuum to the buffer reservoir. Before analysis, BGE in the sample reservoir was replaced with sample solution. Microchips for electrochemical detection were fabricated with two electrode channels perpendicular to the separation channel to incorporate microwire electrodes usingthe design presented in chapter 4.[10] A Pd microwire decoupler (25 μm wide) was placed in the first electrode channel (most upstream electrode) for use as the cathode. The working electrode (25 μm Au) was placed downstream from the decoupler in the second electrode channel. The distance between the two electrodes has been shown to be optimized at 250 μm based on previous work by Lacher *et al.*[15] and experiments in our

lab.[10] After each electrode was aligned and sealed in place, a 0.80 mm copper wire was attached to the exposed microwire end with conductive silver paint and held in place with silicon RTV sealant (Dow Corning 732). A 1000 V (170 V/cm) separation potential was applied to the buffer reservoir while the Pd decoupler was kept at ground. A 300 V push back potential was applied to the sample and sample waste reservoirs to prevent leakage as described in chapter 2..

6.1f Detection

The working electrode was cleaned every 15 runs using cyclic voltammetry (CV) from -1.0 V to 1.0 V at the rate of 0.1 V/s while buffer was electrokinetically pumped over the electrode.[6] CV was allowed to proceed until six consecutive sweep segments overlapped. The Pd decoupler was cleaned and conditioned initially by running a CV from -1.0 V to 1.0 V at 0.1 V/s for 50 cycles. Commercially available potentiostats (CHI812 and CHI660b, CH Instruments) allowed amperometry to be used for the detection of catecholamines and pulsed amperometric detection (PAD) to be used for the detection of doxorubicin and daunorubicin. Amperometry was run at a constant 0.8 V detection potential. The PAD waveform was 1.6 V oxidation/cleaning potential for 0.05 s, -0.5V reduction/regeneration potential for 0.025 s and 0.8 V detection potential for 0.15 s. All experiments were run in a two-electrode configuration using a platinum wire (1.6 mm diameter) in the waste reservoir as the counter electrode. Gold microwire (25μm diameter wire) was used as the working electrode. Noise was determined by measuring peak-to-peak current at $n \geq 30$ random points along the baseline.

6.2 RESULTS AND DISCUSSION

6.2a Surface Chemistry

The effect of air plasma oxidation on the surface composition of native and extracted PDMS was studied using XPS over the period of one week. Figure 6.1 shows a fit of the Si 2p peaks taken from a high resolution XPS scan. Each Si 2p peak is fit with a siloxane ($(Si((CH_3)_2)O-)_n$) peak with a known binding energy of 101.8 – 102.4 eV and a silicon dioxide (SiO_2) peak with a known binding energy of 103.2 – 104.1 eV.[16] Siloxane groups on the surface of native un-oxidized PDMS account for the hydrophobic nature of the polymer and can come from either cross-linked polymer or unreacted oligomer. Native PDMS initially contains Si at the surface in the form of $Si-CH_3$, which can be easily oxidized to form a hydrophilic SiO_2 surface (Figure 6.1). Native PDMS initially contains primarily $Si-CH_3$ Si as expected. 30 min after oxidation, a large peak for SiO_2 in native PDMS is seen; however, 3 hrs after the initial oxidation, the surface has returned to its original state due to hydrophobic recovery caused by unreacted oligomer diffusing to the surface with storage in air as reported previously.[17] The extracted PDMS does not show the same trend. A dominant SiO_2 peak is seen 3 hrs after the oxidation of the extracted PDMS and remains the dominant peak for at least 7 days of storage in air for oxidation times $\geq$ 60s. The extracted PDMS does not show the hydrophobic recovery of native PDMS due to the removal of the unreacted oligomers from the bulk PDMS as determined by loss of mass. The stability of the SiO_2 in air exceeds anything measured

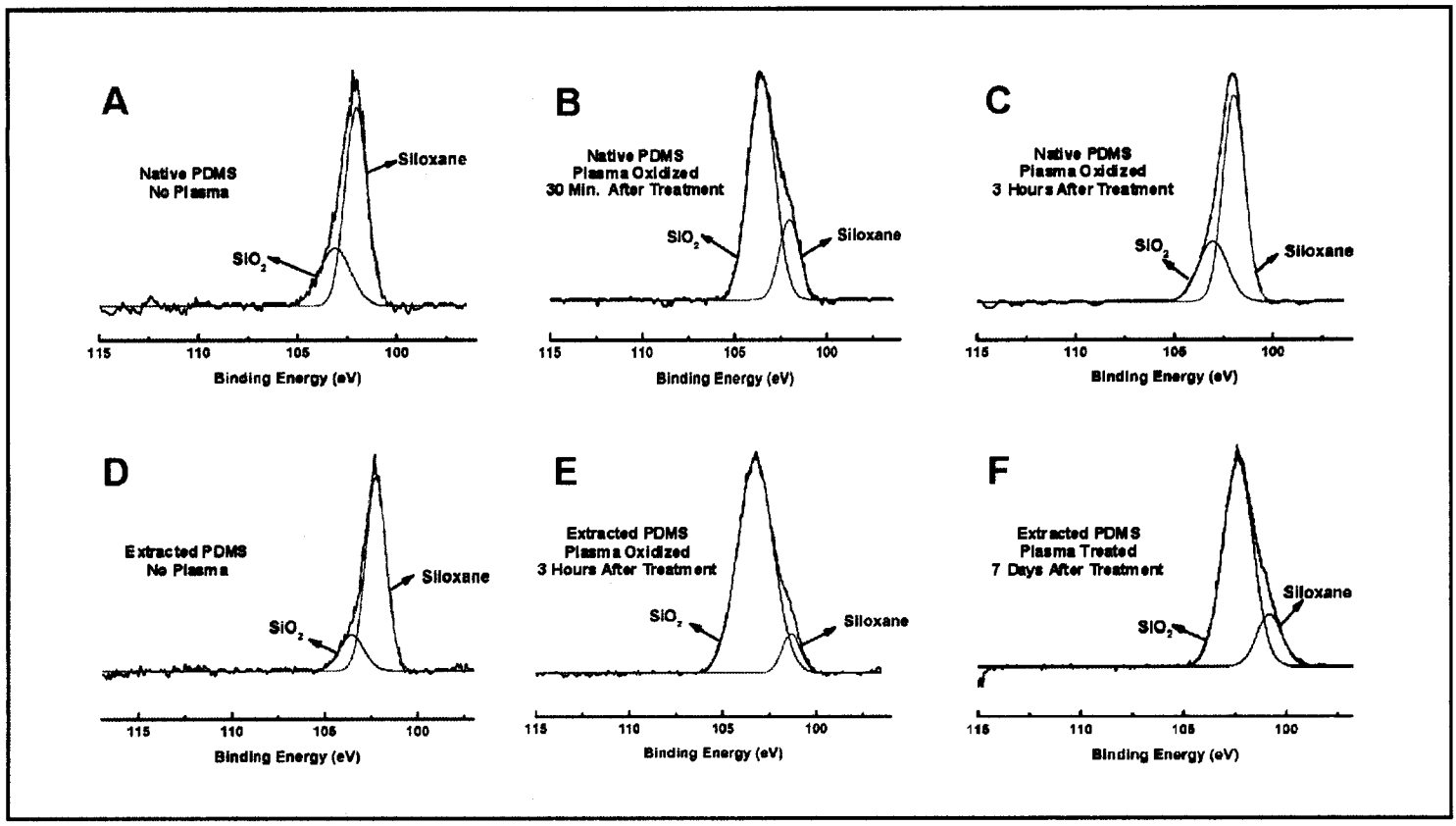

Figure 6.1: Si 2p peak measured by XPS. The Si 2p peaks are fit with a SiO_2 peak (blue) and a siloxane peak (green). Samples were scanned at 30 min, 3 hours and 7days after they were prepared and stored in air. A) Native PDMS with no plasma treatment. B) A 48% increase in SiO_2 calculated from peak areas can be seen 30 min after a 2 min plasma treatment. C) Hydrophobic recovery after 3 hrs seen on native PDMS. D) Extracted PDMS with no plasma treatment. E) A 54% increase in SiO_2 can be seen 3 hrs after a 2 min plasma treatment. F) Only a 7% decrease in SiO_2 can be seen 7 days after oxidation. All samples were stored in air.

previously for PDMS to the best of our knowledge. Studies for longer term stability are currently being performed by another student in the Henry group.

From XPS peak fits, the percentage of total silicon in SiO_2 form on the surface was determined by dividing the area under the SiO_2 peak by the total area of the Si 2p peak from the high resolution XPS scan. Figure 6.2 shows that after oxidation, 79% of the surface silicon is in the SiO_2 form for the native and 91% for the extracted PDMS for the first measured points (30 min and 3 hrs respectively) for a 1200 s oxidation. In the native PDMS, a rapid decline in SiO_2 on the surface is seen, from 79% to 39%, in 3 hrs. After 3 hrs, complete return to native PDMS can be seen. Extracted PDMS on the other hand shows only a 7% decrease in SiO_2 (from 91% to 84%) over a 7 day period while stored in recovery to air. All data was taken from a single XPS run in which multiple scans are taken by the instrument. The stability of this surface can be attributed to the extraction of the unreacted oligomers that are present in native PDMS. The presence of some Si in the siloxane form indicates a very thin SiO_2 film, the presence of a small amount of unreacted oligomer, or some combination thereof. XPS depth profiling experiments were not performed at this time to determine the exact nature of the $Si\text{-}CH_3$ Si. Further experiments are underway to better understand the mechanistic aspects of the material behavior.

Contact angle measurements through the sessile drop method were also made in an effort to further characterize the surface of the PDMS. Contact angle measurements for native and extracted non-oxidized PDMS were 110.2° ± 2.3 and 105.6° ± 4.3,

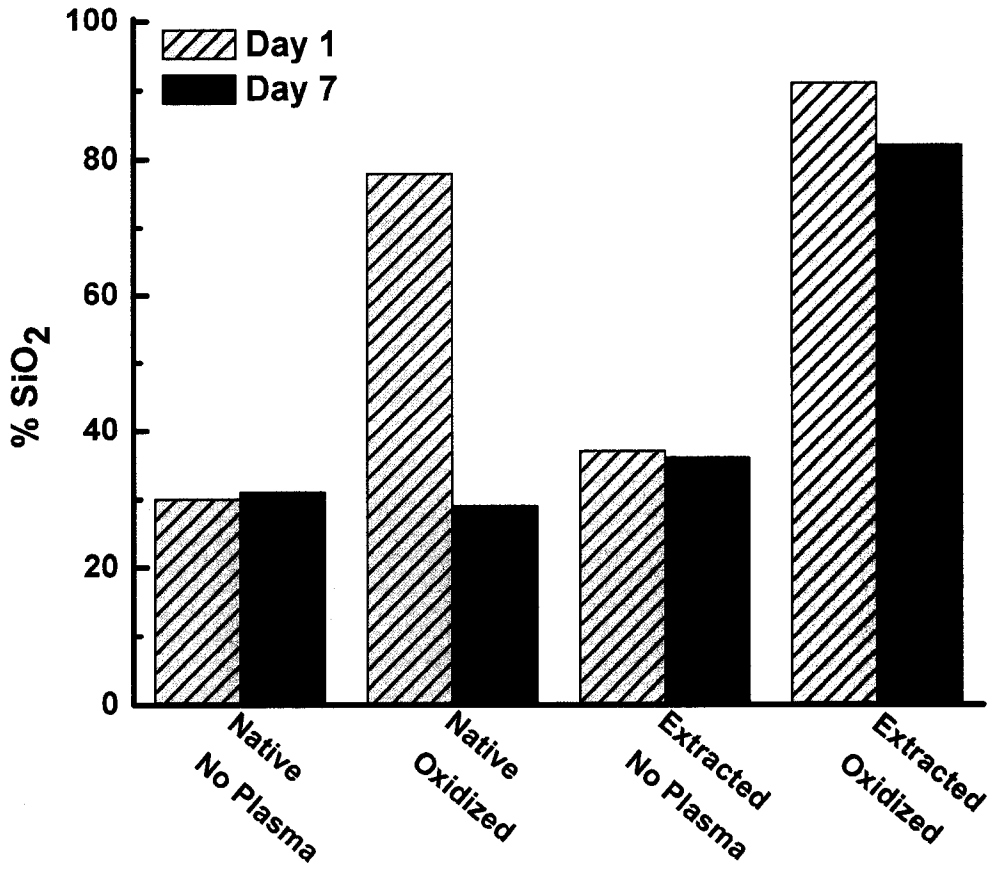

Figure 6.2: % SiO_2 on surface as a factor of time. ▨Represents % SiO_2 on the day the PDMS was oxidized. ■ Represents the % SiO_2 on the 7^{th} day after oxidation. 2 min air plasma prior to sealing the chips was used for oxidation. Percentage determined by area under the SiO_2 peak divided by total area of the Si 2p peak from Figure 6.1.

respectively. Once the PDMS was oxidized, the contact angle decreased to 57.9° ± 3.2 for native PDMS and 30.1° ± 1.9 for extracted PDMS. After seven days both PDMS pieces were tested again. The native oxidized PDMS was 110° ± 3.6 but the extracted oxidized PDMS was 40.3° ± 2.3. The contact angles measured provide additional proof that the oxidized surface is stable over significantly extended times while stored in air relative to native PDMS. The slight increase in contact angle for the extracted oxidized PDMS could be attributed to the small decrease in SiO_2 on the surface of the PDMS over the seven day period. The changes in contact angle and SiO_2 content with extracted oxidized PDMS are most likely due to the slow polymer rearrangement as has been noted previously.[9]

6.2b Oxidation Optimization

Molded and blank PDMS pieces were oxidized in the air plasma for 30 to 1200 s before sealing them together. This allowed for uniform oxidation across the entire PDMS surface. The percent SiO_2 on the surface was determined through XPS. Percent SiO_2 on the day the pieces were oxidized yielded no statistical difference for oxidation times of 60, 120, 600 and 1200 s. After storage in air for 7 days, the percent SiO_2 for the longer oxidation times (600 and 1200 s) showed no decrease from day 1. The shorter oxidation times (30, 60 and 120 s) showed a slight decreases of 19%, 15% and 7%, respectively from day 1. The longer oxidation times (600, 1200 s) also exhibited visible cracking of the PDMS surface (Figure 6.3). A strong irreversible seal was seen in the chips that were treated between 30 and 120 s. For treatment times longer than 120 s the seal was weak or non-existent due to the complete oxidation of the surface rather than the formation of

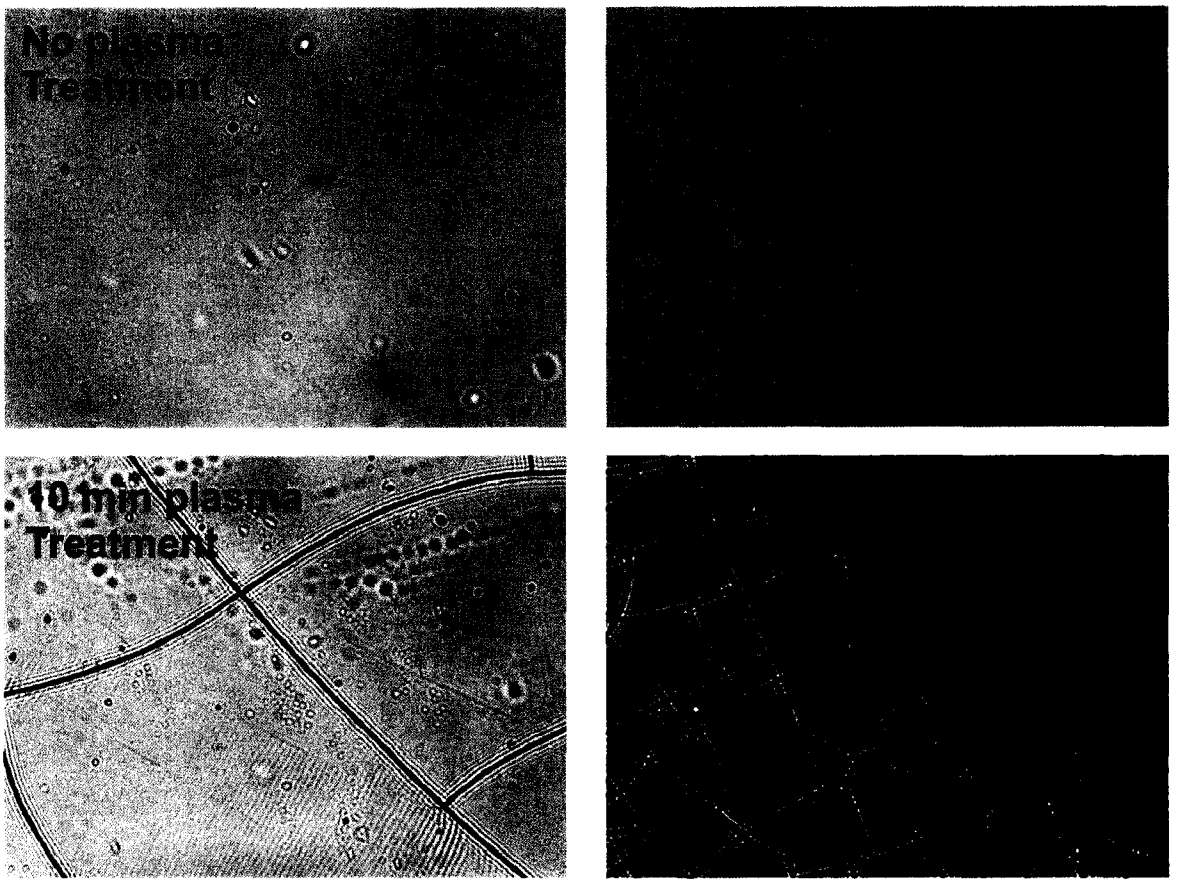

Figure 6.3: Light microscopy of oxidized extracted PDMS for oxidation times of 0, 120, 600 and 1200 s. No cracking can be seen in the 0 and 120s times while an increased amount of surface cracking can be seen in the longer oxidation time.

radicals on the surface that facilitate bonding. After assembly, MCE was performed and separation efficiency and peak skew were measured to determine reproducibility and functionality of the chips. Calculations for peak efficiency and skew are demonstrated in chapter 2. Peak skews of 1.1 – 1.3 were seen for all the microchips and did not change with the changing oxidation times. A 40% increase in separation efficiency was seen from 30 to 60 s oxidation times, above 60 s there was no statistical increase in separation efficiency. From this we determined our optimized protocol was to oxidize the PDMS pieces for 60-120s before sealing them together.

6.2c Separation Efficiency

Extracted PDMS microchips were constructed for both MCE-EC. The electropherograms in Figure 6.4 show the separation of 1 μM dopamine, catechol and ascorbic acid on native (A), extracted non-oxidized (B), and extracted-oxidized PDMS (C). A significant improvement in peak shape, peak height and peak skew can be seen for both forms of the extracted microchips. Peak skews of 3.8, 2.1 and 1.2 for native, extracted and extracted-oxidized, respectively, were measured for catechol. We hypothesize that the decrease in peak skew was the result of an improvement in the overall consistency of the surface composition. Hydrophobic surfaces are known to produce tailing peaks.

Separation efficiencies for dopamine, catechol, and ascorbic acid at a concentration of 1 μM for native PDMS devices are 18,000 ± 1200, 32,000 ± 1900, and 50,000 ± 3000 plates per meter (N/m) respectively. Separation efficiencies of 100,000 ± 5000 N/m for dopamine, 200,000 ± 7000 N/m for catechol and 400,000 ± 16,000 N/m for

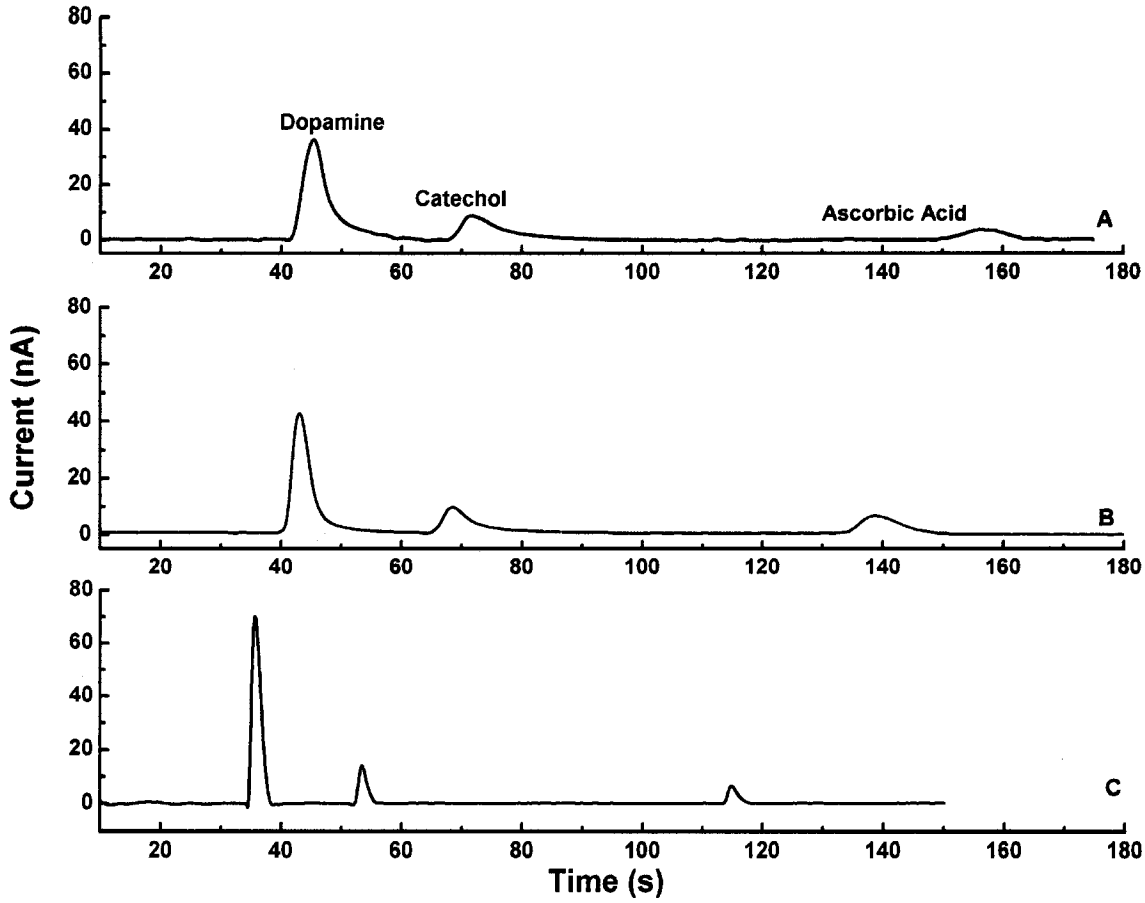

Figure 6.4: Example electropherograms for the separation of 1 μM dopamine, catechol and ascorbic acid using A) Native; B) Extracted; C) Extracted-oxidized PDMS. Experimental conditions: Field strength: 170 V/cm; Pinched injection time: 10 s for native and extracted, 7 s for extracted-oxidized; BGE: 20 mM TES (pH 7.0)

ascorbic acid were measured for the extracted-oxidized chips (n=9). The dramatic increase in separation efficiency can be attributed to the removal of hydrophobic oligomers from PDMS and formation of hydrophilic SiO_2 on the surface that provides uniform flow and resists analyte adsorption.

6.2d Electroosmotic Flow

Decreased migration times were observed for all separations when compared to native PDMS and are attributed to an increase in EOF from 4.1 x 10^{-4} $cm^2/V \cdot s \pm 0.6$ for native PDMS to 6.8 x 10^{-4} $cm^2/V \cdot s \pm 0.3$ for extracted-oxidized PDMS. Native PDMS had a catechol migration time of 71.9 ± 6.1 s (8.6% RSD) (n = 40) and the extracted-oxidized PDMS had a catechol time of 54.2 ± 1.8 s (3.3% RSD) (n = 40). The increased EOF can be attributed to the presence of a glass-like SiO_2 surface and a resulting increase in surface charge. The stability of the surface also lends to a more stable EOF over time as determained by XPS in comparison to native PDMS (Figure 6.5) as noted by the relative standard deviations between the two systems over 40 runs each. Migration times for catechol were measured over a 4 hr period in which 10 separations were run per hour (40 total). The migration time for native PDMS increases from 66 s to 75 s over this time period. The migration times for the extracted-oxidized PDMS showed a slightly upward trend over the 4 hour time, showing that the surface charge is much more stable than the native PDMS. Again, the chemical stability of the resulting surface and the lack of unreacted oligomers in the bulk PDMS facilitate this important characteristic of the modified material.

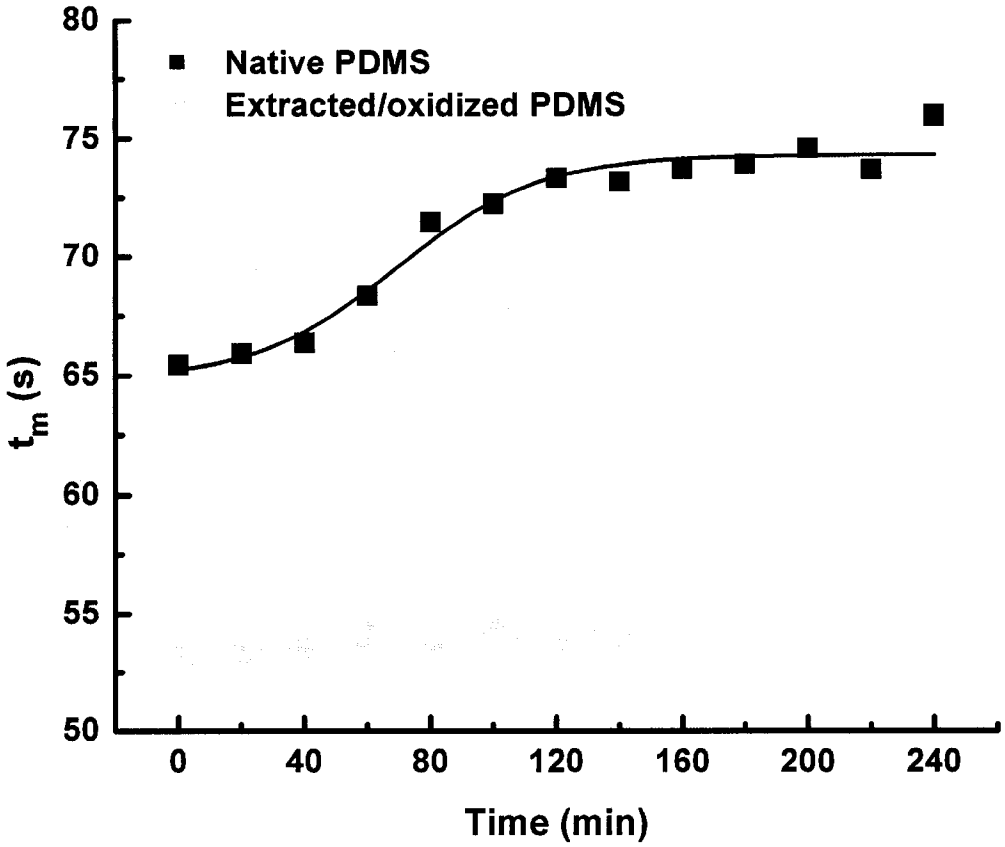

Figure 6.5: Run to run reproducibility over a period of 4 hrs (40 runs). Migration time for catechol was measured over 40 runs without retreating the microchips with NaOH for native PDMS ■ and extracted-oxidized PDMS ●

6.2e Limits of Detection

Electropherograms of the measured limits of detection are shown in Figure 6.6. The measured detection limits were 25 nM ascorbic acid (S/N = 4.23) (A), 2.5 nM catechol (S/N = 4.28) (B) and 600 pM dopamine (S/N = 3.67) (C). The lowest detection limit measured previously with native PDMS devices using electrochemical detection was 5 nM for dopamine as discussed in chapter 4.[10] The reduction in LOD is a result of the increase in peak height associated with a narrower peak. This is the lowest reported detection limit for dopamine to date for MCE-EC to the best of our knowledge. The differences in detection limits in this experiment can be attributed to an electrokinetically biased injection due to the increased EOF seen in the E-PDMS. Biasing can be offset by using longer injection times at the price of larger injection volumes and wider peaks for electrochemical detection or different injection methods. Linear ranges for dopamine, catechol and ascorbic acid were determined by peak height on extracted-oxidized PDMS microchips. Dopamine had a linear range from 600 pM – 1 mM with an R^2 value of 0.989, catechol had a linear range of 100 nM – 1 mM with an R^2 value of 0.998 and ascorbic acid had a linear range of 200 nM – 1 mM with an R^2 value of 0.996 based on peak height.

6.2f Pulsed Amperometric Detection

As a final example of the improvement in material performance, the analysis of two common anthracycline antibiotics was performed. In this example, PAD was used for the detection of the chemotherapy agents doxorubicin (DOX) and daunorubicin

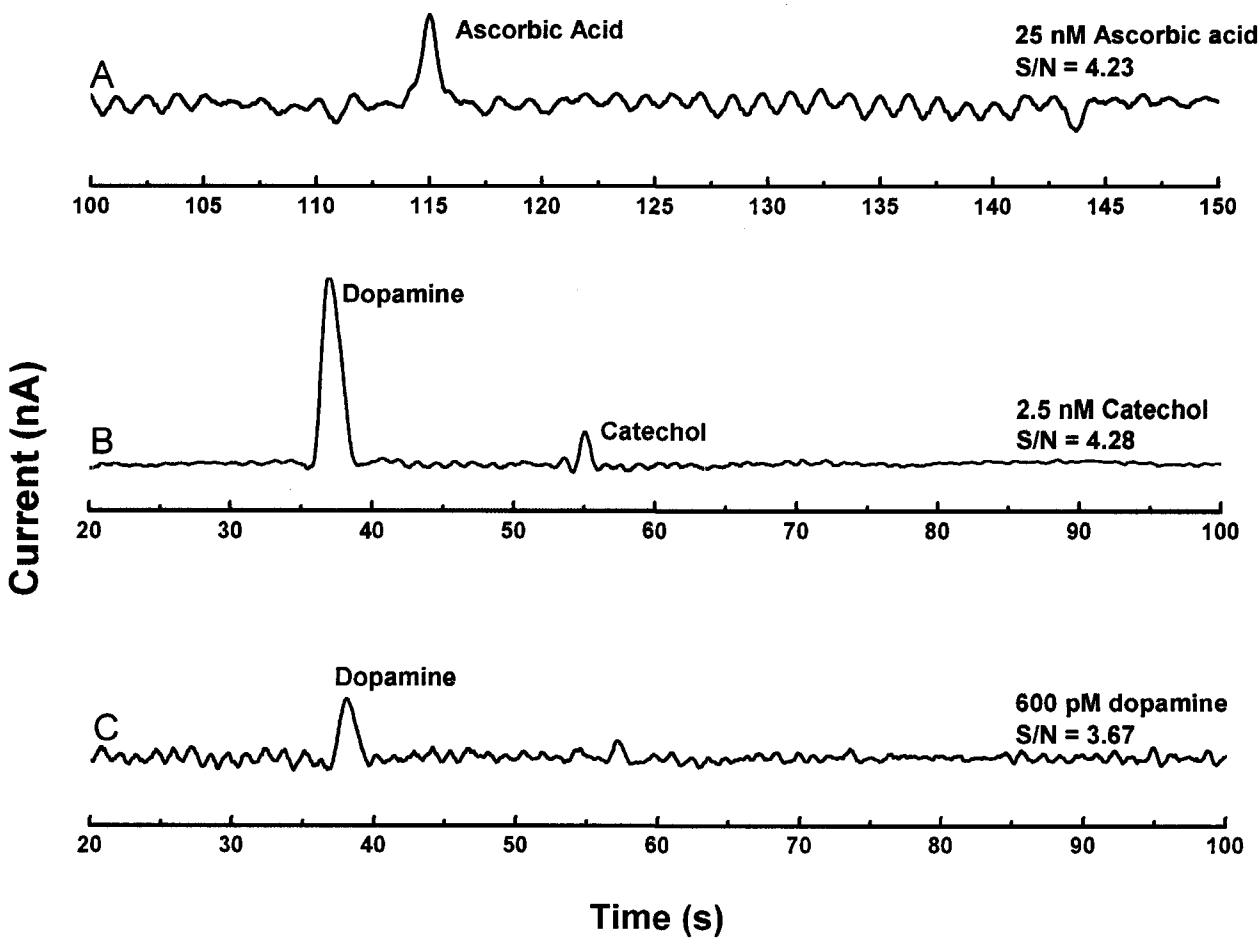

Figure 6.6: Electropherograms showing limits of detection for the three model analytes A) 25 nM ascorbic acid (S/N = 4.23); B) 2.5 nM catechol (S/N = 4.28); C) 600 pM dopamine (S/N = 3.67). Experimental conditions: same as figure 4.4

(DAUN) on an E-PDMS microchip. Figure 6.7 shows a separation of 1mM DOX and DAUN using MCE-PAD. The Culbertson group has reported the absorption of rhodamine, a hydrophobic fluorescent dye, into bulk PDMS.[18] DOX and DAUN, as anthracyclines, are expected to act in a similar manner due to their relative hydrophobicity. The glass like surface of the extracted oxidized PDMS chips lowers the absorption of DOX and DAUN allowing them to be detected at the microwire electrodes. The increased background noise and broadness of the peaks can be attributed to high concentrations, long injection times and some adsorption to the walls of the device. Nevertheless, this is a promising example of the performance that can be achieved. In our laboratory we have never been able to detect either of these analytes on a native PDMS microchip because they strongly absorb into the bulk PDMS before reaching the detection electrodes.

6.3 CONCLUSION

In summary, a simple and effective way to generate a stable hydrophilic SiO_2 surface on PDMS for use with MCE-EC was presented. XPS shows the conversion of Si-CH_3 on the surface of PDMS to SiO_2. An increase from 39% SiO_2 on the surface of native PDMS to 91% SiO_2 on the surface of E-PDMS can be seen. On E-PDMS the SiO_2 surface is stable over 7 days when stored in air. This modification allowed for high separation efficiencies (up to 400,000 N/m) and an increased EOF. These improvements will allow higher resolution of complex samples in shorter amounts of time than they would be on native PDMS.

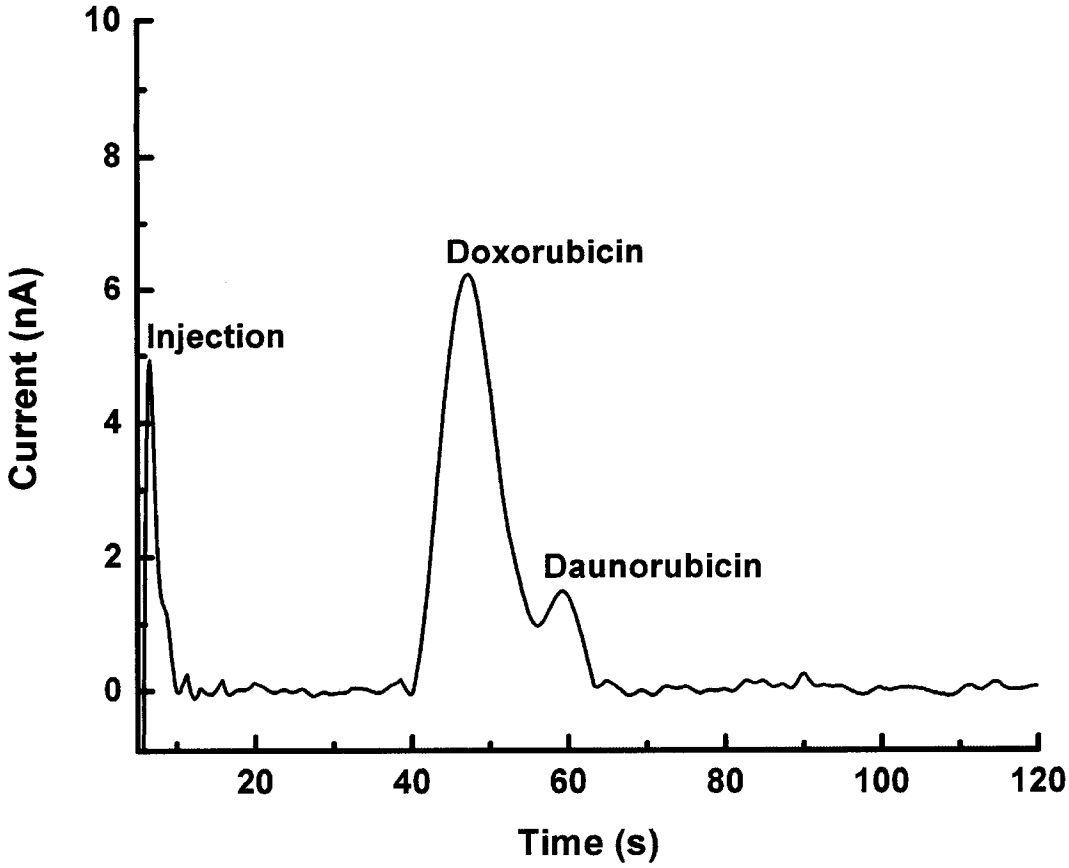

Figure 6.7: Example electropherogram for the separation of 1 mM doxorubicin and daunorubicin by MCE-PAD. PAD waveform: cleaning (1.6 V for 0.05 s), regeneration (-0.5 V for 0.025 s), detection (0.8 V for 0.15 s). Experimental conditions: Field strength: 200 V/cm; Pinched injection: 15 sec; BGE: 20 mM boric acid (pH 10.0)

6.4 Acknowledgments

I would like to thank Dr. Ellen Fisher and her group for instruction and use of the contact angle goneometer and Pat McCurdy for instruction and guidance with XPS experiments. I would also like thank Meghan Caulum and Kanokporn Boonsong for helping with the optimization of oxidation times and help with fluorescent studies for the extracted PDMS. Finally, I would like to thank Christopher Easley, Daniel Leslie, and James Landers for useful discussions regarding extraction protocols.

(1) Lee, J. N.; Park, C.; Whitesides, G. M. *Anal Chem* **2003**, *75*, 6544-6554.
(2) Kim, J.; Chaudhury, M. K.; Owen, M. J. *J Colloid Interface Sci* **2000**, *226*, 231-236.
(3) Kim, J.; Chaudhury, M. K.; Owen, M. J.; Orbeck, T. *J Colloid Interface Sci* **2001**, *244*, 200-207.
(4) Vickers, J. A.; Caulum, M. M.; Henry, C. S. *Anal Chem* **2006**, *78*, 7446-7452.
(5) Liu, Y.; Fanguy, J. C.; Bledsoe, J. M.; Henry, C. S. *Anal Chem* **2000**, *72*, 5939-5944.
(6) Liu, Y.; Vickers, J. A.; Henry, C. S. *Anal Chem* **2004**, *76*, 1513-1517.
(7) Liu, Y.; Wipf, D. O.; Henry, C. S. *Analyst* **2001**, *126*, 1248-1251.
(8) McDonald, J. C.; Duffy, D. C.; Anderson, J. R.; Chiu, D. T.; Wu, H.; Schueller, O. J.; Whitesides, G. M. *Electrophoresis* **2000**, *21*, 27-40.
(9) McDonald, J. C.; Whitesides, G. M. *Acc Chem Res* **2002**, *35*, 491-499.
(10) Vickers, J. A.; Henry, C. S. *Electrophoresis* **2005**, *26*, 4641-4647.
(11) McDonald, J. C.; Metallo, S. J.; Whitesides, G. M. *Anal Chem* **2001**, *73*, 5645-5650.
(12) Shultz-Lockyear, L. L.; Colyer, C. L.; Fan, Z. H.; Roy, K. I.; Harrison, D. J. *Electrophoresis* **1999**, *20*, 529-538.
(13) Jacobson, S. C.; Hergenroeder, R.; Koutny, L. B.; Ramsey, J. M. *Anal Chem* **1994**, *66*, 2369-2373.
(14) Garcia, C. D.; Henry, C. S. *Anal Chem* **2003**, *75*, 4778-4783.
(15) Lacher, N. A.; Lunte, S. M.; Martin, R. S. *Anal Chem* **2004**, *76*, 2482-2491.
(16) Wagner, C. D.; Naumkin, A. V.; Kraut-Vass, A.; Allison, J. W.; Powell, C. J.; Rumble jr, J. R., 2006.
(17) Fritz, J. L.; Owen, M. J. *J Adhes* **1995**, *54*, 33-45.
(18) Roman, G. T.; Hlaus, T.; Bass, K. J.; Seelhammer, T. G.; Culbertson, C. T. *Anal Chem* **2005**, *77*, 1414-1422.

Chapter 7

Thermoset Polyester, an Alternative Microchip Material

Polymer materials have become more widly used with MCE due to their affordability and ease of fabrication. While poly(dimethylsiloxane) (PDMS) has become the most widely used polymer in MCE-EC due to the simplicity of microelectrode incorporation, it suffers from a lack of separation efficiency, low surface stability, and a tendency for analyte adsorption and absorption as discussed in chapter 6. Other polymers such as poly(methylmethacrylate) (PMMA) and poly(carbonate) (PC) have higher separation efficiencies but require more difficult fabrication techniques and have been shown to be more difficult to couple to electrochemical detection. The introduction of thermoset polyester (TPE) as an alternative microchip material has shown promise as a merger between the ease of fabrication and cost effectiveness of PDMS with the higher separation efficiencies and increased stability of PMMA and PC.[1] In this chapter TPE was characterized as an alternative material for MCE-EC. TPE microchips were characterized in their native and plasma oxidized forms and after coating with polyelectrolyte multilayers (PEM). This work has been previously published in Electrophoresis.[2] EOF measurements and PEM experiments were done by Brian M. Dressen, a graduate student in the Henry lab, and Melissa C. Weston, an undergrad in the Henry lab.

The work presented in this chapter was done in order to demonstrate the ability to use various microchip materials and the benefits that they may have over PDMS microchip. TPE was used to show the improvements in separation efficiencies and peak skews seen with ridged, hydrophilic polymers when used as microchip devices. A increase in separation efficiencies and a decrease in peak skews can be seen when using TPE in place of native PDMS.

7.1 Experimental

7.1a Chemicals and Materials.

Sylgard 184 silicone elastomer and curing agent were obtained from Dow Corning (Midland, MI). Sodium phosphate monobasic (F.W. 137.99) was purchased from Acros Organics and *o*-phosphoric acid (85%) and methanol were purchased from Fisher Scientific (Fair Lawn, NJ). Thermoset polyester mixing resin was obtained from TAP Clear-Lite Casting Resin while styrene, 2,2-dimethoxyphenylacetophenone and methyl ethyl ketone peroxide where all obtained from Sigma (St. Louis, Mo, 99%). Gold (99.9% diameter 25 μm) and palladium (99.9% diameter 25 μm) wire were obtained from Goodfellow (Huntingdon, England). SU-8 2035 negative photoresist and XP SU-8 developer were obtained from Microchem Corp (Newton, MA). All polyelectrolytes were obtained from Aldrich. The polymers tested included hexadimethrine bromide (polybrene, 99%) (PB) and dextran sulfate (sodium salt, 99%) (DS) (Av. M.w. 5,000). All chemicals were used as received.

7.1b Microchip Fabrication.

Silicon masters were fabricated following techniques in chapter 2 and published elsewhere. [3] Briefly, SU-8 2035 a negative photoresist, was spun onto a 100 mm silicon wafer (<100>Silicon Inc, Boise, ID) to a thickness of 50 μm. A digitally printed mask was used to define channel structures. After exposure and developing, patterned silicon masters were treated with hexamethyldisilazane (HMDS) by vapor deposition to aid in the removal of the both TPE and PDMS. Vapor deposition was performed by placing the

wafer and a small vial containing 500 μL of HMDS in a crystallization dish, the dish was then covered with foil and placed in a 65° C oven for 4-6 hrs. PDMS walls and posts were used to define the molding area of the TPE and to create reservoirs in the TPE devices. PDMS posted were placed on the mold prior to fabrication of the TPE microchips. After assembly the PDMS posts were removed to open the reservoirs.

TPE was prepared by mixing resin (TAP Clear-Lite Casting Resin) with styrene, UV photoinitiator (2,2-dimethoxyphenylacetophenone) and methyl ethyl ketone peroxide (MEKP) catalyst, following published protocols. [1] Approximately 0.2 g of photoinitiator was dissolved in 0.5 g of styrene and then added to 20 g of resin. Six drops (~ 300 μL) of MEKP catalyst were added and the mixture was stirred (10 min) and degassed in a vacuum desiccator. After degassing, the TPE resin was poured onto the prepared master and either transparency film (polyethylene terephthalate) or a glass microscope slide was used to cover the TPE. The cover material was allowed to make contact with TPE mixture to ensure a flat top surface during UV curing. This was done to ensure even curing throughout the polymer. HMDS was used to treat the glass cover slides to ease removal from cured TPE. TPE was partially cured by UV radiation in a UV flood lamp (364 nm) (Inteli-ray 400) at 50% power for 100 seconds and then, carefully pulled away from the mold while still slightly soft. While the TPE was still soft, the PDMS posts were removed to expose the reservoirs. Microwire electrodes were then placed in the designated electrode channels located at the end of the separation channel according to previously published work in PDMS microchips.[4, 5] Care had to be taken while inserting the microwires because TPE is easily scratched, torn or otherwise damaged when not

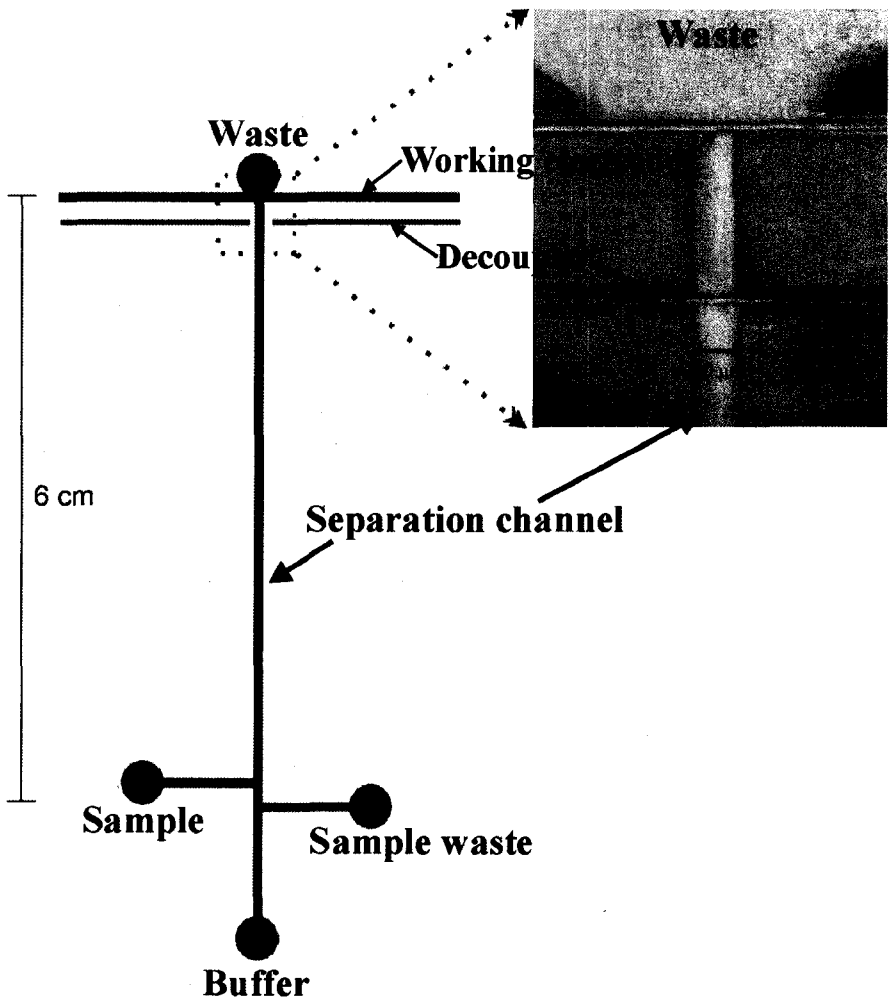

Figure 7.1: Schematic of the TPE microchips (50 μm x 50 μm x 6 cm) showing the double-T injector (100 μm, 250 nL) and electrode alignment channels (decoupler 25 μm x 50 μm and working 50 μm x 50 μm). A 50 μm gap separates the decoupler channel from the separation channel. To the right is a photograph showing the electrode alignment in a completed microchip.

fully cured. While the electrodes were being placed on the molded TPE, a blank piece of TPE was prepared in the same manner with a UV exposure of 100 s. The two pieces were then placed together to form the microchannels. A final UV exposure was necessary to set the bond between the two pieces and fully cure the TPE (Four, 30 s exposures separated by 90 s cooling periods). The chip was then placed on a 65° C hot plate for 30 min followed by transfer to a 120° C hotplate for 90 min for final curing. Figure 7.1 shows a schematic of the microchip design as well as a zoomed in picture of the detection electrodes in a fully assembled TPE microchip.

7.1c Electroosmotic Flow Measurements.

The current monitoring method (developed by Huang *et al* [6]) was used to measure electroosmotic flow. All EOF measurement were done on a single 50 x 50 μm channel with a length of 4.5 cm. One of the reservoir and the channel were filled with a 20 mM phosphate buffer while the opposite reservoir was filled with 18 mM phosphate buffer. When a potential was applied between the reservoirs the lower concentration BGE in the second reservoir displaced the higher concentration BGE in the channel. This results in an increase in the electrical resistance and therefore a different separation current. The time required to see the change in current under a constant applied electric field was monitored and was used to calculate EOF. Current was monitored with a digital multimeter (Fluke 189) across a 1 kΩ resistor in series between cathode and ground. A 900 V separation potential (200 V/cm) was used for all EOF measurements. EOF measurements were preformed by Melissa Weston.

7.1d Coating Procedure.

TPE microchips were coated with polyelectrolyte multilayers using previously reported methods used with PDMS microchips.[7] Polyelectrolytes are known to form alternating polymer layers on virtually any surface.[8, 9] Preconditioning of the channel was done with 0.1 M NaOH for 10-15 min, followed with a 5 min water rinse. Polybrene (PB), a cationic material, was deposited onto the channel wall by filling the channel with a 5% PB solution in water. The channel was then immediately rinsed with water for 5 min. A reversed EOF was observed to ensure that PB was on the surface. A second coating layer was formed by repeating the same procedure with an anionic polyelectrolyte solution, dextran sulfate (DS). After a water rinse, the channel was filled with buffer and an electric field was applied. PEM studies were preformed in coordination with Brian Dressen.

7.1e Electrochemical Detection.

Amperometric detection and PAD were used for the analysis of electrochemically active analytes using the chip design discussed in chapter 4.[4, 10] Amperometry was used for the detection of dopamine, catechol, and ascorbic acid. PAD was used in the detection of carbohydrates and thiols. Both amperometry and PAD were done using a commercially available potentiostat (CHI812 or CHI660b, CH Instruments). Amperometry had a constant potential of 0.8 V applied to the working electrode. The PAD waveform had a cleaning/oxidation potential of 1.6 V for 0.05 s, the reduction/regeneration potential was -0.5 V for 0.025 s and the detection potential was 0.6 V for 0.15 s. Amperometry and PAD experiments were run in a two-electrode

configuration with a Pt wire (1.6 mm diameter) as the counter electrode in all cases. A Au microwire (25 μm) was placed in the microfluidic devices and used as the working electrode. Cleaning and conditioning of the Pd decoupler was done initially by running cyclic voltammetry (CV) from -1.0V to 1.0V at 0.1 V/s for 50 cycles. Cleaning of the working electrode was done initially by running a CV from -1.0V to 1.0V at 0.1 V/s until 6 sweep segments overlapped each other. While using amperometry the working electrode was cleaned every 15 runs via CV with 20 sweep segments from -1.0V to 1.0V at the rate of 0.1 V/s while buffer was flowed over the electrode.[10]

7.2 Results and Discussion

TPE for the use with MCE has been reported previously in three separate publications.[1, 11, 12] In the previous work, EOF was measured for only five days. Furthermore, no surface modification studies were presented. Finally, all previous detection was performed using laser-induced fluorescence (LIF). LIF in previous reports was complicated by background fluorescence inherent in the polymer. In our quest to achieve high efficiency separations for MCE-EC using polymer microchips, we sought to both further establish the material characteristics of TPE as well as demonstrate its use with EC detection.

7.2a Electroosmotic Flow Studies.

EOF values were measured over an 18-day time frame (Figure 7.2). Over the first four days no statistical decrease in EOF was seen, the chips stored in water. Microchips

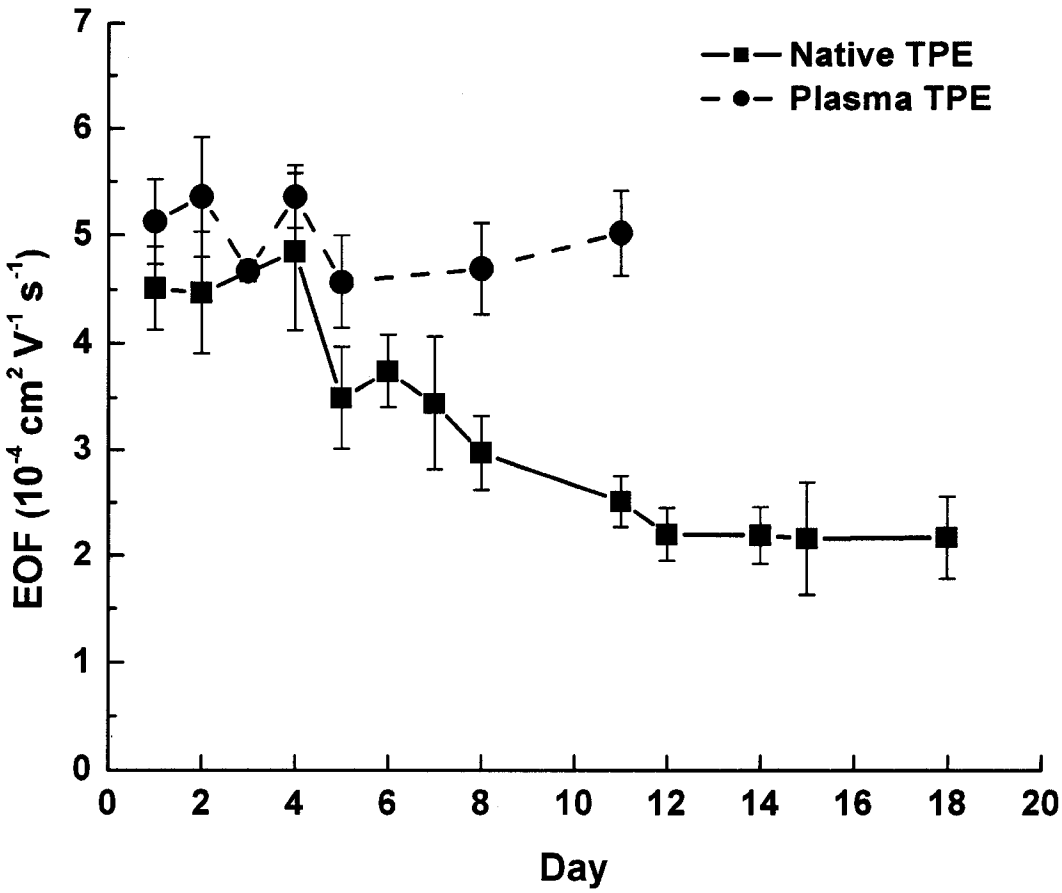

Figure 7.2: Day-to-day EOF reproducibility of TPE microchips. EOF stability is shown for native TPE over an 18 day period (■) and for plasma treated TPE over an 11 day period (●). EOF was determined by the current monitoring method. Lines are added to aid in visualization of the relative trends. Errors are expressed as standard deviations a n = 4. Experimental conditions: Field strength: 200 V/cm; Background electrolytes: 20 mM phosphate (high ionic strength) and 18 mM phosphate (low ionic strength). Data collected by Brian Dressen.

stored in air showed similar EOF values and trends. EOF values were also measured for plasma oxidized microchips over a period of 11 days. A comparison of EOF values as seen for a change in pH on PDMS, native TPE and plasma oxidized TPE can be seen in Figure 7.3. EOF values showed a 22% increase and were more stable for native TPE across all pH values than on PDMS microchips. EOF values of plasma oxidized TPE devices were 5.13 ± 0.34, 5.56 ± 0.22 and 5.61 ± 0.35 $cm^2/V{\cdot}s \times 10^{-4}$ (n = 5) for pHs 4, 7 and 10 respectively. This is a 38% increase in EOF over PDMS and a 21 % increase in EOF over native TPE. Chip-to-chip reproducibility was also established on TPE microchips. The RSD over 5 different chips was 2.7, 5.1 and 7.1% for pH 4, 7 and 10 respectively. Reproducibility of the EOF on TPE microchips shows that small variations in the volume or mass of the different components in TPE have little or no effect on EOF. The stability of the EOF for both native and oxidized TPE is improved over PDMS microchips and on par with EOFs measured in PMMA or PC.[13] The comparison to PDMS is more relevant in our laboratory because of the similar fabrication methods, cost for the two materials and microchip design. PDMS lacks the stability seen in TPE devices because of diffusion of hydrophobic low molecular weight oligomer to the surface (refer to chapter 6 for more detail).[14-16] TPE does not undergo hydrophobic recovery because it has a higher density and the starting materials are less hydrophobic determined by contact angle measurements. Decreases in the long-term stability of native TPE can be attributed to the conversion of the surface carboxylic acids to esters over time. Plasma treatment presumably perturbs the surface enough to separate reactive acids and alcohols. The exact chemical mechanism that leads to enhanced stabilization is unknown at this time.

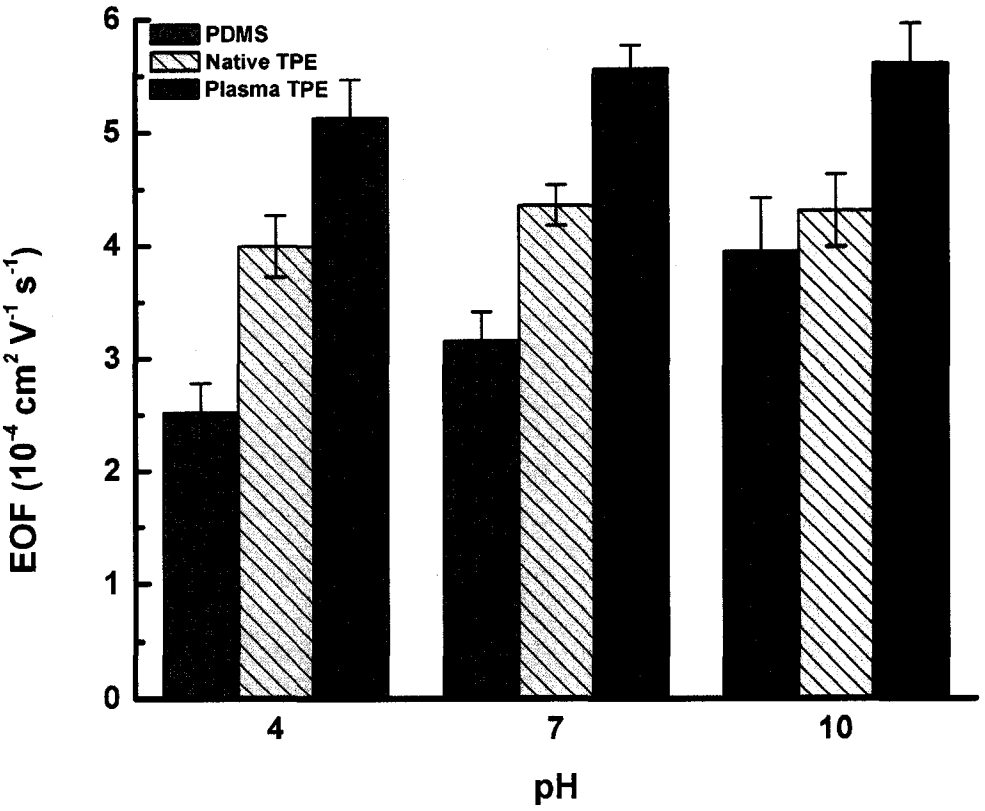

Figure 7.3: EOF measured for five microchips made at different times from different batches of TPE. Each chip was run multiple times at varying pHs (4, 7 and 10) to determine pH effects on reproducibility. Errors expressed as standard deviation a an n = 4. Other experimental protocols as in Figure 7.2. Data collected by Melissa Weston and analyzed by Jon Vickers.

7.2b Polyelectrolyte Modification.

A method for controlling the surface chemistry in microchip devices has been used in the Henry group in the form of PEMs.[7, 8] Benefits of PEMs when used with PDMS microchips include an increase in the EOF, an increased surface stability and hydrophilicity of the devices.[9] The control over the surface chemistry through these simple and effective PEM coating will allow TPE microchips to be used in variety of ways such as being used to reverse, reduce or even eliminate EOF. Reversal of EOF is useful in the separation of negatively charged species because the flow direction would parallel anion migration. A second benefit to adsorbed PEM coatings is that no additional polyelectrolyte needs to be added to the BGE as is needed with dynamic coatings as is the case with surfactants. Figure 7.4 shows EOF values measured for native (untreated) TPE, TPE coated with PB, and TPE coated with a bilayer of PB and DS over a pH range of 3 to 10. Addition of the PB cationic layer serves to reverse the flow through a change in the surface charge, as expected, but also significantly reduced the magnitude. Addition of the anionic DS layer to the PB coated surface, gave EOF values similar to the native TPE. Here, the PEMs are strongly held to the surface through electrostatic interactions with the walls of the channel or the adjacent PEM layer. This work was done by Melissa C. Weston.

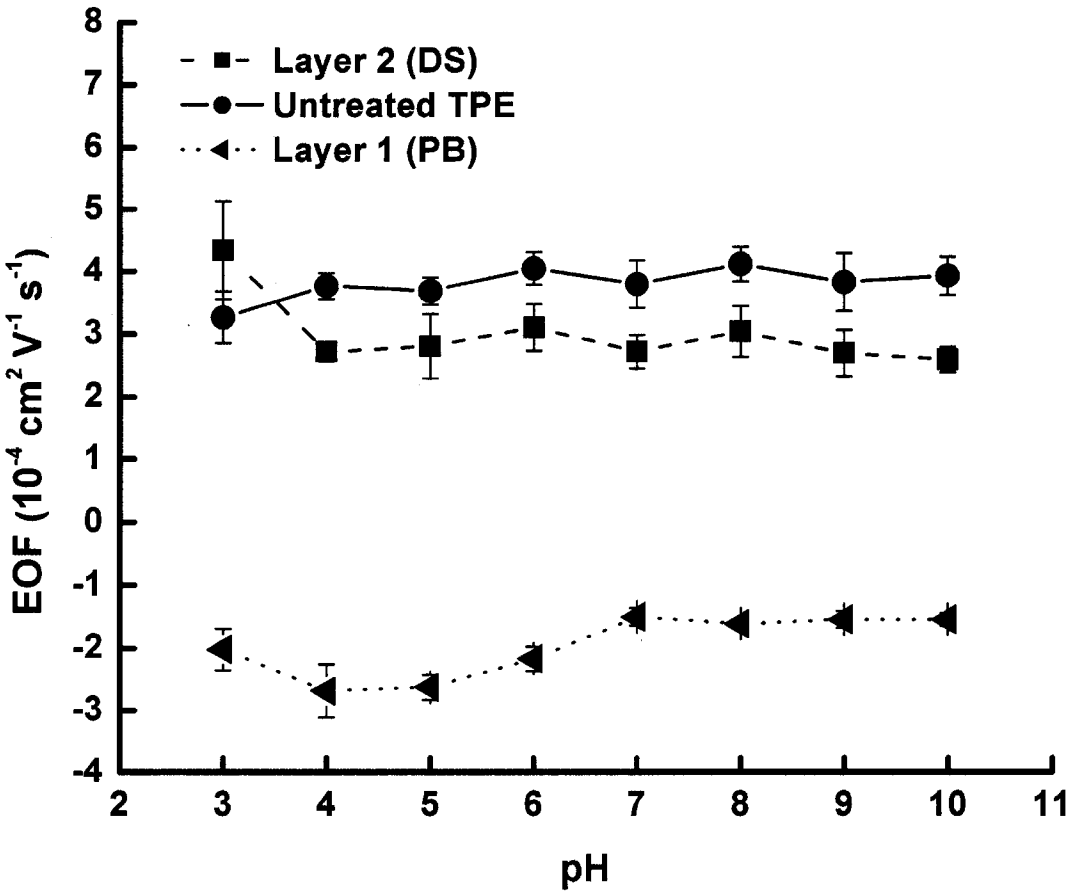

Figure 7.4: EOF values of native TPE (●) modified with a single layer of polybrene (anionic polyelectrolyte) (◀) and a double layer of dextran sulfate (cationic polyelectrolyte) (■) over a pH range from 3 to 10. Other experimental protocols as in Figure 7.2.

7.2c Microchip CE-Amperometry.

Dopamine, catechol and ascorbic acid were chosen as model analytes to characterize TPE microfluidic devices and to provide a comparison to PDMS microchips. Figure 7.5 shows representative electropherograms for the separation of 1 μM dopamine, catechol and ascorbic acid on TPE (top) and PDMS (bottom) microchips. Peak tailing and width were dramatically decreased when using TPE over PDMS. Peak skews of 3.2 and 3.8 are observed for dopamine and catechol respectively on the PDMS microchip compared to 1.2 and 1.3 for dopamine and catechol on the TPE devices. The large peak skew values can be attributed to analyte adsorption to the hydrophobic surface of PDMS. An 8-fold increase in separation efficiency is seen when going from PDMS to TPE as shown in Figure 7.6. On TPE, separation efficiencies of 49,000 ± 2600, 148,000 ± 4500 and 295,000 ± 12,000 N/m are seen for dopamine, catechol and ascorbic acid respectively as compared to 18,000 ± 1200, 24,000 ± 1400 and 42,000 ± 2100 for PDMS. Separation efficiencies were calculated at an n = 9 (3 different chips with 3 runs each). The higher separation efficiencies seen on the TPE devices can be attributed to the increased hydrophilic nature of the TPE, increased surface charge stability and lack of hydrophobic recovery as discussed previously. The increased separation efficiency allows for a complete baseline resolved separation of all three analytes on TPE in the same time that dopamine is seen on a PDMS device. The higher separation efficiencies, better peak skews and larger EOF values seen for TPE will allow for a faster and better resolved separation of complex samples.

The effect of field strength on migration time and peak shape were investigated next. Figure 7.7 shows the separation of dopamine, catechol and ascorbic acid on a TPE

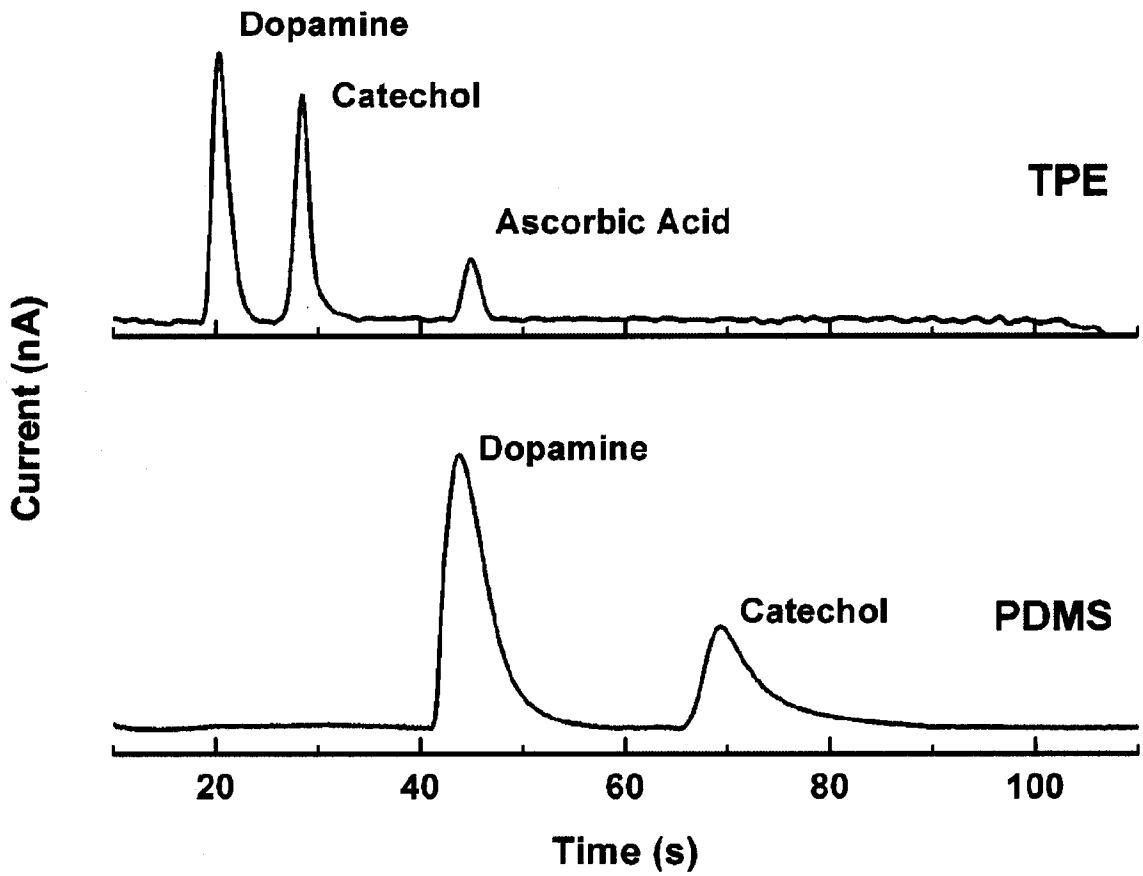

Figure 7.5: Example electropherograms for 1 μM dopamine, catechol and ascorbic acid on a TPE microchip (Top) and PDMS microchip (bottom). Experimental conditions: Field strengths: 300 V/cm and 200 V/cm for TPE and PDMS microchips respectively; pinched injection time: 15 s; Background Electrolyte: 20 mM TES (pH 7.0)

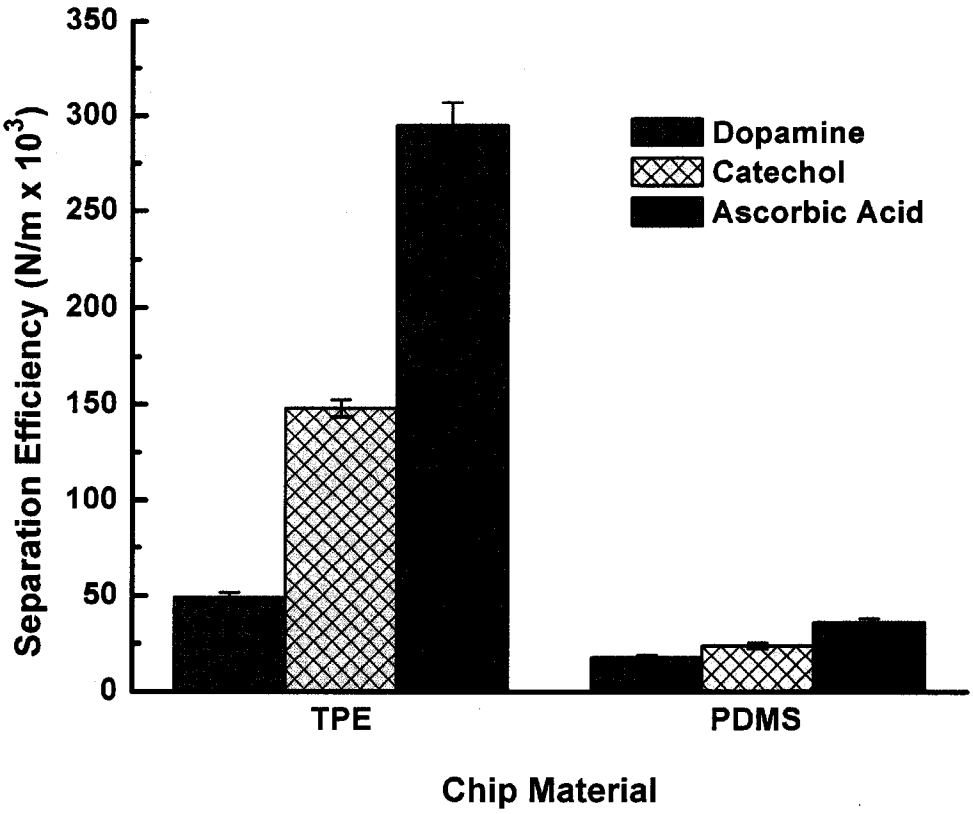

Figure 7.6: Separation efficiencies for 1 μM dopamine, catechol and ascorbic acid on Errors expressed as standard deviations at an n = 9. TPE (left) and PDMS (right) microchips made from the same mold.

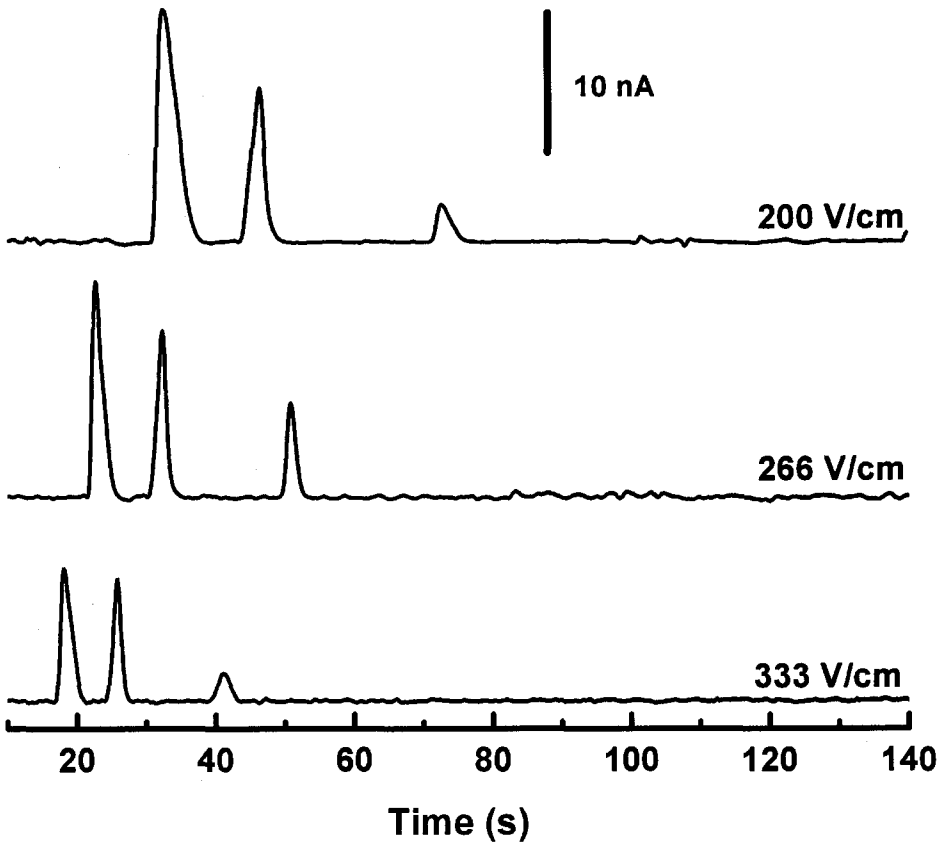

Figure 7.7: Separation of 1 μM dopamine, catechol and ascorbic acid on a TPE microchip as a function of separation potential. Optimized separation potential is determined to be 266 V/cm (1600V). Experimental conditions as in Figure 7.5.

microchip as a function of separation potential using pH 7.0, 20 mM TES as the run buffer. As expected, as the field strength is increased, the migration times decrease. Migration times were reduced by 31% with microchips at the same field strengths and by 58% with the higher field strength that are possible on TPE microchips compared to PDMS microchips. TPE was able to handle higher field strengths than PDMS in our experiments without the generation of bubbles. The maximum field strength used with the TPE devices before failure was 366 V/cm (2200 V). The exact mechanism that allows higher field strengths to be used is not known, however, improvements of this kind are normally the result of improved heat transfer properties of the substrate material. The optimal separation potential was determined to be 266 V/cm (1600 V) because it offered the fastest separation without sacrificing peak height.

7.2d Microchip CE-PAD.

As a final test of the compatibility of TPE for MCE-EC, PAD detection of carbohydrates and thiols was performed. Homocysteine, cysteine and glutathione were chosen as model analytes. Direct detection has the potential to simplify the quantification of these biologically important compounds. An example electropherogram of the separation of these three analytes is shown in Figure 7.8. The separation was performed using 20 mM boric acid, 0.8 mM SDS (pH 10.0) as the background electrolyte at field strengths of 233 V/cm with a 15 s injection. Baseline resolution of all three analytes is seen. Migration times of 71.7 ± 1.5 s, 93.4 ± 2 s and 103.9 ± 3.2 s (n=4) were seen for homocysteine, cysteine and glutathione respectively. This example shows the compatibility of the more general PAD mode with TPE microchips. The increased

separation efficiencies and decreased peak widths allow for a baseline separation of cysteine and glutathione which was not observed on native PDMS (Chapter 4, Figure 4.8B)

7.3 Conclusion

In summary, the suitability of TPE, as a material for MCE-EC, to perform the separation of several analytes has been demonstrated. EOF values for TPE microchips have shown to be very stable over a wide pH range and an extended period of time relative to PDMS. Chip-to-chip reproducibility of these devices has also been shown to be very good. The improvement of separation efficiencies on TPE microchips when compared to other chip materials gives a good indication of the increased complexity of samples that may be studied with these chips.

7.4 Acknowledgments

I would like to thank Brian Dressen and Melissa Weston for assistance with EOF measurements and chip fabrication. I would also like to thank Kanokporn Boonsong for help with the preparing polyelectrolyte multilayers and optimization of some of the fabrication procedures.

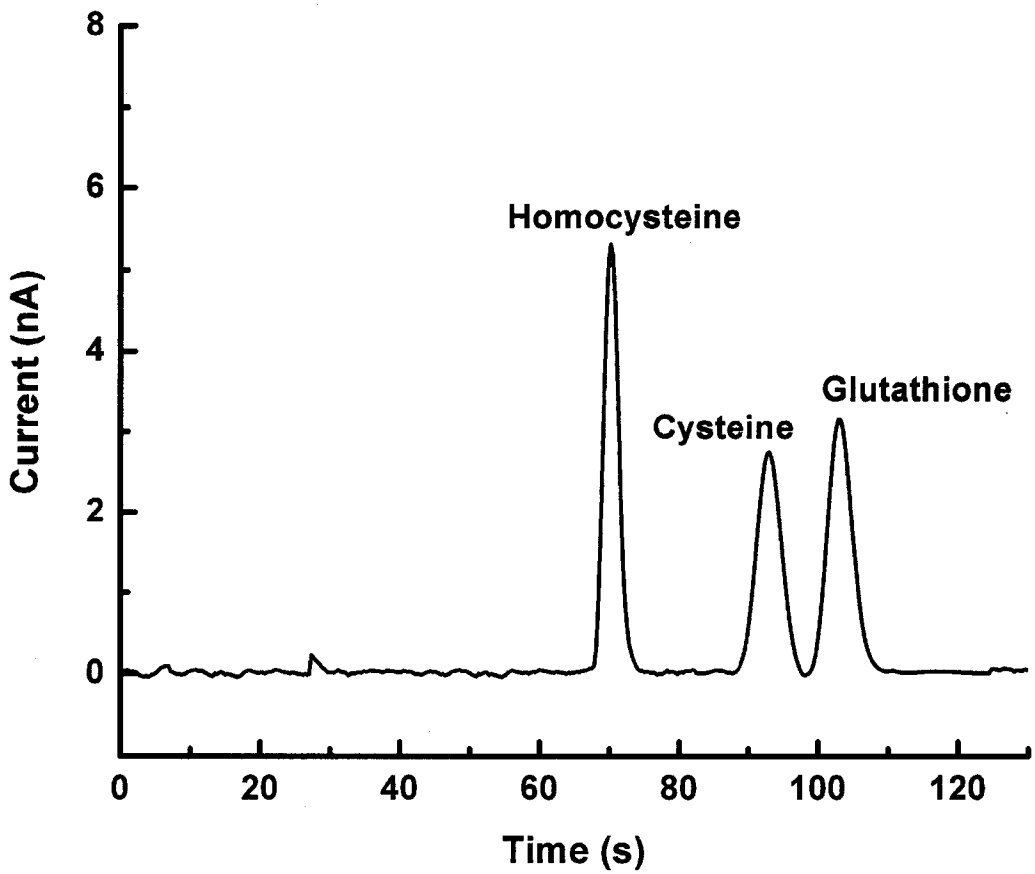

Figure 7.8: Electropherogram for the separation of 100 μM homocysteine, glutathione and cysteine on a TPE microchip. Experimental conditions: Field strength: 233 V/cm; Pinched injection time: 15 s; Background electrolyte: 20 mM boric acid (pH 10.0)

(1) Fiorini, G. S.; Lorenz, R. M.; Kuo, J. S.; Chiu, D. T. *Anal Chem* **2004**, *76*, 4697-4704.
(2) Vickers, J. A.; Dressen, B. M.; Weston, C. M.; Boonsong, K.; Chailapakul, O.; Cropek, D. M.; Henry, C. S. *Electrophoresis* **2007**, *28*, 1123.
(3) Duffy, D. C.; McDonald, J. C.; Schueller, O. J. A.; Whitesides, G. M. *Anal Chem* **1998**, *70*, 4974-4984.
(4) Garcia, C. D.; Henry, C. S. *Anal Chem* **2003**, *75*, 4778-4783.
(5) Vickers, J. A.; Henry, C. S. *Electrophoresis* **2005**, *26*, 4641-4647.
(6) Huang, X.; Gordon, M. J.; Zare, R. N. *Anal Chem* **1988**, *60*, 1837-1838.
(7) Liu, Y.; Fanguy, J. C.; Bledsoe, J. M.; Henry, C. S. *Anal Chem* **2000**, *72*, 5939-5944.
(8) Barker, S. L. R.; Tarlov, M. J.; Canavan, H.; Hickman, J. J.; Locascio, L. E. *Anal Chem* **2000**, *72*, 4899-4903.
(9) Henry, C. S.; Liu, Y.; Bledsoe, J. M.; Hopkins, C. D. *Abstrat Papers - ACS* **2001**, *221st*, ANYL-212.
(10) Liu, Y.; Vickers, J. A.; Henry, C. S. *Anal Chem* **2004**, *76*, 1513-1517.
(11) Fiorini, G. S.; Jeffries, G. D. M.; Lim, D. S. W.; Kuyper, C. L.; Chiu, D. T. *Lab Chip* **2003**, *3*, 158-163.
(12) Xu, W.; Uchiyama, K.; Shimosaka, T.; Hobo, T. *Chem Letters* **2000**, 762-763.
(13) Kirby, B. J.; Hasselbrink, E. F., Jr. *Electrophoresis* **2004**, *25*, 203-213.
(14) Kim, J.; Chaudhury, M. K.; Owen, M. J. *J Colloid Interface Sci* **2006**, *293*, 364-375.
(15) Kim, J.; Chaudhury, M. K.; Owen, M. J. *J Colloid Interface Sci* **2000**, *226*, 231-236.
(16) Fritz, J. L.; Owen, M. J. *J Adhes* **1995**, *54*, 33-45.

Chapter 8

Microchip CE-EC for Label Free Detection of Heme and non-Heme Proteins

Proteins play key roles in many biological systems. There are already many methods for the analysis of proteins. In this chapter I will show a rapid, sensitive and specific identification of proteins. With MCE devices, a single integrated chip can perform many of the steps necessary for biochemical analysis.[1, 2] Detection methods such as mass spectrometry (MS),[3-5] protein arrays,[6-8] laser induced fluorescence (LIF)[9-11] and UV absorption spectroscopy (UV)[4, 12, 13] are commonly used in the detection and qualitative analysis of proteins. However, these techniques can require expensive instrumentation, consume relatively large amounts of protein or require difficult and tedious fluorescent labeling procedures.

Labeling is often done to aid in the detection of proteins.[14, 15] Although labels have significantly improved protein research by increasing the sensitivity of detection, they are not without drawbacks. Labels can hinder the behavior of proteins. Increased steric hindrance, a possible denaturing or altered electrophoretic mobility could result from the change in the behavior of the proteins.[14] Another drawback is that the experimental conditions must also favor optimal label performance rather than the optimal conditions for the proteins. This forces many proteins to perform outside of their optimal chemical environments. Consequently, labeling technology limits protein detection.

One alternative method for the detection of proteins is the utilization of electrochemical systems. Electrochemical systems when combined with MCE devices provide the benefits of miniaturization, speed, sensitivity and low cost. This chapter shows the use of our microwire MCE-EC system for the label-free direct detection of heme and non-heme centered proteins. Heme centered proteins such as hemoglobin and

myoglobin are important in the transport of oxygen through the body and in muscles. Many non-heme centered proteins have functions include enzymatic, structural, storage or receptors. The ability to selectively and quantitatively detect either the heme or non-heme proteins has the possibility to provided a plethora of information on biological processes and/or disease states.

8.1 EXPERIMENTAL

8.1a Chemicals and Materials.

The following chemicals and materials were used as received: SU-8 2035 photoresist (Micro Chem. Corp., Newton, MA), propylene glycol methyl ether acetate (Aldrich), 4" silicon wafers (Silicon Inc., Boise, ID), poly(dimethylsiloxane) (PDMS) (Dow Corning), Sygard 184 elastomer curing agent (Dow Corning), sodium hydroxide (Fisher, 99%), boric Acid (Fisher, 99%), sodium dodecyl sulfate (SDS) (Fisher, 99%), N-dodecyl-B-D-maltoside (DDM, 99%), methanol (Fisher, ACS), 2-propanol (Fisher, ACS), sodium hydrosulfite (Sigma, 85%) and Sephadex G-25 (GE healthcare). Proteins were in powder form and are as follows hemoglobin (Hb) (Sigma, 99%), myoglobin horse heart (Mb) (Sigma, 99%), concanavalin A (Con A, 99%) (Calbiochem) and human serum albumin (HSA) (Sigma, 99%). Microwires made of 99.99 % Pd (diameter 0.025 mm) and 99.99 % Au (diameter 0.025 mm) were obtained from Goodfellow (Huntingdon, England).

8.1b MCE

A 250 μm double-T PDMS microchip with a 5.3 cm separation channel was employed for all experiments.[16-18] The buffer reservoir was filled with 1.0 M NaOH and forced through the microchannels with pressure. NaOH was used to pretreat the channels at the beginning of each day for 30 min. The channels were then filled in the same manner with a micellar electrokinetic chromatography (MEKC) background electrolyte (BGE) and allowed to equilibrate for a minimum of 15 min. Before analysis, BGE in the sample reservoir was replaced with a 1 mg/ml protein solution in BGE. Microchips were fabricated with two electrode channels perpendicular to the separation channel to incorporate microwire electrodes using the design reported in chapter 4.[19] A Pd microwire decoupler (25 μm wide) was placed in the first electrode channel (most upstream electrode) for use as the cathode. The working electrode (25 μm Au) was placed 250 μm downstream from the decoupler in the second electrode channel.[20] After each electrode was aligned and sealed in place, a 0.80 mm copper wire was attached to the exposed microwire end with conductive silver paint and held in place with silicon RTV sealant (Dow Corning 732). A 1200 V (230 V/cm) separation potential was applied to the buffer reservoir while the Pd decoupler was kept at ground. A 450 V push back potential was applied to the sample and sample waste reservoirs to prevent leakage.

8.1c Detection

A commercially available potentiostat (CHI812b, CH Instruments) was used for pulsed amperometric detection (PAD) of Hb, Mb, Con A and HSA. A Pd decoupler was cleaned and conditioned initially by running a CV from -1.0 V to 1.0 V at 0.1 V/s for 50

cycles. The working electrode was cleaned initially using CV from -1.0 V to 1.0 V at the rate of 0.1 V/s while buffer was electrokinetically pumped over the electrode for 30 cycles.[21] The PAD waveform was 1.6 V oxidation/cleaning potential for 0.05 s, -0.5V reduction/regeneration potential for 0.025 s and a varied detection potential for 0.15 s. Due to the PAD waveform no additional cleaning of the working electrode was required during experiments with the exception of experiments with albumin. The microchip was flushed with NaOH and CV was preformed from -1.0 V to 1.5 V while buffer was electrokinetically pumped over the electrode for 40 cycles after each consecutive run while using albumin. All experiments were run in a two-electrode configuration using a platinum wire (1.6 mm diameter) in the waste reservoir as the counter electrode and a gold microwire (25μm diameter wire) as the working electrode. Hydrodynamic voltamograms (HDV) from -0.5 V to 1.8 V were taken for all of the proteins.

8.2 Results and Discussion

8.2a Microchip MEKC-EC

The effects of MEKC on the migration times of the proteins were studied to help determine optimal separation conditions. 20 mM boric acid with 0.8 mM SDS, pH 9.4 was used as a standard non-MEKC buffer for migration time comparison. The migration times for each of the proteins increased with the use of the SDS MEKC buffer but no appreciable improvement was seen in the separation of the proteins from the standard non-MEKC buffer. Migration times of 76.6 ± 5.3 s, 79.5 ± 7.3 s and 94.9 ± 6.2 s and were seen for Hb, Con A and HSA in the non-MEKC buffer respectively. The migration times slowed to 81.3 ± 6.2 s for Con A, 87.2 ± 4.1 s for Hb and 95.5 ± 3.8 s for HSA

when using the 20 mM SDS MEKC buffer. The second MEKC buffer used was 20 mM boric acid with 0.4 mM DDM. Unlike charged surfactants such as SDS, DDM will not denature the proteins in solution. Migration times using the DDM buffer were 44.1 ± 4.6 for Con A, 60.13 ± 3.6 s for Hb and 89.7 ± 5.2 s for HSA (Figure 8.1). Table 8.1 show a comparison of migration times for the proteins in each BGE. DDM was chosen as a surfactant due to its neutral charge. The increased migration times seen when using the

Table 8.1: Migration times (t_m) for proteins

BGE Surfactant	CMC (mM)	t_m Hb (s)	t_m Con A (s)	t_m HSA (s)
No surfactant	N/A	76.6 ± 5.3	79.5 ± 7.3	94.9 ± 6.2
SDS	7.5 - 8.0	87.2 ± 4.1	81.3 ± 6.2	95.5 ± 3.8
DDM	0.15 - 0.2	60.1 ± 3.6	44.1 ± 4.6	89.7 ± 5.2

SDS micellar buffer can be attributed to the interaction of the proteins with the negatively charged micelle.[22] The increased overall negative charge will have a higher mobility toward the anode causing the analyte to remain in the separation channel longer. A second factor can be attributed to the unfolding of the proteins in the SDS buffer. In contrast, DDM micelles have a neutral charge and will therefore travel with the EOF causing the decreased migration times seen for Hb and Con A. The large change in migrations times seen for Con A can be attributed to a few factors. First is the difference in charge of the micelles (Figure 8.2). SDS is negatively charged, while DDM is neutral (Figure 8.2). Second, ionic surfactants have been shown to denature proteins whereas neutral surfactants retain protein structure.[23-25] Denaturing the proteins will change the overall shape and hydrodynamic radius, which will in turn affect the partitioning or association between the proteins and the micelles and their overall mobility.[26, 27]

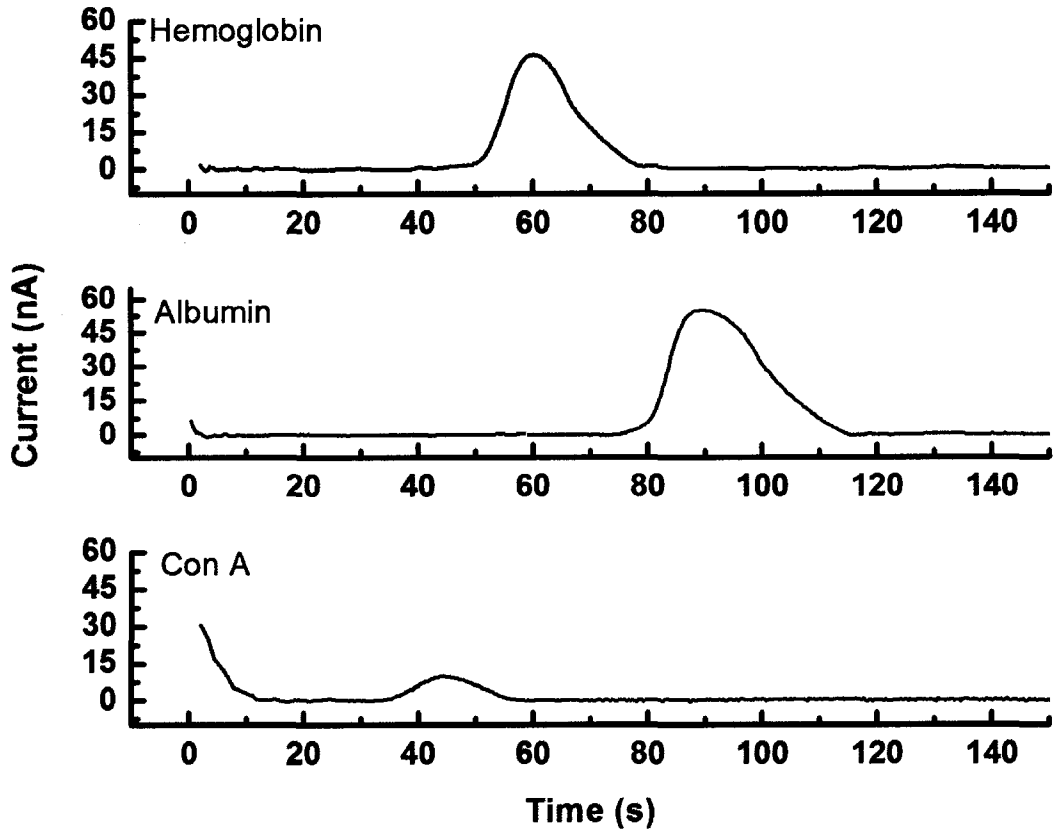

Figure 8.1: Proteins Hemoglobin, Albumin and concanavalin A run using microchip MEKC-PAD. Experimental conditions: 20 mM boric acid, 0.4 mM DDM (pH 9.4), Detection potential +1.2 V.

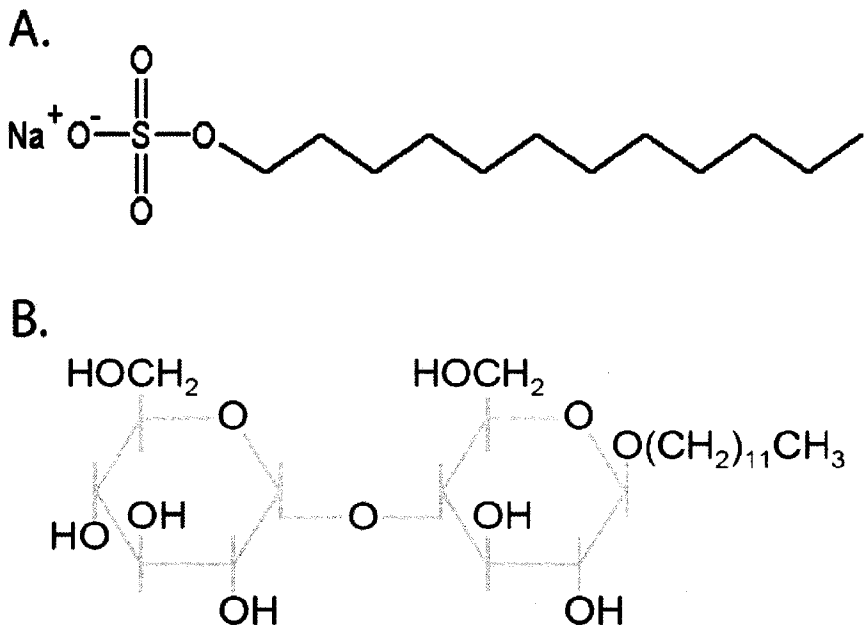

Figure 8.2: A) Structure of sodium dodecyl sulfate (SDS) surfactant. B) Structure of N-dodecyl-B-D-maltoside (DDM) surfactant

8.2b Hydrodynamic voltamograms

Hydrodynamic voltamograms were taken for Hb, Mb, HSA and Con A from -0.5 to 1.8 V detection potentials to determine optimum detection potentials for each protein. Figure 8.3 shows the resulting HDVs for each protein. HSA and Con A showed an optimal detection of 1.1 V and 1.2 V respectively. Heme centered proteins have two distinct maximum detection potentials of 0.1 V and 1.4 V for Hb and 0.2 V and 1.4 V for Mb. The high detection potentials in all four proteins may be attributed to specific amino acid residues on the surface of each protein.[28, 29] Electrochemically active residues include those with a primary amine (arginine, asparagine, lysine and glutamine), an alcohol (serine, tyrosine and threonine) or thiol (cysteine) group. The lower detection potentials of 0.1 and 0.2 V seen in the heme centered proteins are not completely understood at this time. I speculate that they are a function of the heme center itself. Whether the heme center is affecting specific amino acid residues or if it is a direct detection of the heme center is not known. Another possibly factor is the folded or unfolded state of the protein.

Figure 8.4 shows a breakdown of electrochemical signal vs. number of specific electrochemically active amino acids. Peak heights were measured for a 1mg/ml protein sample. Peak heights for Hb, HSA, Con A and Mb were 92.1 ± 5.2 nA, 62.2 ± 7.3 nA, 13.8 ± 1.7 nA and 2.96 ± 0.75 nA, respectively (n = 4). While the total electrochemical signal can not be directly linked to the number of electrochemically active amino acids, the proteins seem to be increasingly apt to adsorb to the electrode as the number of thiol residues increases. This would explain the need for additional cleaning CVs when

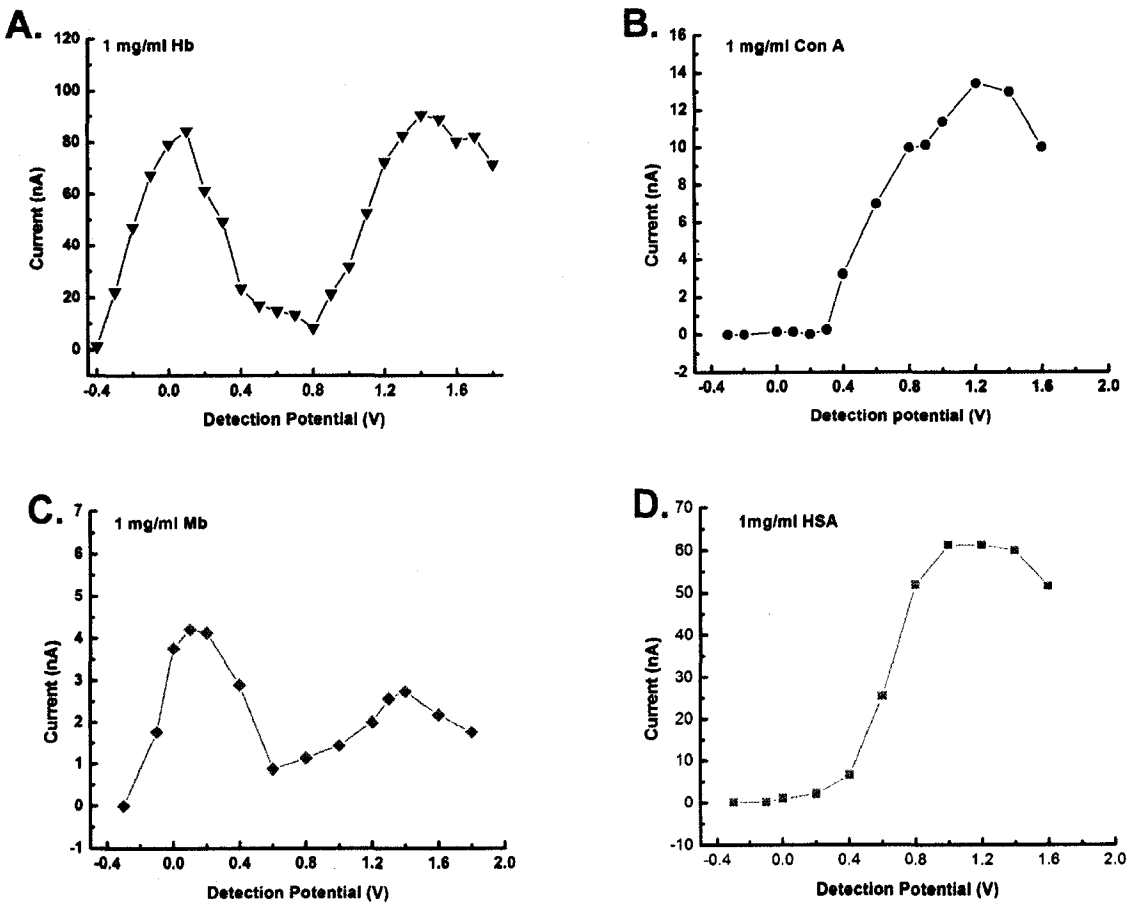

Figure 8.3: A) HDV for 1 mg/ml hemoglobin. B) HDV for 1 mg/ml concanavalin A. C) HDV for 1 mg/ml myoglobin. D) HDV for 1 mg/ml human serum albumin. All proteins were prepared in run buffer (20 mM boric acid, 0.4 mM DDM (pH 9.4))

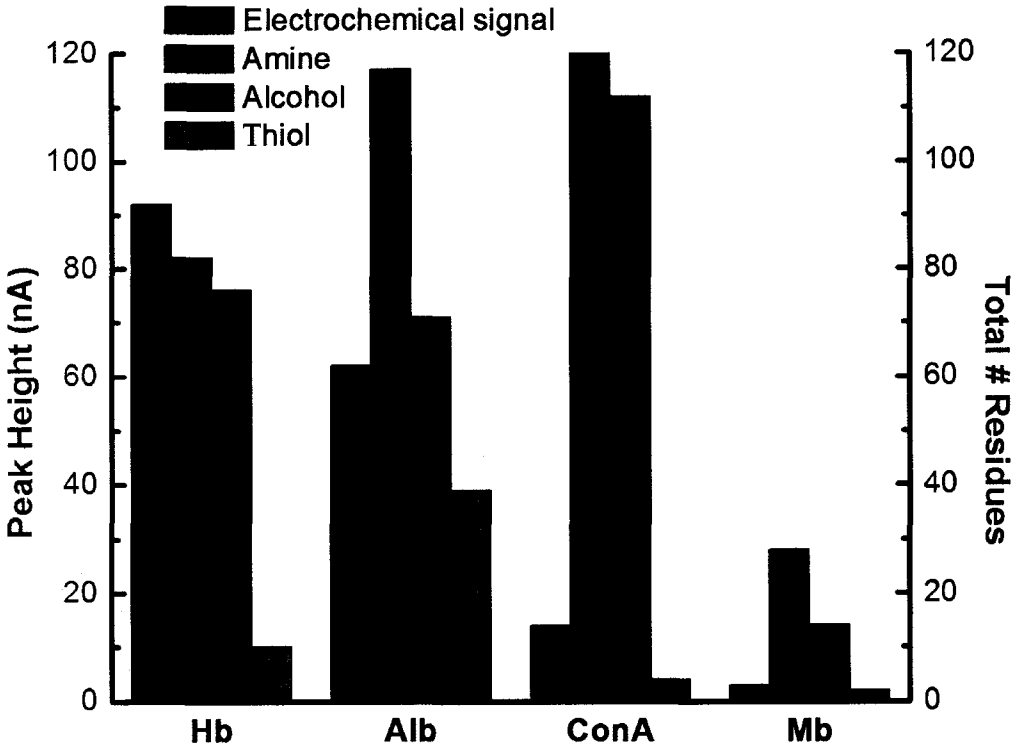

Figure 8.4: The total number of electrochemically active residues vs the electrochemical signal based on peak height. The left axis (red) and the red bar represent the electrochemical signal (peak height) for each of the proteins. The right axis (blue) and the blue bars show the number of specific electrochemically active amino acid residues in each protein. This was made to determine if there was any correlation between a specific type of amino acid and the electrochemical signal observed.

running albumin. Figure 8.5 shows the percentage of electrochemically active amino acids based on the overall total number of amino acids per protein. The percentage of alcohol containing amino acids, shows the same trend as the electrochemical signal from each analyte seen in Figure 8.4. Hb having the highest followed by HSA, then Con A and finally Mb.

8.2c Hemoglobin oxidation state

To determine if the low oxidation potential seen in the HDV's of hemoglobin is a direct oxidation/detection of the heme center, chemical oxidation and reduction of the heme center was done prior to microchip MEKC-PAD. Chemical reduction of the heme center was preformed using a Sephadex G-25 column modified with sodium hydrosulfite.[30] Reduced hemoglobin samples were bright red in color indicating a reduced iron center (Fe^{2+}). The oxidized hemoglobin (methemoglobin) samples were a dark brown color indicating an oxidized iron center (Fe^{3+}).[31, 32] An HDV of oxidized Hb is shown in Figure 8.6. As in previous experiments, two optimal oxidation potentials are seen for the oxidized Hb at +0.1 V and +1.4 V. Figure 8.7 is an HDV for Hb that was chemically reduced with sodium hydrosulfite to the Fe^{2+} state. Excess sodium hydrosulfite was removed by dialysis before running on the microchip system. Only one optimal detection potential was seen for the reduced Hb at +1.4 V. Little to no signal was seen at detection potentials between 0.0 V and +0.3 V. This data shows a correlation between the heme center, its oxidation state and the maximum detection potentials from the HDVs between 0.0 V and +0.3 V. The exact nature of the relationship between the oxidation state of the

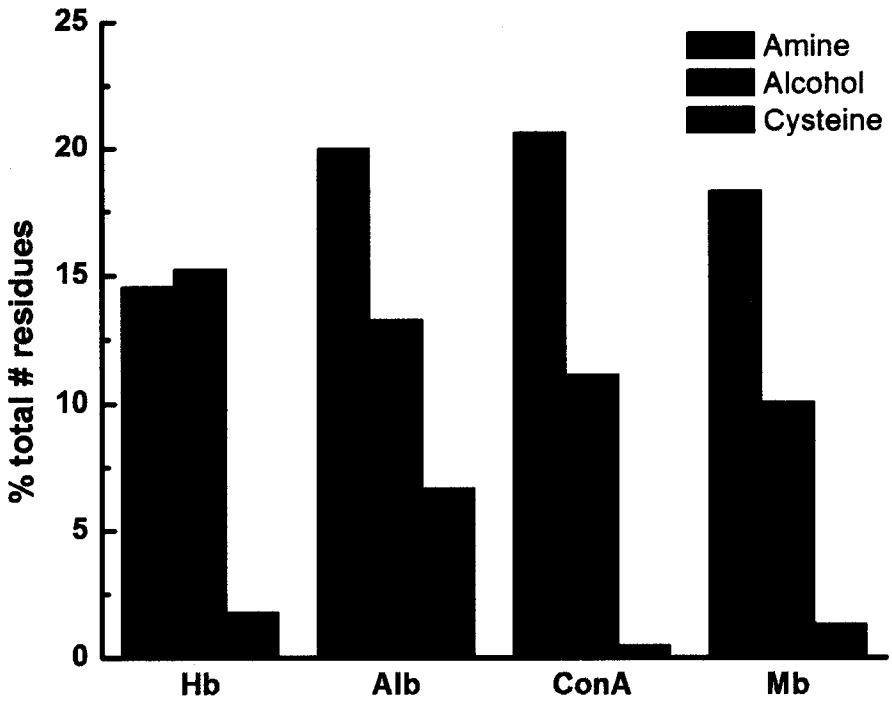

Figure 8.5: Percentage of amine, alcohol and thiol containing residues on hemoglobin, albumin, concanavalin A and myoglobin.

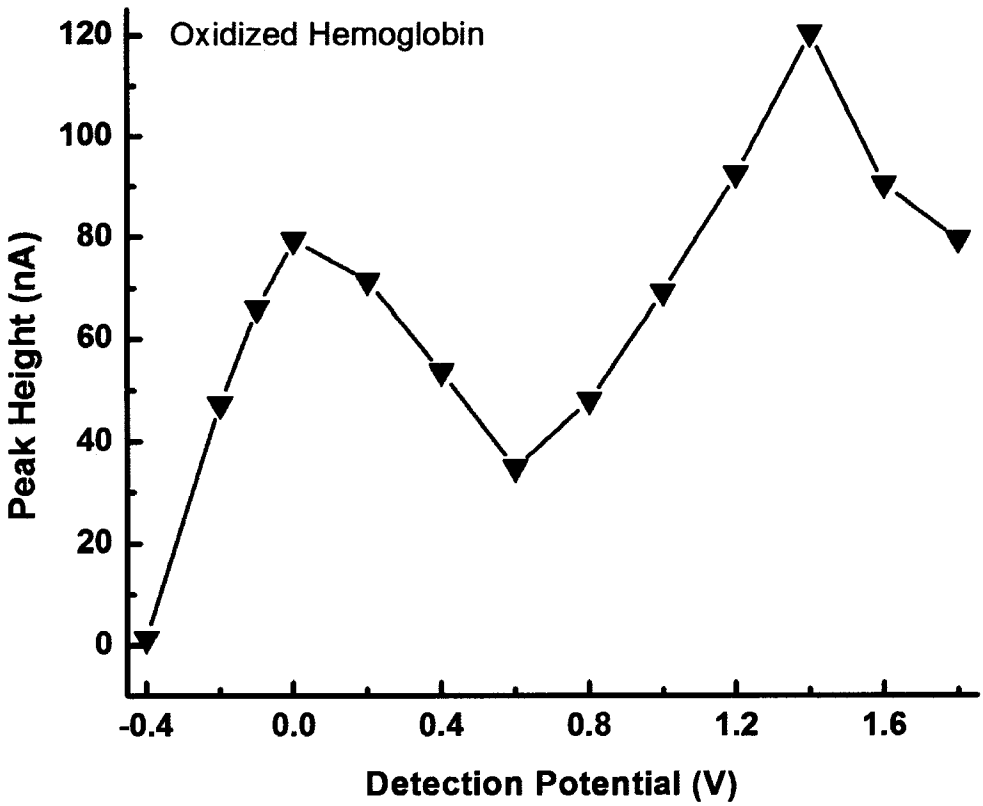

Figure 8.6: HDV for oxidized Hemoglobin run through a Sephadex G-25 column. Optimal detection potentials around 0.1V and 1.4 V. Experimental conditions same as figure 8.1.

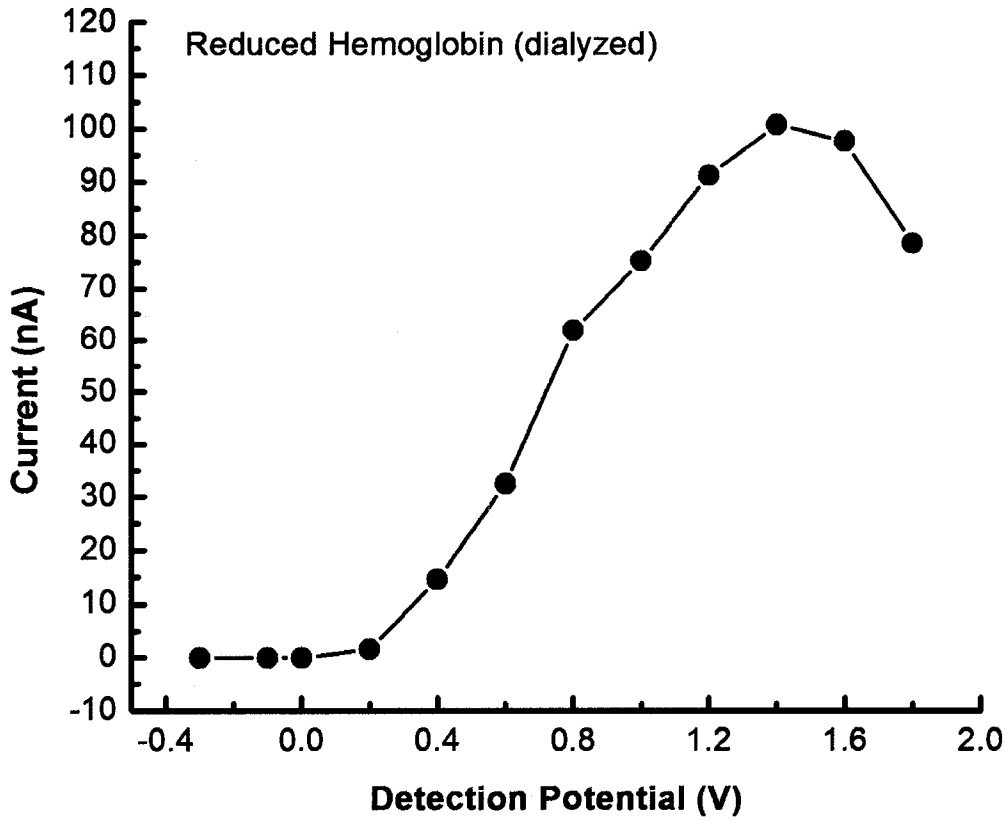

Figure 8.7: HDV for reduced Hemoglobin. Hb was reduced by running a Sephadex G-25 column with sodium hydrosulfite. Samples were then dialyzed to remove excess sodium hydrosulfite from solution. Experimental conditions were the same as Figure 8.1.

heme center and the optimal detection potential is unknown at this time but will be characterized in more depth.

Several possible theories are presented to explain the lower detection potential (0.0 - +0.3 V) seen for hemoglobin in the ferric state (oxidized state). The first theory revolves around the reduction potential of the ferric heme center and the effects of the PAD waveform. The reduction/regeneration step in the PAD waveform could be reducing some of the hemoglobin as it passes over the electrode which in turn is reoxidized at a low oxidation potential during the detection step. This theory would explain the appearance of the low positive (oxidation) peak for an already oxidized heme center. A problem with this theory is the disappearance of the low oxidation potential for the reduced hemoglobin. If the low detection potential corresponds to the oxidation of the heme center then it should be seen in the reduced hemoglobin to an equal or greater signal than seen with the oxidized hemoglobin. A second theory is that the reduction process could cause a conformational change of the protein and the heme center. This would explain the appearance of the two optimal oxidation potentials. The high detection potential, much like in all the proteins studied, can be attributed to the amino acid residues of the protein, while the low detection potential may be attributed to a ligand preferentially bound to the iron center in the ferric state rather than the ferrous state. Another possible explanation for a ligand bound to the heme center of hemoglobin would be that the ease of oxidation of the ligand could increase as the heme center is oxidized. This would mean that for the oxidized hemoglobin, the ligand could be oxidized at a lower potential appearing as the low optimal detection potential in the HDV. The ligand could still be oxidized in the reduced form but at a higher potential which would be

encompassed by the high detection potential of the amino acid residues. The determination of the mechanism at work here is beyond the scope of this dissertation, but these theories would be a good place to start.

A few possible experiments to determine which, if either, of these theories is correct are presented here. The first and simplest experiment would be to alter the PAD waveform. By simply switching the oxidation/cleaning and reduction/regeneration steps we should be able to determine if the low oxidation peak is coming from the reduction and subsequent re-oxidation of the oxidized heme center. The reversal of the steps will add noise to the system and could allow for more electrode fouling but will eliminate the possibility for the heme to be reduced directly before the detection. An experiment to determine if ligand binding or a conformational change in the hemoglobin affects detection potential wouldl be to run a HDV of hemoglobin in the oxidized form. Then chemically reduce it and run the reduced form in the same manner. Finally, chemically re-oxidize the hemoglobin to determine if the HDV is the same as the original sample. This will help determine if it is a factor of a bound ligand or simply of conformational change between the oxidized and reduced forms of hemoglobin.

8.3 Conclusions

These studies demonstrated a label-free detection of proteins on a MCE-PAD device. Direct detection of four proteins varying in size from 17 kDa to 104 kDa was been presented. Non-Heme containing proteins, HSA and Con A, showed optimal detection potentials of around +1.2 - +1.4 V, while the heme containing proteins, Hb and Myo, in their oxidized form gave two separate maximum detection potentials at 0.0 -

+0.2 V and +1.2 - +1.4 V. Two possible theories for the explanation of the two optimal detection potentials along with possible experiments are presented for future students. The capabilities of this label-free protein separation and detection greatly enhance the utility of microfluidic devices for protein analysis. Electrochemical detection will allow for a wider range of separation conditions due to the lack of labeling constraints.

(1) Dittrich, P. S.; Manz, A. *Nature Rev Drug Discov* **2006**, *5*, 210-218.
(2) Srinivasan, V.; Pamula, V. K.; Fair, R. B. *Lab on a Chip* **2004**, *4*, 310-315.
(3) Huber, C. G.; Premstaller, A.; Kleindienst, G. *J Chrom A* **1999**, *849*, 175-189.
(4) Larive, C. K.; Lunte, S. M.; Zhong, M.; Perkins, M. D.; Wilson, G. S.; Gokulrangan, G.; Williams, T.; Afroz, F.; Schoeneich, C.; Derrick, T. S.; Middaugh, C. R.; Bogdanowich-Knipp, S. *Anal Chem* **1999**, *71*, 389R-423R.
(5) Chaurand, P.; Fouchecourt, S.; DaGue, B. B.; Xu, B. J.; Reyzer, M. L.; Orgebin-Crist, M. C.; Caprioli, R. M. *Proteomics* **2003**, *3*, 2221-2239.
(6) Eickhoff, H.; Konthur, Z.; Lueking, A.; Lehrach, H.; Walter, G.; Nordhoff, E.; Nyarsik, L.; Bussow, K. *Adv Biochem Eng Biotechnol* **2002**, *77*, 103-112.
(7) Zhu, H.; Snyder, M. *Curr Opin Chem Biol* **2001**, *5*, 40-45.
(8) Cutler, P. *Proteomics* **2003**, *3*, 3-18.
(9) Colyer, C. L.; Mangru, S. D.; Harrison, D. J. *J Chrom A* **1997**, *781*, 271-276.
(10) Gilman, S. D.; Pietron, J. J.; Ewing, A. G. *J Microcolumn Sep* **1994**, *6*, 373-384.
(11) Chang, H.-T.; Huang, Y.-F.; Chiou, S.-H.; Chiu, T.-C.; Hsieh, M.-M. *Current Proteomics* **2004**, *1*, 325-347.
(12) Jenkins, M. A.; Guerin, M. D. *J Chrom B Biomed Sci Appl* **1997**, *699*, 257-268.
(13) Salloum, D. S.; Schlenoff, J. B. *Biomacromolecules* **2004**, *5*, 1089-1096.
(14) Cooper, M. A. *Anal Bioanal Chem* **2003**, *377*, 834-842.
(15) Craig, D. B.; Polakowski, R. M.; Arriaga, E.; Wong, J. C. Y.; Ahmadzadeh, H.; Stathakis, C. *Electrophoresis* **1998**, *19*, 2175-2178.
(16) Shultz-Lockyear, L. L.; Colyer, C. L.; Fan, Z. H.; Roy, K. I.; Harrison, D. J. *Electrophoresis* **1999**, *20*, 529-538.
(17) Jacobson, S. C.; Hergenroeder, R.; Koutny, L. B.; Ramsey, J. M. *Anal Chem* **1994**, *66*, 2369-2373.
(18) Garcia, C. D.; Henry, C. S. *Anal Chem* **2003**, *75*, 4778-4783.
(19) Vickers, J. A.; Henry, C. S. *Electrophoresis* **2005**, *26*, 4641-4647.
(20) Lacher, N. A.; Lunte, S. M.; Martin, R. S. *Anal Chem* **2004**, *76*, 2482-2491.
(21) Liu, Y.; Vickers, J. A.; Henry, C. S. *Anal Chem* **2004**, *76*, 1513-1517.
(22) Ramsey, J. D.; Jacobson, S. C.; Culbertson, C. T.; Ramsey, J. M. *Anal Chem* **2003**, *75*, 3758-3764.
(23) Gudiksen, K. L.; Gitlin, I.; Whitesides, G. M. *Proc Natl Acad Sci U S A* **2006**, *103*, 7968-7972.
(24) Banerjee, P.; Joo, J. B.; Buse, J. T.; Dawson, G. *Chem Physics Lipids* **1995**, *77*, 65-78.
(25) Seddon, A. M.; Curnow, P.; Booth, P. J. *Biochemica et Biophysica Acta* **2004**, *1666*, 105-117.
(26) Franzin, C. M.; Gong, X. M.; Thai, K.; Yu, J. H.; Marassi, F. M. *Methods* **2007**, *41*, 398-408.
(27) Rabel, S. R.; Stobaugh, J. F. *Pharm Res* **1993**, *10*, 171-186.
(28) Lunte, S. M.; Martin, R. S.; Gawron, A.; Lacher, N.; Fogarty, B.; Reagan, F. *Abstr Papers - ACS* **2001**, *221st*, ANYL-214.
(29) Wang, J.; Chen, G.; Pumera, M. *Electroanalysis* **2003**, *15*, 862-865.
(30) Dixon, H. B. F.; Mcintosh, R. *Nature* **1967**, *213*, 399-&.

(31) Mansouri, A. *Clin Res* **1985**, *33*, A348-a348.
(32) Mansouri, A. *Fed Proceed* **1985**, *44*, 1427-1427.

Chapter 9

Summary and Future Work

9.1 DISSERTATION SUMMARY

The focus of this dissertation has been on the development, improvement and application of capillary electrophoresis microchips with microwire electrodes for electrochemical detection (MCE-EC). Development of these microchips has gone through two main stages. The first stage involved the use of a single microwire as a working electrode on a microchip. The development of the microwire detection electrode in MCE allows for a robust, simple electrode. The use of microwires also allows for the incorporation of multiple electrode materials (Au, Pt and Cu) and differing electrode diameters (25 and 50 μm). Limits of detection for 25 and 50 μm wires were 250 nM and 100 nM respectively. At the time of publication these were the lowest detection limits reported on a MCE-EC device. The second stage in the development of these microchips saw the addition of multiple microwire electrodes of varying composition for use as working electrodes and current decouplers. The microwire design allowed the use of two different electrode materials without extensive electrode fabrication that is seen with thin film electrodes. Pd was used as the decoupling electrode because of its ability to absorb hydrogen during the electrolysis process. The incorporation of a palladium current decoupler gave lower limits of detection than seen in the previous single electrode chips. A 50 fold decrease in the limit of detection was seen when using a decoupled microchip with a 50 μm Pt wire in comparison to a non-decoupled chip with the same working electrode. The decoupler also allows for the use of multiple working electrodes on a single microchip. The ability to use multiple working electrodes in two different modes was shown to add selectivity to the devices. Selective detection of analytes with reversible redox reactions was achieved when running the dual electrode microchips in

the oxidation/reduction mode. Looking for easily oxidizable analytes in a more complex matrix was shown when using the increasing potential mode of detection. MCE-EC devices with microwire electrodes have shown improvements over standard thin film and off-column disk electrode in every facet of their construction and use.

The second focus of this thesis was the investigation of different microchip materials. Multiple microchip materials, as well as modified chip materials, were studied and showed improved separation efficiencies and peak skew as well as an increased electroosmotic flow (EOF). Although, inexpensive and easy to fabricate, poly(dimethylsiloxane) (PDMS) has inherent flaws. The largest problem with PDMS devices is the hydrophobic recovery of the material. After oxidation of siloxane groups to SiO_2, unreacted oligomers migrate to the surface and convert the hydrophilic SiO_2 back to hydrophobic siloxane groups. This hydrophobic recovery also leads to the non-uniform surface charge seen in PDMS devices. A simple solvent extraction and oxidation process was developed in order to prevent the hydrophobic recovery of unreacted oligomers from the bulk PDMS to the surface. The process consists of a simple three part organic extraction of unreacted oligomers followed by plasma oxidation of the surface. This process was shown to render a stable hydrophilic surface for up to 7 days while stored in air. An 8-fold increase in separation efficiencies can be seen when comparing native PDMS (50,000 N/m) and E-PDMS (400,000 N/m). Thermoset polyester (TPE) was also used as a material for CE-EC microchips. Devices made from TPE showed increased separation efficiency, increased EOF and a decreased peak skew when compared to native PDMS. Peak skews of 1.2 - 1.3 and separation efficiencies as

high as 300,000 N/m were seen in the TPE devices as compared to 3.2 and 50,000 N/m on native PDMS respectively.

Finally, extracted PDMS microchips with incorporated microwire decouplers and working electrodes were used in the direct detection of heme and non-heme centered proteins. Pulsed amperometric detection (PAD) was used in the detection of hemoglobin, albumin, myoglobin and concanavalin-A at a concentration of 1 mg/ml. PAD at a detection potential of 1.2 - 1.4 V was used for the analysis of all of the proteins, while a detection potential of 0.0 – 0.2 was used for the analysis of only the proteins that contained a heme center (Hb, gHb, and myoglobin). This allows for selective differentiation between heme and non-heme centered proteins by simply changing the detection potentials.

9.2 FUTURE WORK

The future of this project lies in a few main areas. The first was the development of alternate microchip material. Second was to improve upon selectivity and the number of detectable analytes. The final goal would be to integrate these changes for the detection of important small molecules and proteins in biological samples.

Microchip materials such as PMMA and PC have been used by many groups with good results while using MCE-LIF but have not made a great impact when used with MCE-EC. This was because the ability to incorporate electrodes was more difficult than when using PDMS. The ability to incorporate microwires directly onto the chip before bonding should increase the versatility of these materials in MCE devices. These materials should also give better separation efficiencies, a more uniform surface charge

and a resistance to absorbing hydrophobic materials. With these improvements, more complex samples could be analyzed with less concern about the hydrophobicity of the analytes.

Selectivity can be improved in our microchips through the expansion of the dual electrode detection. New modes of detection, which incorporate amperometry and PAD at parallel working electrodes as well as dual electrode PAD, will help to increase the number of detectable analytes as well as the selectivity for specific analytes. Detection potentials as well as the PAD waveforms will need to be optimized to coincide with one another in order to specifically detect an analyte of interest.

Homocysteine, which plays an important role in the early detection of cardiovascular disease, and 8-hydroxydeoxyguanosine (8OH-dG), which is a marker for oxidation damage, are important electrochemically active small molecules. Therefore, it is important to detect biologically relevant levels in blood or serum samples. Blood and/or serum are extremely complex samples that contain a variety of electrochemically active analytes such as carbohydrates, amines, proteins and other thiol containing compounds. The use of carbon or chemically modified carbon electrodes may need to be employed to enhance the detection of specific analytes in a complex mixture.

The specific mechanism that allows for the determination between heme and non heme centered protein and more importantly the oxidation state of the heme center needs to be better understood. The ability to differentiate between heme centered and non-heme centered proteins with electrochemical detection has brought about a question as to whether or not this method could be used for proteins with various metal centers (Cu, Co, etc.). PAD waveforms will need to be modified to accommodate for the detection

potentials needed for the oxidation/reduction of the proteins depending on factors such as protein metal composition, location of metal center within the protein and oxidation state of the protein.

APPENDIX A:

List of Publications

- Y. Liu, **J.A. Vickers**, C.S. Henry. *2004.* Simple and Sensitive Electrode Design for Microchip Electrophoresis/Electrochemistry. Analytical Chemistry. **76(5)**:1513

- **J.A. Vickers**, C.S. Henry. *2005.* Simplified Current Decoupler for Microchip Capillary Electrophoresis with Electrochemical and Pulsed Amperometric Detection. Electrophoresis. **26(24)**: 4641

- **J.A. Vickers**, M.M. Caulum, C.S. Henry. *2006.* Generation of Hydrophilic Poly(Dimethylsiloxane) for High Performance Microchip Electrophoresis. Analytical Chemistry. **78(21)**: 7446

- **J.A. Vickers**, B.M. Dressen, M.C. Weston, K. Boonsong, O.Chailapakul, D.M. Cropek and C.S. Henry. *2007.* Thermoset Polyester as an Alternative Material for use with Microchip CE-EC. Electrophoresis. **28(7)**: 1123

APPENDIX B:

Micro-Total Analysis Chips for the Detection of Proteomic Biomarkers of Alzheimer's disease in Cerebrospinal Fluid

Jonathan A. Vickers, Department of Chemistry, Colorado State University

Original Research Proposal

A. Specific Aim

Alzheimer's disease (AD) is classified as a progressive neurodegenerative disorder which affects the parts of the brain that control thought, memory, and language.[1] AD affects as many as 4.5 million Americans and 18 million worldwide with cost of diagnosis and treatment estimated at close to 100 billion dollars a year in the United States alone.[2] There is presently no known cure for AD and diagnosis while approximately 80-90% accurate at specialized clinics is limited to a "possible" or "probable" verdict while the patient is alive.[1] In recent history there has been a push to look for proteomic biomarkers for the early diagnosis and progression monitoring of AD and other neurodegenerative disorders in body fluids such as plasma, urine and cerebrospinal fluid (CSF).[3] Human CSF is an ideal source for identification of protein biomarkers for neurodegenerative diseases such as AD because of it's close proximity to the site of pathology within the ventricles of the brain and the surrounding subarachnoid space.[3] A major issue in the use of CSF is the limited volumes that can be taken from the body at any given point in time. Changes in the concentration of tau, β-amyloid, glycosylation patterns of glycoproteins α-1-antitrypsin, β-trace, α-1β glycoprotein and apolipoprotein E (apoE) in CSF have all shown great promise in the early diagnosis of AD.[4-6] *Here, we propose a novel micro-total analysis system (μ-TAS) for the detection and quantification of glycoprotein biomarkers specific to Alzheimer's disease in a small*

volume sample of human cerebrospinal fluid. The novelty of this system will revolve around the small volumes needed for analysis (μL), the convenience of an all in one device and short analysis times in comparison to standard methods. The specific aims of this proposal are as follows:

1. Develop microchip for the injection and purification of glycoproteins from CSF using known microfluidic methods.
2. Develop a multidimensional microchip for the separations and qualification of CSF proteins.
3. Couple a microchip device to mass spectrometry for the quantification of CSF proteins of interest.
4. Merge the development of specific aims one, two and three through the addition of a series of valves to create a total analysis microchip for the detection of glycoproteins in CSF for the diagnosis of Alzheimer's disease.

The proposed μ-TAS will have a significant impact on the diagnosis of Alzheimer's disease in a clinical setting and will allow for the detection and quantification of multiple biomarkers simultaneously using sample volumes and short analysis times.

B. Background

Alzheimer's disease is a complex genetic disorder arising from the interaction of multiple genes as well as environmental factors that affects approximately 10% of the population over the age of 65 and is regarded as the most common form of dementia.[1, 7] Therefore, there is merit to approaches that will simultaneously assay multiple biological markers and their interactions. Current diagnosis is based on a combination of clinical and psychological examinations, progression of the disease and measurements of biological markers β-amyloid and tau proteins. These techniques combined with the exclusion of other dementias have shown a > 80% accuracy in the diagnosis of AD.[6, 8] No ante mortem test has shown the same accuracy and reliability to diagnosis AD as autopsy, which remains the gold standard for the confirmation of AD. The inability to accurately diagnosis AD in live patients has implications beyond the diagnostic domain. Without an early diagnosis of the disease available pharmacological treatment can be delayed. This delay can lead to an earlier onset of symptoms and a faster progression of the disease. Figure 1 shows a comparison of the cross section of a normal human brain with cross section of a human brain with an advanced case of Alzheimer's disease. The areas of the brain that control memory and language are greatly deteriorated, as are the sulcus, gyrus and the ventricles due to AD.

http://www.crystalinks.com/alzheimers.html

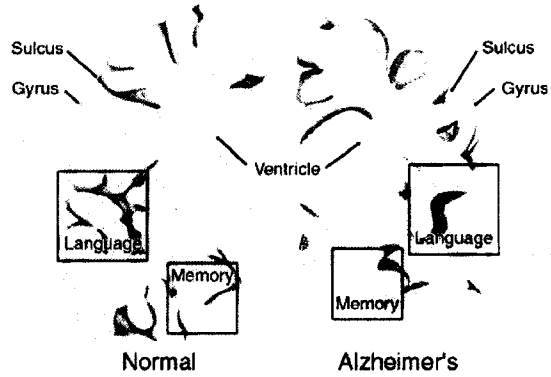

Figure 1: Cross -Section for a normal (left)brain and advanced Alzhemeimer's (Right) brain.

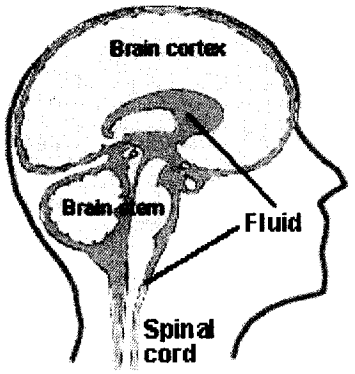

Figure 2: Cerebrospinal fluid (blue) surrounds the brain and central nervous system

Cerebrospinal fluid is a clear, colorless liquid that is the main component of the extracellular space around the brain and central nervous system (Figure 2). At any give point in time there is approximately 125-150 mL of CSF surrounding the CNS. The primary function of CSF is to cushion the brain within the skull and serve as a shock absorber for the central nervous system; CSF also circulates nutrients, chemicals filtered from the blood and removes waste products from the brain. The CSF participates in free exchange of many biochemical products within the brain including small molecules, peptides and proteins.[9] Consequently the CSF is a complex mixture which can reflect the physiological processes occurring in the central nervous system (CNS). Changes in protein composition and concentrations can be indicative of disease-related changes in the CNS protein expression patterns.[10] These changes in protein expression can lead to altered levels of certain proteins within the CSF. Changes in specific protein concentrations can then be used as biomarkers for diseases related to the CNS. CSF is obtained by performing a procedure called a lumbar puncture or spinal tap. A long, thin, hollow needle is inserted between the L4 and L5 vertebrae in the lower spine and into the subarachnoid space. Approximately 15-30 mL (10-20%) of CSF is removed for analysis. About half of the people who have a lumbar puncture preformed report sever headaches after the procedure but serious side effect are rare. [11]

Unfortunately, resolution is typically not adequate using a single liquid chromatography (LC) or capillary electrophoresis (CE) procedure to separate a complex

protein mixture. Therefore, the use of different LC or CE modes and a combination of these techniques (multidimensional separations) to generate the required resolution for proteome analysis is needed. Traditional techniques for separation and detection of CSF proteins include two-dimensional gel electrophoresis coupled with matrix-assisted laser desorption/ionization time of flight mass spectrometry (2DE-MALDI-TOF-MS)[6, 9, 12], liquid chromatography coupled to mass spectrometry (LC-MS)[3, 12, 13] and most recently capillary electrophoresis coupled to mass spectrometry (CE-MS)[14, 15]. These methods will be discussed in more detail in the following sections.

B.1. 2-D Gel Electrophoresis. Two-dimensional gel electrophoresis (2DE) is a powerful and widely used method for the analysis of complex protein mixtures and the most common preparative technique for CFS. 2DE separates proteins in a gel matrix two different ways. Isoelectric focusing (IEF) is used as the first dimension of separation. Proteins are separated according to their isoelectric points (pI). The second-dimension is SDS-polyacrylamide gel electrophoresis (SDS-PAGE) where separation of proteins is done according to their molecular weights (MW). 2DE requires large amounts of sample (μL-mL) and is time consuming with each dimension requiring hours to run plus additional time for preparation, staining, excising and analysis of the proteins of interest.

B.2. Liquid Chromatography Methods. The majority of LC analysis used in proteomics is based on a two-dimensional separation.[4, 16] The first dimension is typically size-exclusion chromatography (SEC) to first separate the proteins by molecular weight. The second dimension is run in-line and is normally reversed-phase liquid

chromatography (RPLC) to further separate the proteins by hydrophobicity. While this method reduces the analysis time from hours (2DE) to minutes (2D-LC), large sample volumes and sample consumption are still limiting factors.

B.3. Capillary Electrophoresis Methods. Capillary electrophoresis (CE) is used in a variety of ways in the analysis of proteins. CE can be used as the second dimension in a multidimensional LC-CE separation[17, 18], as a single dimension separation technique[15, 19, 20] or in multidimensional CE-CE[21-23]. While one dimensional CE uses very small sample volumes and has fast analysis times the resolution is not adequate for complex protein mixtures. Using CE as a second dimension coupled to RPLC adds a separation mechanism, electrophoretic mobility (separation based on charge to hydrodynamic radius ratios), which is not attainable with LC. Difficulties lie in the coupling of LC to CE. While there are some in-line coupling methods,[24] the majority of LC-CE experiments are preformed in a off-line manner where fractions are collected from the LC and then run on CE. The off-line method is more labor intensive and time consuming but easily accommodates the differences in flow rates and volumes between LC and CE. 2D-CE allows for a simple on-line coupling of CE to CE because differences in flow and volumes are not as great a factor as with LC-CE. 2D-CE couples capillary gel electrophoresis (CGE) with either micellar electrokinetic chromatography (MEKC) or capillary zone electrophoresis (CZE). In the 1st dimension, CGE, separation is done based on molecular weight and in the 2nd dimension resolution is improved by separations based on differential partitioning between a pseudostationary micellar phase and an aqueous mobile phase (MEKC) or by the ratio of charge to hydrodynamic radius

of the analyte (CZE). 2D-CE systems have shown a easier on-line adaptation, smaller sample volumes and faster analysis times than LC-LC and LC-EC methods while retaining the high resolution needed to separate complex protein mixtures.

Table 1 gives a comparison of capillary electrophoresis (CE), gel electrophoresis (SGE) and high performance liquid chromatography (HPLC) as separation techniques for the analysis of complex protein mixtures.[17]

Table 1. Comparison of HPLC, CE, and SGE

Function	CE	SGE	HPLC
Automation	Yes	No	Yes
Speed	Fast, seconds–minutes	Slow, minutes–hours	Minutes
Sensitivity	nM–femtomoles	μM	μM
Sample size	nL	μL	μL
Detection	On–column	Staining, fluorescence	Off–column
Quantitation	Yes, area under peak	Possible, but not simple	Area under peak
Multi samples	Yes, 96–384 capillaries	Yes	No
Multidimensional	Yes	Yes	Yes

B.4. Mass Spectrometry Methods. MALDI-TOF-MS is considered by many the workhorse of proteomics. In this method, the sample is mixed with a matrix solution and allowed to co-crystallize on a target plate. This solid matrix absorbs light at the same wavelength of the excitation laser. When the laser is fired at the target the matrix desorbs from the surface and carries some of the sample with it. At the same time the laser is pulsed, a voltage is applied to the target plate to accelerate the ionized sample towards a time-of-flight mass spectrometer. A second method used for the introduction of sample

to a MS for proteomic analysis is electrospray ionization (ESI-MS). ESI is an ionization method in which a liquid sample is forced through a charged capillary creating dispersed droplets containing the liquid mobile phase as well as the ions of interest. As the liquid evaporates off the ions are accelerated to the MS by the high potential charge applied between the capillary tip and cathode. A schematic of this process can be seen in Figure 3. ESI allows for a direct injection of Liquid samples into a MS which other ionization processes such as MALDI can not do. This makes ESI an extremely attractive method of coupling both LC and CE to mass spectrometry.

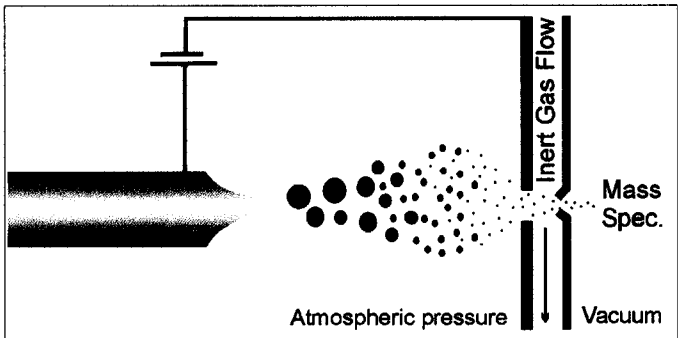

Figure 3: Electrospray ionization

B.5. Summary. The aforementioned techniques while frequently used in the diagnosis of AD from CSF have slow analysis times, many of them can consume large volumes of sample (μL - mL) and are limited in the number of markers that can be simultaneously detected. This proposed total analysis microchip will allow for the simultaneous detection of multiple markers in a small sample (nL). A decrease in analysis time will also be seen using the microchip format in comparison to conventional instrumentation.

C. Research Methods/Experimental Design

Development of a total analysis microchip for the purification, separation and detection of glycoproteins from human cerebrospinal fluid is presented. The development of this microchip will take place in 4 parts.

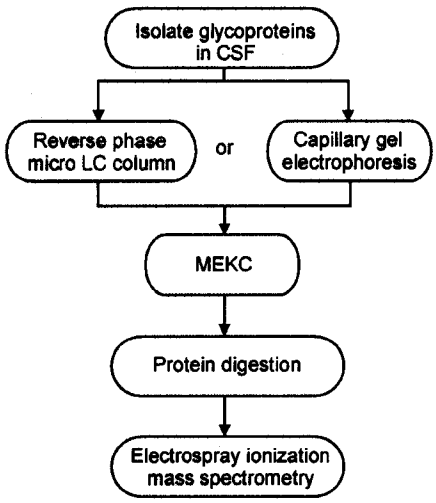

Figure C1: Steps in the development of μTAS for glycoproteins in CSF

1. Develop microchip for the injection and purification of glycoprotein from CSF using known microfluidic methods.

2. Develop a multidimensional microchip for the separations and qualification of CSF proteins.

3. Couple a microchip device to mass spectrometry for the quantification of CSF proteins of interest.

4. Merge the development of specific aims one, two and three through the addition of a series of valves to create a total analysis microchip for the detection of glycoproteins in CSF for the diagnosis of Alzheimer's disease.

The basic steps for the analysis of glycoproteins in CSF are shown in Figure C1. Many of these procedures have been preformed previously on conventional instrumentation. The aim and novelty of this proposal is to incorporate all of these steps into a single, on-line, microchip for complete glycoprotein analysis of CSF.

C.1. Isolation of glycoproteins in CSF. The first specific aim of this project will be to isolate glycoproteins from the complex protein mixture found in CSF. This will be accomplished through the use of affinity chromatography. Affinity chromatography is the process of selective adsorption and subsequent recovery of a compound from an

immobilized ligand. This process allows for a highly specific and efficient purification of many diverse proteins and other compounds. Binding is based on a highly specific interaction such as interactions between antigen and antibody, enzyme and substrate, or receptor and ligand. The ligand is generally immobilized on a beaded, porous matrix which may be in the form of a packed column. Within this specific aim there will be two major tasks.

Task 1: Optimization of affinity chromatography for glycoproteins. This task with be preformed on conventional LC instrumentation with either commercially available affinity particles or particles modified in the lab. The conventional LC instrument is automated and equipped with an autosampler which will allow us to run multiple affinity columns with a variety of buffer conditions to quickly optimize the binding and elution of glycoproteins.

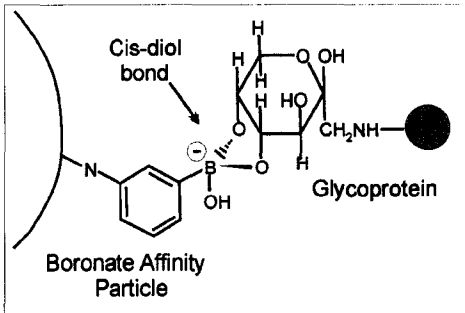

Figure C2: Capture of glycoprotein by boronate affinity chromatography through a Cis-diol

Boronate[25] and Multilectin[26] are two affinity chromatography variants that have been shown to bind glycoproteins. Boronate columns bind through cis-diols on carbohydrates, while in a multilectin affinity column, specific lectins such as concanavalin A or wheat germ agglutinin bind to specific carbohydrates. In this proposal we will focus on the use of boronate affinity particles for the isolation of glycoproteins in CSF. Boronate affinity particles can be purchased commercially or made in the lab. Due to ease of fabrication, the boronate affinity particles will made by modifying ToyoPearl Formyl particles with 3-aminophenylboronic acid.[27] Carbohydrates such as glucose bound to the exterior of

proteins (glycoprotein) contain cis-diols which bind to the boronate modified particles (Figure C2). The bound glycoprotein can then be eluted off of the column in one of two ways. First a buffer with a higher affinity for the cis-diols on the glycoprotein such as borate can be or second a buffer containing compounds with a higher affinity to the column than the glycoprotein such as sorbitol can be used.

Task 2: Miniaturization of boronate affinity chromatography for total analysis microchip. This task will focus on the adaptation of the boronate affinity column, task 1, to a small scale polymer microchip. This microchip will be used to test the viability of small scale affinity chromatography (AC) in the isolation of glycoproteins in CSF. A simple microchip design is given in Figure C3. This microchip will consist of 3 distinct parts. The first part is the multiple inlets to the column. Three inlets will be used for sample (A), binding buffer (B) and elution buffer (C). When pressure is applied to a specific reservoir, solution from that reservoir will flow through the column. The second major part of the microchip affinity column is the packed particle column. Affinity modified beads will be pushed into the chip under pressure to form a tightly packed lattice. The tapered outlet will serve two purposes, first to act as a frit to contain the particles to the column and second is to reduce the width of the capillary for easy coupling to microchip LC or CE for later parts of this proposal. The third distinct part is the outlet to a UV-Vis absorbance spectrometer. UV will be used in this part of the design process because of its simplicity,

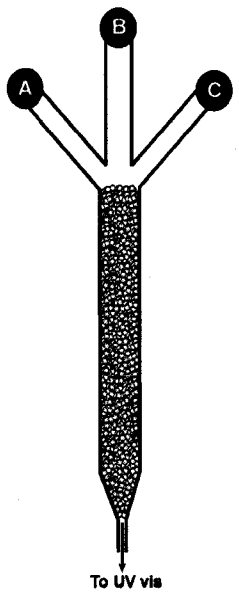

Figure C3: Proposed microchip boronate affinity column

cost and universal detection. Flow rates and pressures will be adjusted through syringe pumps.

The development of the micro-LC affinity column in this specific aim will allow glycoproteins to be isolated from CSF. The isolation of the glycoproteins will be able to be done on small sample volumes (nL) in short time periods (sec.) in comparison to standard instrumentation. The micro-LC column will also allow for an easy on-line coupling to the following parts of the μ-TAS device.

C.2. Multidimension protein separation on a microchip. Specific aim 2 is crucial for a high resolution separation of proteins. 2 dimensional separations whether they are 2DE, 2D-LC, 2D-CE or a combination of other separation methods have proven to be the best way of resolving complex protein mixtures. In this specific aim we plan to develop a two dimensional separation on a microchip for the separation of CSF proteins. We plan on using a 2D-CE method. The first dimension will separate the proteins by molecular weight by using capillary gel electrophoresis (CGE). The second dimension will further separate the protein mixtures based on the partitioning of the proteins between an aqueous mobile phase and the interior of a micellar pseudostationary phase. An alternative method to explore if unforeseen problems occur in the use of 2D-CE will be to use LC-CE in which the size exclusion chromatography could be used in place of CGE in the first dimension.

Task 1: 1st dimension, molecular weight separation on a microchip. Our primary focus will be on capillary gel electrophoresis (CGE) for the 1st dimension of separation. The

microchip will consist of two distinct parts. The first part will be the injector. A 250 μm double- T injector will be used for the injection of proteins. The second distinct part is the gel electrophoresis sieving matrix. This sieving matrix will be photopolymerized in the microchannel and is what allows the separation based on molecular weight. As the proteins migrates through the sieve they will be hindered, with larger proteins being more hindered and have longer migration times than smaller ones. CGE has been shown to be effective on the microchip scale.[23, 28] Soper's method for the photopolymerization of a sodium dodecyl sulfate polyacrylamide gel will be followed to contain the sieving gel in capillary. [23, 29] In this approach, the microchannels will be filled with a monomer solution including a photoinitiator. The polymerization is initiated by UV light, and using a mask or a shaped beam, the polymerization is restricted to the UV-exposed regions. The unpolymerized portions of the monomer can then be washed out of the microchip. Borate buffer will be used in the microchip CGE separation to better provide a smooth junction between the affinity column (borate elution buffer) and the electrophoretic separation.

A second method that may be used is size exclusion chromatography (SEC). In SEC, much like CGE, the separation is based on molecular weight. However, in SEC, larger molecules are the first to come off the column. This will require the addition of another micro LC column much like the one described in specific aim 1 for use with affinity chromatography.

Task 2: 2nd dimension, microchip MEKC. MEKC has been done on the microchip scale by numerous groups with numerous surfactants.[30-32] The microchip design will be very

similar to that used in the microchip CGE mentioned previously. The chip will contain a double-T injector and a separation channel. In this case, however, the separation channel will be an open channel. Micelles acting as a pseudostationary phase will allow proteins to partition between the aqueous and non-aqueous phases of the micelle depending on the hydrophobicity of the protein. Buffer solutions in this separation phase will have SDS concentrations above the critical micellar concentration (8 mM). Sodium dodecyl sulfate (SDS) is the most commonly used surfactant in MEKC applications. The anionic character of the sulfate groups of SDS cause the surfactant and micelles to have electrophoretic mobility that is counter to the direction of the strong electroosmotic flow. As a result, the surfactant monomers and micelles migrate slowly, but their net movement is still toward the cathode. Selectivity in MEKC can be varied, if need be, by altering the nature of the micelle. This is achieved by altering the surfactant and thereby changing the size, charge or geometry of the micelle.

Task 3: Coupling 1st and 2nd dimension on a microchip. One of the benefits to coupling CGE and MEKC on a microchip is the fact that both methods are electrophoretic separations. Figure C4 show a schematic layout of the microchip that will be used for the 2D separation. A glycoprotein sample will be introduced into the CGE portion of the chip from the reservoir labeled sample 1 in figure C4. An electric field will be applied between the sample 1 and sample

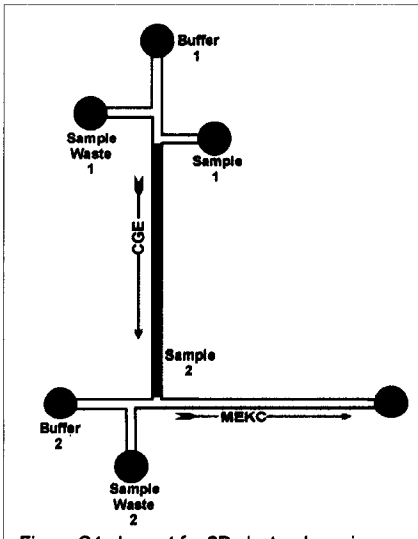

Figure C4: Layout for 2D electrophoresis microchip. Capillary gel electrophoresis will be the first dimension. Micellar electrokenetic chromatography will be the second dimension.

waste 1 reservoirs causing an electroosmotic flow. When the sample has filled the double T injector the injection potential will be turned off and a potential between buffer 1 and sample waste 2 will be turned on. This will cause the injected sample to flow through down the separation channel and through the CGE sieving matrix. As proteins are separated and come off the CGE portion of the chip (sample 2) they are automatically injected onto the MEKC portion of the chip. As proteins are injected onto the second dimension an electric field will be applied between the buffer 2 reservoir and the unlabeled reservoir at the end of the MEKC separation channel to perform the MEKC separation. The SDS MEKC buffer will be introduced into the chip from the buffer 2 reservoir. Determination of a properly functioning chip will be done with fluorescently labeled proteins and fluorescent monitoring on an inverted microscope.

C.3. Coupling microchip device to mass spectrometry. Specific aim 3 will involve the incorporation of trypsin protein digestion with the coupling of the microchip to a TOF-MS. All experiments will be done on polymer microchips fabricated in lab. This will allow for the quantification and qualification of the CSF glycoproteins.

Task 1. On-chip protein digestion. Traditional trypsin protein digestion is done by incubating a protein solution for 15-20 hours at 37° C. This however is too time consuming to be integrated in-line on a μ-TAS device. The Landers' group has developed a method for the in-line fast digestion of proteins on a microchip device.[33] An integrated micro LC column filled with trypsin modified agarose particles will be used. This method has shown a comparable tryptic digestion to traditional methods with the

low flow rate associated with CE.[33] The trypsin modified particles will be introduced into a microchannel shaped similarly to the micro LC column in specific aim 1 from an upstream side channel. The same side channel will later be used to introduce acetic acid to adjust the pH of the CE run buffers (8-10) to the pH needed for digestion (4-5). Optimization of flow will be done by adjusting the separation potential applied during the CE separation.

Task 2. Coupling ESI to microchip. Using electrospray ionization to couple electrophoretic microchips with mass spectrometry has been published previously.[34-38] We will incorporate an external, in-line ESI emitter for introduction to the mass spectrometer (Figure C5). An apparatus similar to this has been described previously by Harrison *et al.* [38] with low dead volume. This device will allow for a good decoupling between the separation potentials used in CE and the high voltages needed for the ionization process. It also allows for an introduction of a sheath buffer to eliminate problems of ionization associated with aqueous CE buffers and ESI. This will decrease chip cost and increase the ease of fabrication when compared to microchips with on chip emitters. An external fused silica capillary or a capillary fabricated into the polymer microchip will be used to connect the microchip to this emitter.

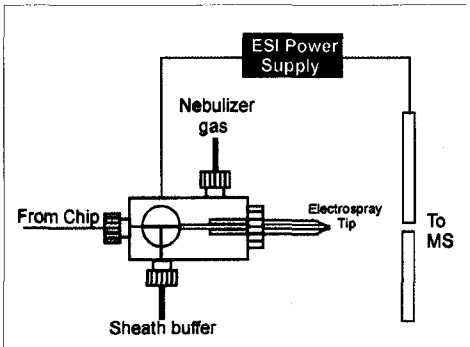

Figure C5: An external in-line electrospray emitter for coupling microchip CE to MS.

An ultra-fast tryptic digest coupled to an external ESI emitter will allow a simple but effective coupling of MEKC to mass spectrometry. Trypsin functionalized particles

will allow for protein digestion to be done in seconds without having to stop or slow the flow in the microchip. The external ESI emitter will be beneficial in adjusting flow rates needed for the electrospray as well as decoupling the voltages needed for the ionization process from the voltages used to drive CE separations.

C.4. Construction of μ-TAS device. Specific aim 4 involves the merger of specific aims one, two and three through the addition of a series of valves to create a μ-TAS device for the detection and quantification of glycoproteins in CSF. In Figure C6 (left) a schematic of the final chip is proposed. The chip itself can be broken into 3 major parts; affinity

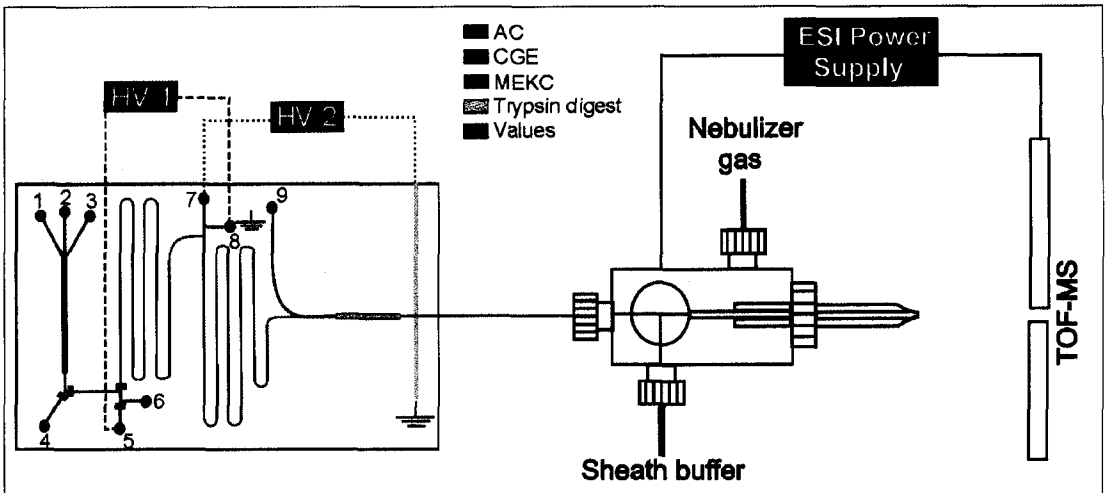

Figure C6: Proposed μ-TAS chip coupled to ESI-TOF-MS

chromatography, 2D-CE and ESI-TOF-MS. In total there will be 9 reservoirs, 2 high voltage power supplies, and 4 valves (figure C6, green rectangle). The valves used in this device will be based on work from the Mathies' group. These valves operate in a normally closed manner and are actuated using pressure when flow is needed in a specific channel.[39] Other methods such as electromagnetically driven valves may be explored.

The first major part of the microchip is the μ-AC column (figure C6, blue) described in specific aim 1. Reservoirs 1, 2 and 3 will be used as described previously for the sample, binding buffer and elution buffer respectively. Reservoir 4 will be used as the waste reservoir. Valving can be opened or closed depending on the path of desired flow travel. For example, when washing particles, flow goes to waste, requiring the valve that leads to reservoir 4 to be opened and all the others to remain closed. If flow is desired toward the CE portion of the chip, the valve to reservoir 4 remains closed while the valve that leads to the next stage of the chip is open.

The second major part of the microchip is the 2D-CE portion. Pressure driven flow will force the eluted glycoproteins into the double T injector to perform CGE (figure C6, red). Once the glycoproteins are injected the valves blocking reservoir 5 and the CGE separation channel will be opened and a high electric field applied between reservoir 5 and reservoir 8 to drive the separation through the CGE sieving matrix. Junction between CGE and MEKC (figure C6, purple) separation steps will be done as described in specific aim 2. The separation potential for MEKC will be applied between reservoir 7 and the electrode near the edge of the microchip.

The third major section of the microchip device is the protein digestion (figure C6, orange) and ESI emitter. Protein digestion is done at the end of the MEKC separation channel where a side channel (reservoir 9) introduces acetic acid into the buffer to adjust pH for the protein digestion. The addition of acetic acid will be done by appling a pressure to reservoir 9 and allowing it to mix with the MEKC buffer before entering the trypsin modified column. Linking the microchip to the ESI emitter will be done by a process described by the Harrison group.[38] Briefly a small hole will be drilled

in the side of the microchip in-line with the end of the channel where a capillary will be inserted for connection

D. Summary

Neurodegenerative diseases such as Alzheimer's affects millions of people worldwide. There is no definitive ante mortem way to diagnose AD. Current diagnosis for this disease is done through a combination of clinical and psychological examinations but is only around 80% accurate. Because of this there is merit to approaches that will simultaneously assay multiple biological markers. Cerebrospinal fluid offers a good medium for the discovery and analysis of biological markers relevant to the diagnosis of AD because of its close proximity to the brain. The CSF participates in free exchange of many biochemical products within the brain including small molecules, peptides and proteins. A change in concentration of specific proteins, both glycated and non-glycated, have been shown in patients with AD. In this proposal we focus on glycoproteins in the CSF. A micro total analysis system is proposed for the purification, separation and detection of the glycoproteins in CSF. This novel all in one device will allow the accurate analysis of multiple glycoproteins in CSF and their relative concentrations from small sample volumes (μL) in a fraction of the time it takes for conventional instrumentation.

The proposed μ-TAS can be implemented in much broader areas than for the detection of AD biomarkers in CSF. Various complex biological samples such as blood or urine could also be run on these chips depending on the interests of the researcher. Specificity can also be easily changed in this device by simply changing the affinity

column. Specific proteins, groups of proteins or even small molecules could be isolated depending on the affinity composition.

E. References

1. National Institute on Aging; U.S. National Institute of Health. **2006**, http://www.nia.nih.gov/Alzheimers/Publications/adfact.htm.
2. The Facts on Alzheimer's Disease; American Health Assistance Foundation. **2005**, www.ahaf.org.
3. Xu, J.; Chen, J. Z.; Peskind, E. R.; Jin, J. H.; Eng, J.; Pan, C.; Montine, T. J.; Goodlett, D. R.; Zhang, J., Characterization of proteome of human cerebrospinal fluid. *International Review of Neurobiology, Vol 73* **2006,** 73, 29-98.
4. Davidsson, P.; Sjogren, M., The use of proteomics in biomarker discovery in neurodegenerative diseases. *Disease Markers* **2005,** 21, (2), 81-92.
5. Merched, A.; Serot, J. M.; Visvikis, S.; Aguillon, D.; Faure, G.; Siest, G., Apolipoprotein E, transthyretin and actin in the CSF of Alzheimer's patients: relation with the senile plaques and cytoskeleton biochemistry. *Febs Letters* **1998,** 425, (2), 225-228.
6. Puchades, M.; Hansson, S. F.; Nilsson, C. L.; Andreasen, N.; Blennow, K.; Davidsson, P., Proteomic studies of potential cerebrospinal fluid protein markers for Alzheimer's disease. *Molecular Brain Research* **2003,** 118, (1-2), 140-146.
7. Choe, L. H.; Dutt, M. J.; Relkin, N.; Lee, K. H., Studies of potential cerebrospinal fluid molecular markers for Alzheimer's disease. *Electrophoresis* **2002,** 23, (14), 2247-2251.
8. Andreasen, N.; Minthon, P.; Davidsson, E.; Vanmechelen, H.; Winblad, B.; Blennow, K., Evaluation of CSF-Tau and CSF-Abeta42 as diagnosic markers for Alzheimer disease in clinical practice. *Arch. Neurol.* **2001,** 58, 373-379.
9. Li, X.; Miyajima, M.; Mineki, R.; Taka, H.; Murayama, K.; Arai, H., Analysis of potential diagnostic biomarkers in cerebrospinal fluid of idiopathic normal pressure hydrocephalus by proteomics. *Acta Neurochirurgica* **2006,** 148, (8), 859-864.
10. Rohlff, C., Proteomics in molecular medicine: Applications in central nervous systems disorders. *Electrophoresis* **2000,** 21, (6), 1227-1234.
11. WebMD; Lumbar Puncture. **2004**, http://www.webmd.com/hw/lab_tests/hw234563.asp.
12. Fountoulakis, M.; Kossida, S., Proteomics-driven progress in neurodegeneration research. *Electrophoresis* **2006,** 27, (8), 1556-1573.
13. Wenner, B. R.; Lovell, M. A.; Lynn, B. C., Proteomic analysis of human ventricular cerebrospinal fluid from neurologically normal, elderly subjects using two-dimensional LC-MS/MS. *Journal of Proteome Research* **2004,** 3, (1), 97-103.
14. Fliser, D.; Wittke, S.; Mischak, H., Capillary electrophoresis coupled to mass spectrometry for clinical diagnostic purposes. *Electrophoresis* **2005,** 26, (14), 2708-2716.
15. Wittke, S.; Mischak, H.; Walden, M.; Kolch, W.; Radler, T.; Wiedemann, K., Discovery of biomarkers in human urine and cerebrospinal fluid by capillary electrophoresis coupled to mass spectrometry: Towards new diagnostic and therapeutic approaches. *Electrophoresis* **2005,** 26, (7-8), 1476-1487.
16. Opiteck, G. J.; Ramirez, S. M.; Jorgenson, J. W.; Moseley, M. A., Comprehensive two-dimensional high-performance liquid chromatography for the isolation of

overexpressed proteins and proteome mapping. *Analytical Biochemistry* **1998,** 258, (2), 349-361.
17. Issaq, H. J., The role of separation science in proteomics research. *Electrophoresis* **2001,** 22, (17), 3629-3638.
18. Issaq, H. J.; Chan, K. C.; Liu, C. S.; Li, Q. B., Multidimensional high performance liquid chromatography - capillary electrophoresis separation of a protein digest: An update. *Electrophoresis* **2001,** 22, (6), 1133-1135.
19. Weissinger, E. M.; Wittke, S.; Kaiser, T.; Haller, H.; Bartel, S.; Krebs, R.; Golovko, I.; Rupprecht, H. D.; Haubitz, M.; Hecker, H.; Mischak, H.; Fliser, D., Proteomic patterns established with capillary electrophoresis and mass spectrometry for diagnostic purposes. *Kidney International* **2004,** 65, (6), 2426-2434.
20. Wittke, S.; Fliser, D.; Haubitz, M.; Bartel, S.; Krebs, R.; Hausadel, F.; Hillmann, M.; Golovko, I.; Koester, P.; Haller, H.; Kaiser, T.; Mischak, H.; Weissinger, E. M., Determination of peptides and proteins in human urine with capillary electrophoresis-mass spectrometry, a suitable tool for the establishment of new diagnostic markers. *Journal of Chromatography A* **2003,** 1013, (1-2), 173-181.
21. Kraly, J.; Fazal, M. A.; Schoenherr, R. M.; Bonn, R.; Harwood, M. M.; Turner, E.; Jones, M.; Dovichi, N. J., Bioanalytical applications of capillary electrophoresis. *Analytical Chemistry* **2006,** 78, (12), 4097-4110.
22. Kraly, J. R.; Jones, M. R.; Gomez, D. G.; Dickerson, J. A.; Harwood, M. M.; Eggertson, M.; Paulson, T. G.; Sanchez, C. A.; Odze, R.; Feng, Z. D.; Reid, B. J.; Dovichi, N. J., Reproducible two-dimensional capillary electrophoresis analysis of Barrett's esophagus tissues. *Analytical Chemistry* **2006,** 78, (17), 5977-5986.
23. Shadpour, H.; Soper, S. A., Comprehensive on-chip 2-D electrophoresis of proteins using photopolymerized gel and microemolsions. *Abstracts of Papers of the American Chemical Society* **2006,** 231, -.
24. German, I.; Roper, M. G.; Kalra, S. P.; Rhinehart, E.; Kennedy, R. T., Capillary liquid chromatography of multiple peptides with on-line capillary electrophoresis immunoassay detection. *Electrophoresis* **2001,** 22, (17), 3659-3667.
25. Narayanan, S. R., Preparative affinity chromatography of proteins. *Journal of Chromatography A* **1994,** 658, 237-258.
26. Yang, Z. P.; Harris, L. E.; Palmer-Toy, D. E.; Hancock, W. S., Multilectin affinity chromatography for characterization of multiple glycoprotein biomarker candidates in serum from breast cancer patients. *Clinical Chemistry* **2006,** 52, (10), 1897-1905.
27. Valente, J. J.; Verma, K. S.; Manning, M. C.; Wilson, W. W.; Henry, C. S., Second virial coeffcient studies of cosolvent-induced protein self-interaction. *Biophysical Journal* **2005,** 89, (6), 4211-4218.
28. Hatch, A. V.; Herr, A. E.; Throckmorton, D. J.; Brennan, J. S.; Singh, A. K., Integrated preconcentration SDS-PAGE of proteins in microchips using photopatterned cross-linked polyacrylamide gels. *Analytical Chemistry* **2006,** 78, (14), 4976-4984.
29. Shadpour, H.; Soper, S. A., Two-dimensional electrophoretic separation of proteins using poly(methyl methacrylate) microchips. *Analytical Chemistry* **2006,** 78, (11), 3519-3527.
30. Collier, A.; Wang, J.; Diamond, D.; Dempsey, E., Microchip micellar electrokinetic chromatography coupled with electrochemical detection for analysis of

synthetic oestrogen mimicking compounds. *Analytica Chimica Acta* **2005,** 550, (1-2), 107-115.
31. Roman, G. T.; Carroll, S.; McDaniel, K.; Culbertson, C. T., Micellar electrokinetic chromatography of fluorescently labeled proteins on poly(dimethylsilokane)-based microchips. *Electrophoresis* **2006,** 27, (14), 2933-2939.
32. Wallenborg, S. R.; Bailey, C. G., Separation and detection of explosives on a microchip using micellar electrokinetic chromatography and indirect laser-induced fluorescence. *Analytical Chemistry* **2000,** 72, (8), 1872-1878.
33. Yue, G. E.; Roper, M. G.; Balchunas, C.; Pulsipher, A.; Coon, J. J.; Shabanowitz, J.; Hunt, D. F.; Landers, J. P.; Ferrance, J. P., Protein digestion and phosphopeptide enrichment on a glass microchip. *Analytica Chimica Acta* **2006,** 564, (1), 116-122.
34. Akashi, S.; Suzuki, K.; Arai, A.; Yamada, N.; Suzuki, E. I.; Hirayama, K.; Nakamura, S.; Nishimura, Y., Top-down analysis of basic proteins by microchip capillary electrophoresis mass spectrometry. *Rapid Communications in Mass Spectrometry* **2006,** 20, (12), 1932-1938.
35. Kameoka, J.; Orth, R.; Ilic, B.; Czaplewski, D.; Wachs, T.; Craighead, H. G., An electrospray ionization source for integration with microfluidics. *Analytical Chemistry* **2002,** 74, (22), 5897-5901.
36. Lion, N.; Rohner, T. C.; Dayon, L.; Arnaud, I. L.; Damoc, E.; Youhnovski, N.; Wu, Z. Y.; Roussel, C.; Josserand, J.; Jensen, H.; Rossier, J. S.; Przybylski, M.; Girault, H. H., Microfluidic systems in proteomics. *Electrophoresis* **2003,** 24, (21), 3533-3562.
37. Ramsey, R. S.; Ramsey, J. M., Generating electrospray from microchip devices using electroosmotic pumping. *Analytical Chemistry* **1997,** 69, (6), 1174-1178.
38. Li, J. J.; Thibault, P.; Bings, N. H.; Skinner, C. D.; Wang, C.; Colyer, C.; Harrison, J., Integration of microfabricated devices to capillary electrophoresis-electrospray mass spectrometry using a low dead volume connection: Application to rapid analyses of proteolytic digests. *Analytical Chemistry* **1999,** 71, (15), 3036-3045.
39. Grover, W. H.; Skelley, A. M.; Liu, C. N.; Lagally, E. T.; Mathies, R. A., Monolithic membrane valves and diaphragm pumps for practical large-scale integration into glass microfluidic devices. *Sensors and Actuators B-Chemical* **2003,** 89, (3), 315-323.